THE NUCLEATION OF NICKEL DIOXIMATES
FROM AQUEOUS SOLUTION

THE NUCLEATION OF NICKEL DIOXIMATES
FROM AQUEOUS SOLUTION

By

JOSEPH DEREK HANNA, B.Sc., M.Sc.

A Thesis
Submitted to the Faculty of Graduate Studies
in Partial Fulfilment of the Requirements
for the Degree
Doctor of Philosophy

McMASTER UNIVERSITY
September 1971

DOCTOR OF PHILOSOPHY (1971)
(Chemistry)

McMASTER UNIVERSITY
Hamilton, Ontario

TITLE: The Nucleation of Nickel Dioximates from Aqueous Solution

AUTHOR: Joseph Derek Hanna, B.Sc., M.Sc. (Queen's University, Belfast)

SUPERVISOR: Dr. O. E. Hileman

NUMBER OF PAGES: xiv, 161

SCOPE AND CONTENTS:

A brief review of the theoretical and experimental aspects of liquid droplet nucleation from vapours and of crystal nucleation from aqueous solution is presented. In order to study the nucleation and crystal growth of several analytically important metal chelates, methods were developed to measure the size distribution of crystals growing in a supersaturated solution. These methods involved rapid mixing techniques followed by measurement of the size distribution of the precipitated particles using a Coulter counter and multichannel analyser. The size distributions were dumped from the analyser onto magnetic tape and recovered using computer methods. The mixing and counting techniques were calibrated and tested using barium sulphate and spheres of known size distribution.

From the size distributions obtained for the metal chelates, conclusions were made regarding the nucleation step, and the parameters important in the classical Volmer-Weber-Becker-Doring theory of nucleation were calculated. The validity of the values were evaluated and comparisons made with values obtained by other workers.

The laws controlling the crystal growth of the metal chelates and their importance in elucidating the type of nucleation process were also investigated.

To

ANNA

and

MY PARENTS

ACKNOWLEDGEMENTS

I should like to thank Dr. O. E. Hileman for his advice and enthusiasm throughout the course of this research. I should also like to thank the fellow members of our research group for stimulating and useful discussions.

Financial assistance by the Province of Ontario and McMaster University is gratefully acknowledged.

I wish to thank Mrs. Susan Hawley for typing and correcting this thesis.

Fianlly I am especially grateful to my wife, Anna, and my parents for their constant encouragement and understanding.

TABLE OF CONTENTS

LIST OF TABLES

LIST OF TABLES (cont.)

LIST OF FIGURES.

LIST OF SYMBOLS

A	pre-exponential factor (defined in the text).
A'	$= \sigma O^*/i^{*\frac{2}{3}}$
a_1	activity of the supersaturated solute.
$a_{1\infty}$	activity of the saturated solute.
c_t	concentration of the solute at time t.
d	diameter of a crystal.
D	diffusion coefficient.
G	Gibbs free energy.
ΔG	Gibbs free energy of formation of an embryo.
ΔG^*	Gibbs free energy of formation of a critical nucleus.
$\Delta G'^*$	Gibbs free energy of activation for surface nucleation.
h	Plancks constant.
I	moment of inertia of the embryo.
i	number of molecules in an embryo.
i*	number of molecules in a critical nucleus.
J	rate of nucleation
kT	4.12×10^{-14} ergs at $T = 298.16\ ^0K$
m	mass of a molecule.
n_i	number of clusters containing i molecules.
N(d,t)	number of crystals with a diameter > d at time t.
O_i	surface area of a cluster containing i molecules.
O*	surface area of a cluster containing i* molecules.

p_1	partial pressure of the supersaturated vapour.
$p_{1\infty}$	partial pressure of the saturated vapour.
q_r	rotational partition function of a cluster.
q_{rep}	replacement factor.
r	radius of a crystal.
r^*	radius of the critical nucleus.
r_i	radius of an embryo containing i molecules.
s	solubility.
S	supersaturation.
S^*	critical supersaturation (where $J=1$).
t	time.
T	absolute temperature.
v_2	molecular volume = v
w_1	rate of condensation of vapour molecules to a cluster.
w_{2i}	rate of evaporation of molecules from an i cluster.
W	molecular weight.
α	degree of reaction
β	shape factor.
μ_1	chemical potential of a single molecule in the vapour.
$\mu_{2\infty}$	chemical potential of a single molecule in the liquid.
ω	shape factor.
ρ	crystal density.
σ	surface free energy of a cluster.

1. INTRODUCTION

1.A. Statement of the problem

The literature concerning the nucleation of one phase from another contains many theoretical and experimental contradictions. This is especially true for the nucleation of crystals from aqueous solution. The nucleation step and the subsequent crystal growth determine the variation with time, of the number, size and shape of the crystals formed in a precipitation. The purpose of this investigation was, therefore, to measure these parameters in order to elucidate the type of mechanism controlling the initial phase transformation and to assess the validity of the classical nucleation theory. For metal chelates this required the development of new experimental techniques. These also enabled comparisons to be made with the results obtained by other authors, for similar compounds, using widely different techniques.

1.B. Historical Background

The process of nucleation and growth of a new phase has been known and used for over a millenium in the purification of substances. The literature on the subject is very substantial and while much is known empirically and theoretically about the subject it has often been difficult to put unequivocable theoretical interpretations on the empirical results. Any knowledge gained regarding the interpretation of experimental results in the light of known theory is therefore of considerable interest.

Any advance in the understanding of the nucleation phenomenon is of added interest as problems involving phase changes occur in many widely diverse scientific and technological disciplines. Among these are metallurgy, meteorology, physics, biology, astrophysics, geochemistry, engineering, aerodynamics and chemistry.

In particular analytical chemists are interested in the problem because the nucleation of crystals from solution is important both in its own right and as a process which controls the number, size and morphology of the precipitated crystals. This knowledge is important in the elucidation of empirical problems encountered by the analytical chemist such as the unfilterability of certain precipitates, the presence of coprecipitated foreign ions and poor fractional crystallization.

Probably the most important fact regarding the nucleation and growth of one phase from another is that any vapour or liquid or solution can be supercooled or supersaturated beyond the point where the old phase and the new phase should be in equilibrium. This phenomena of supercooling was first investigated scientifically in the early eighteenth century by Fahrenheit (1) who found that water could be kept overnight at 15°F in sealed air free glass vessels without freezing. He also found that crystallization could be induced by addition of some ice crystals and by violent concussion. These observations were confirmed and extended by many other workers in the eighteenth century. For example Lowitz (2) discovered supersaturation phenomena in aqueous salt solutions. Gay Lussac (3,4) showed that supersaturation was a very general phenomenon occurring wherever a phase change occurred.

Many methods of inducing crystallization in supersaturated salt solutions, such as shaking, scratching and rubbing, were investigated. Gay Lussac found that sound had no effect in inducing crystallization. The recent literature, on the other hand, contains many references to experiments where crystallization has been induced by ultrasonic radiation (5,6,7) and by magnetic fields (8,9).

At this time it was realized (10) that atmospheric dust could contaminate the supersaturated solutions of salts and act as centres of growth. Significant steps forward were made by de Coppet (11) and Ostwald (12). The former measured the average time lag before crystallization occurred in solutions of known supersaturation and the latter recognized two types of supersaturation - metastable and labile. Metastable solutions did not crystallize after long periods of time whereas labile solutions crystallized very quickly. Tamman (13) and von Weirman (14) showed that the metastable state could be made labile by increasing the concentration of the solute and also that if the metastable state was left for a sufficiently long time crystallization would in fact occur.

At this time therefore it was clear that crystallization probably consisted of two steps. The first step (termed nucleation) consisted of the formation of discrete submicroscopic nuclei and the second their growth to a visible size. It was also clear that the nuclei could be formed either entirely of the new phase or that growth could occur on foreign particles already present in solution. The former process is termed homogeneous nucleation and the latter, heterogeneous nucleation. The formation of the nuclei is difficult to study experimentally as they are usually smaller than 100 Å in diameter and so are not amenable to direct study. In this respect, some recent work using molecular beams (15-18) appears promising for the case of the condensation of a liquid from its vapour.

Theories of nucleation have been developed primarily for the condensation of liquids from their vapours. These, in modified form, also describe the nucleation of solids from condensed phases. Vapour to liquid nucleation can be treated more rigorously and is more exactly described by theoretical models. The theories have developed along two main lines. The first is the approach, using a procedure suggested by Szilard (19), of Volmer and Weber (20) who recognized that the phenomenon of metastability of supersaturated phases was the result of kinetic effects. Their approach has subsequently been improved by many authors, notably Farkas (21), Stranski (22), Becker and Doring (23), and Zeldovich (24). This theory, known as the classical theory, has been widely accepted because it is in agreement with much of the experimental evidence found since it was proposed.

The second approach is a statistical mechanical one based on Mayers' (25) theory of condensation. This theory has been developed by Frenkel (26), Becker (27), Rodebush (28), Reiss (29), Dunning (30), Lothe and Pound (31) and Oriani and Sundquist (32). Lothe and Pound (31) obtained theoretical rates of nucleation which were as much as 10^{17} times greater than those predicted by the classical theory for supersaturated water vapour. Reiss and Katz (33) have challenged the conclusions found by Lothe and Pound (31), although the latter authors (34) and Abraham and Pound (35) have shown Reiss and Katz to be in error. In a very recent paper Abraham and Pound have modified the factor of 10^{17} to a factor of 10^{8}. The evaluation of this factor is a matter of continuing discussion at the present time.

1.C. Nucleation Theory

1.C.1. The nucleation of liquid drops from the vapour phase

The literature on the subject of vapour to liquid nucleation is extensive and together with the original papers previously mentioned (Section 1.B.) many excellent reviews (36-41) on the subject exist.

The experimental aspects of vapour to liquid nucleation for which any theory of nucleation must account are as follows. All phases can be made supersaturated without spontaneous formation of a new phase. This implies that as the two phases are not in thermodynamic equilibrium there is a free energy barrier to the formation of the new phase analogous to the activation energy for a normal chemical reaction. Also, the new phase forms in large numbers of discrete particles which do not become visible until a finite length of time has elapsed. A theory of nucleation must therefore account for this energy barrier and predict the rate of formation of the particles of the new phase.

Statistical fluctuations with a supersaturated vapour of pressure p_1 give rise to aggregates containing various numbers of molecules. It has been shown (42) that the clusters are probably built up by the addition of single molecules

$$A + A \rightleftharpoons A_2$$
$$A_2 + A \rightleftharpoons A_3$$
$$- - - - - - - - -$$
$$A_{i-1} + A \rightleftharpoons A_i$$
$$A_i + A \longrightarrow A_{i+1}$$

where A_i represents a cluster containing i molecules of A. If the supersaturation is small these clusters tend to evaporate and disappear. As the supersaturation is increased, however, the frequency of cluster-molecular collisions increases so rapidly that there are an appreciable number of large clusters.

In order to account for the energy barrier the energy of formation of a cluster of i molecules must be calculated. If the cluster is at rest then the free energy of formation is simply (neglecting the change in energy due to changes in volume)

$$\Delta G = i\mu_{2\infty} + \sigma O_i - i\mu_1 \qquad [1]$$

A plot of ΔG versus i is found to have a maximum at ΔG* and i*. If the cluster has a size i* then the addition of a single molecule to it decreases the free energy of the cluster and it grows unhindered into a macroscopic part of the new phase. Clusters with the size i* have the maximum free energy ΔG* and are termed critical nuclei. This maximum in the free energy versus size curve is the reason for the existence of the phenomenon of supersaturation. Putting $i = 4\pi r_i^3 / 3v_2$ in Equation [1] it is found that

$$r^* = \frac{2\sigma v_2}{\mu_1 - \mu_{2\infty}} = \frac{2\sigma v_2}{kT\ln(p_1/p_{1\infty})} \qquad [2]$$

where r* is the radius of the critical nucleus. The ratio $(p_1/p_{1\infty})$ is usually referred to as the supersaturation S. Equation [2] is the well known Gibbs-Thompson equation. Further, the following equations for ΔG* and i*, the free energy of formation of the critical nucleus and the number of molecules in the critical nucleus may be derived from Equation [2]. For a spherical nucleus:

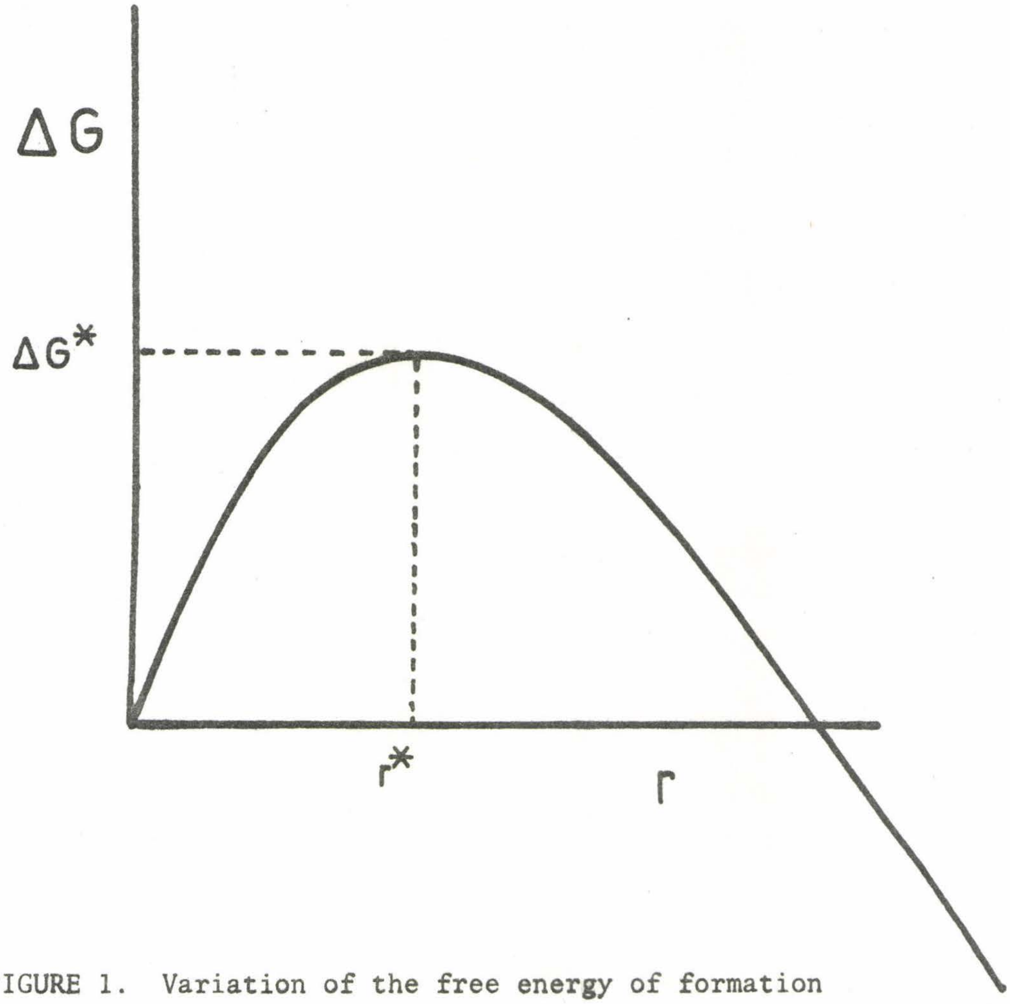

FIGURE 1. Variation of the free energy of formation of a cluster with radius.

$$\Delta G^* = \frac{16\pi\sigma^3 v_2{}^2}{3k^2T^2\ln^2(p_1/p_{1\infty})} , \qquad [3]$$

$$i^* = \frac{32\pi\sigma^3 v_2{}^2}{3k^3T^3\ln^3(p_1/p_{1\infty})} . \qquad [4]$$

The next problem is then to calculate the rate of nucleation J. The "classical" theory is derived largely from the treatment of Becker and Doring (23). The assumption is made that the supersaturated phase is in a state of quasi-equilibrium in which the size distribution of clusters of all sizes up to the critical size is essentially stationary with time and that drops may form and grow. These are removed when they reach a size just greater than the critical size. The vapour pressure is maintained at a constant level by the continuous introduction of single molecules so that there is a steady stream of molecules from one cluster size to the next. Also a spherical surface, of area $0_i'$, surrounding the embryo is chosen such that a molecule passing through it from the vapour is regarded as captured and on passing through it from the embryo is regarded as having escaped. The steady state flux through the system is then

$$J = n_i w_1 0_i' - n_{(i+1)} w_{2(i+1)} 0_i' \qquad [5]$$

where w_1 is the impingment frequency and $w_{2(i+1)}$ is the evaporation frequency per unit area.

Becker and Doring solved these equations for J by the successive elimination of n_i and the use of the Gibbs-Thompson theory in the form

$$w_1/w_{2i} = p_1/p_i = \exp \frac{2\sigma v_2}{kT} \left(\frac{1}{r^*} - \frac{1}{r_i}\right) \qquad [6]$$

This involves the assumption that the Gibbs-Thompson equation is valid for all sizes of embryos. This assumption cannot be justified for small embryos which consist of only a few molecules. Using this method however Becker and Doring (23) and Zeldovich (24) found that the rate of nucleation was given by

$$J = Z\beta^{*}n_1 \exp(-\Delta G^{*}/kT) \qquad [7]$$

where ΔG^* is given by Equation [3], Z, the Zeldovich factor, is $(\Delta G^*/3\pi kTn^{*2})^{1/2}$ and $\beta^* = p_1 0^*/(2\pi mkT)^{1/2}$. For typical condensations from the vapour $Z = 10^{-2}$ and the pre-exponential factor is 10^{25}.

The form of this equation is such that J remains negligibly small until the supersaturation ratio $(p_1/p_{1\infty})$ reaches a critical value, the Ostwald metastable limit, at which J suddenly and dramatically increases. Although J is a smooth function of the supersaturation the change in J is so dramatic that the value of the supersaturation at this point is sharply defined and is termed the critical supersaturation. The theory therefore qualitatively accounts for all the experimental observations regarding phase changes.

Theoretically the equation has been questioned by many authors. The criticism has been based on the recalculation, using statistical mechanics, of the energy of formation of the clusters. The value of this formation energy dictates the equilibrium concentration of the critical nucleus. This concentration is in turn the most important factor in determining the nucleation rate.

The classical theory of nucleation described thus far, completely ignores the translational and rotational partition functions of clusters and nuclei. Frenkel (43) and Rodebush (44) provided the first improved derivation of the free energy of the embryos. Kurt (45) also provided a complete derivation of the equilibrium distribution of clusters in a vapour. According to Lothe and Pound (46) an error in Kurt's work made the work of formation of the nucleus nearly equal to that of the classical theory. Allowing the translational and rotational contributions, the free energy of a cluster is given by

$$F = i\mu_{2\infty} + \sigma O_i - \frac{kT}{n_i} \ln[\lambda^{n_i}/n_i!] - kT \ln q_r + kT \ln q_{rep}. \qquad [8]$$

where $\lambda = (2\pi nmkT)^{3/2}/h^3$

is the translational partition function, and

$$q_r = (2kT)^{3/2}(\pi I^3)^{3/2}/h^3$$

is the rotational partition function.

The replacement term, $kT\ln q_{rep}$, takes into account the increase in free energy arising from the deactivation of six degrees of freedom in taking the cluster from the bulk liquid. From Equation [8] the equilibrium distribution of clusters was found to be

$$n_i = n_1 \exp \{ - [\Delta G^o - kT\ln(\frac{\lambda q_r}{n_1 q_{rep}})] / kT \} \qquad [9]$$

Much controversy exists in the literature (48) at present, the main arguments centering around the evaluation of the replacement factor in Equation [8]. Estimates of the factor by which nucleation rates should be adjusted vary from 1 (33) to 10^{17} (31). The classical theory and statistical mechanical version make the assumption that there is a steady state size distribution. In a real situation however each cluster may not be in dynamic equilibrium with the next size and also a time lag will be present before the supposed steady state is built up. Zeldovich (24) was the first to attempt an estimate of the time lag for approach to the steady state. Several other authors (49-52) have also studied the time lag problem. Abraham (53) gives an overall picture of how the system relaxes into a steady state. In general the estimates of the time lag are approximately 10^{-6} seconds.

1.C.2. Nucleation of crystals from condensed phases

Qualitatively the calculation of the rate of nucleation of crystals from either melts or solutions follows the same path as that outlined above for vapour to liquid nucleation. The work of formation of each cluster, the steady state concentration of clusters and the flux of monomers impinging on the clusters are calculated. The rate of nucleation is then found. Quantitatively differences exist in all of these calculations.

Analogous with Equation [2], the radius of the critical nucleus was shown (12) to be

$$r^* = \frac{2\sigma v_2}{kT\ln(a_1/a_{1\infty})} \qquad [10]$$

Analogous with Equation [3], the free energy of formation of clusters is

$$\Delta G^* = \frac{\beta\sigma^3 v_2{}^2}{k^2T^2\ln^2(a_1/a_{1\infty})} \qquad [11]$$

The free energy of a crystal will include the contributions from edges and corners. In Equation [11], these have been neglected and also the surface free energies for each face of the crystal are replaced by an average surface energy σ. β is a shape factor and for a spherical nucleus equals $16\pi/3$.

Turnbull and Fisher (54) have calculated the rate of nucleation in condensed systems using the theory of absolute reaction rates. They have shown the steady state concentration of clusters to be

$$n_i = n_1 \exp(-\Delta G_i/kT) \qquad [12]$$

and the rate of nucleation to be

$$J = n^*(A'/9\pi)^{1/2}(N'kT/h) \exp[-(\Delta g^* + \Delta G^*)kT] \qquad [13]$$

where Δg^* is the free energy of activation for the short range diffusion of molecules. By separating the exponential powers, putting

$$A = n^*(A'/9\pi)^{1/2}(NkT/h)\ e^{-\Delta g^*} \qquad [14]$$

and replacing ΔG^* by $\dfrac{\beta\sigma^3v^2}{k^3T^3(\ln S)^2}$, the rate of nucleation may be written

$$J = A \exp\left(\frac{-\beta\sigma^3v^2}{k^3T^3(\ln S)^2}\right) \qquad [15]$$

The assumptions made in developing the theory for aqueous solutions are the same as those made in the theory of vapour to liquid nucleation. These assumptions are, that the Gibbs-Thompson equation is valid for the smallest clusters, that a steady state cluster size distribution is obtained and that the time lag taken to obtain this distribution is small compared with the length of time over which nucleation occurs. Several authors also have shown that assumptions that the time lag is small and the steady state instantaneous are good except for very viscous liquids.

In the condensed phase the free energy of formation of a cluster found by excluding the rotational and vibrational contributions is probably accurate as both are relatively small. Values of the pre-exponential factor A lie in the region $10^{33\pm3}$ for both the nucleation of crystals from pure liquids and the nucleation of crystals of solute from solution. For the latter case, however, this value may well be much lower due to the fact that desolvation of the monomers must occur before clusters can form.

1.C.3. Heterogeneous nucleation

The theories of nucleation already discussed in Section 1.C.1. and Section 1.C.2. apply to nucleation which occurs solely as the result of fluctuations in the sizes and numbers of clusters in the original phase. This type of nucleation is termed homogeneous. Macroscopic crystals may, however, also grow by the addition of monomers to microscopic particles or motes, already present in the system. This type of nucleation is termed heterogeneous. The heterogeneous particles on which growth is initiated may be dust particles, the walls of the vessels, or seed particles of the new phase deliberately introduced into the system. When nucleation and growth occur in this way the energy of formation of a heterogeneous cluster is much lower than that for a homogeneously formed cluster. Consequently heterogeneous nucleation occurs at much smaller supersaturations than homogeneous nucleation. This fact is used to advantage in many crystallization procedures by chemists who induce heterogeneous nucleation by scratching the walls of the vessel or adding seed crystals to the supersaturated solutions.

It has been shown (68) that the ability of a heterogeneous particle to act as a growth site is related to the match between its crystal lattice and that of the growing crystal. Consequently, other authors (98) have postulated that heterogeneous particles have a range of nucleating abilities. As dust particles are probably always inadvertently present in solutions, heterogeneous nucleation on them and the walls of the vessel is probably always present in any crystallization process from solution. It is therefore a very important consideration when evaluating the validity of the theory of homogeneous nucleation as applied to nucleation of solids from aqueous solution.

1.D. Experimental Assessment of Nucleation Theory

1.D.1. Nucleation of liquid droplets from the vapour phase

Experimental investigations of vapour to liquid nucleation fall into three classes:

(i) adiabatic expansions using cloud chambers;
(ii) adiabatic expansions using supersonic jets; and
(iii) molecular beams.

The classical experiments of Volmer and Flood using a cloud chamber to detect the onset of condensation of the vapour of several organic liquids have provided the best experimental vindication of the classical theory of nucleation. In these experiments no actual measurement of the nucleation rate is made. The critical supersaturation, being that supersaturation which just produces a visible vapour, is measured and compared with theory. The results of the experiments of Volmer and Flood are shown in Table I. The point at which condensation was just observable was made equal to a rate of 1 particle/cm^3/sec. The agreement between calculated and observed values is good for all the vapours studied except methanol.

From Equation [3] $T^{3/2} \ln \frac{p_1}{p_{1\infty}}$ should be constant when the critical supersaturation is measured at various temperatures. Powell (56) has measured the temperature dependence of the critical supersaturation for water and found that the relationship holds. Katz and Ostermier (57) have also found that similar relationships hold for methanol, ethanol and hexane. In all these cases the values found agree with the classical theory and not with Lothe and Pound's (31) modification of it.

TABLE 1

Observed and calculated values of P/P_∞ (critical).

Substance	P/P_∞ (critical)	
	Calculated	Observed
Water	4.2	4.2
Methanol	1.8	3.2
Ethanol	2.3	2.3
n-Propanol	3.2	3.0
Isopropanol	2.9	2.8
n-Butanol	4.5	4.6
Nitromethane	6.2	6.1

Hill (58), using supersonic nozzles to induce nucleation, finds that, for water, the experimental results verify the classical theory and that the critical supersaturations found are much lower than those predicted by Lothe and Pound (31). Experimental investigations with supersonic molecular beams have recently given direct evidence of the presence in the beams of clusters of various sizes. This technique coupled with mass spectrometry is potentially very powerful for the study of homogeneous nucleation of liquids from their vapours.

1.D.2. Nucleation of solutes from aqueous solution

(a) Interpretation of the experimental results for solutions

The nuclei formed in precipitation from solution are usually very small and as such are not amenable to direct observation. It is necessary, therefore, that the nuclei grow to macroscopic size before their numbers, sizes and rate of appearance at the detector may be measured. The period between the formation of the critical nucleus and the detection of a macroscopic crystal is determined by its rate of crystal growth. As many factors, which may change discontinuously throughout the precipitation, control the rate and type of crystal growth, the interpretation of experimental results in terms of liquid nucleation theory becomes very difficult. The effect of crystal growth on the observed nucleation rates must therefore be taken into account in order to assess the experimental results.

Nielsen (42,59,60) has discussed the interpretation of nucleation results in detail. A generalized diagram showing the nucleation velocity as a function of the supersaturation ratio for various values of the surface energy for nickel dimethylglyoximate is shown in Figure 2. This plot is very useful in interpreting experimental results and also in evaluating how a variation in any one parameter affects the value of the others. From Figure 2, it can be seen that the plots of lnJ against lnS are almost straight lines over several decades of J. Therefore it is a fairly good approximation to write

$$\ln J = \ln k_n + n \ln S \qquad [16]$$

or $$J = k_n S^n \qquad [17]$$

for intervals of restricted lengths. This formula is the same as that first proposed by Christiansen (61). Equation [14] is useful in that the power n is easily found from the slope of lnJ against lnS curves and can be shown (42) to be equal to i* the number of molecules in the critical nucleus. The size of the critical nucleus may then be determined directly from experiments.

Perhaps the best test for correspondence between experimental results and theory is obtained by rewriting Equation [15] in logarithmic form

$$\ln J = \ln A - B'(\ln S)^{-2} \qquad [18]$$

where $B' = \frac{\beta \sigma^3 v^2}{k^3 T^3}$.

A plot of lnJ against $(\ln S)^{-2}$ should therefore yield a straight line. Experiments on nucleation from solution have as their objectives to verify the functional relationship between J and S and to measure the values of the parameters in Equation [13], primarily the values of the pre-exponential factor A and of the surface tension σ. In many experi-

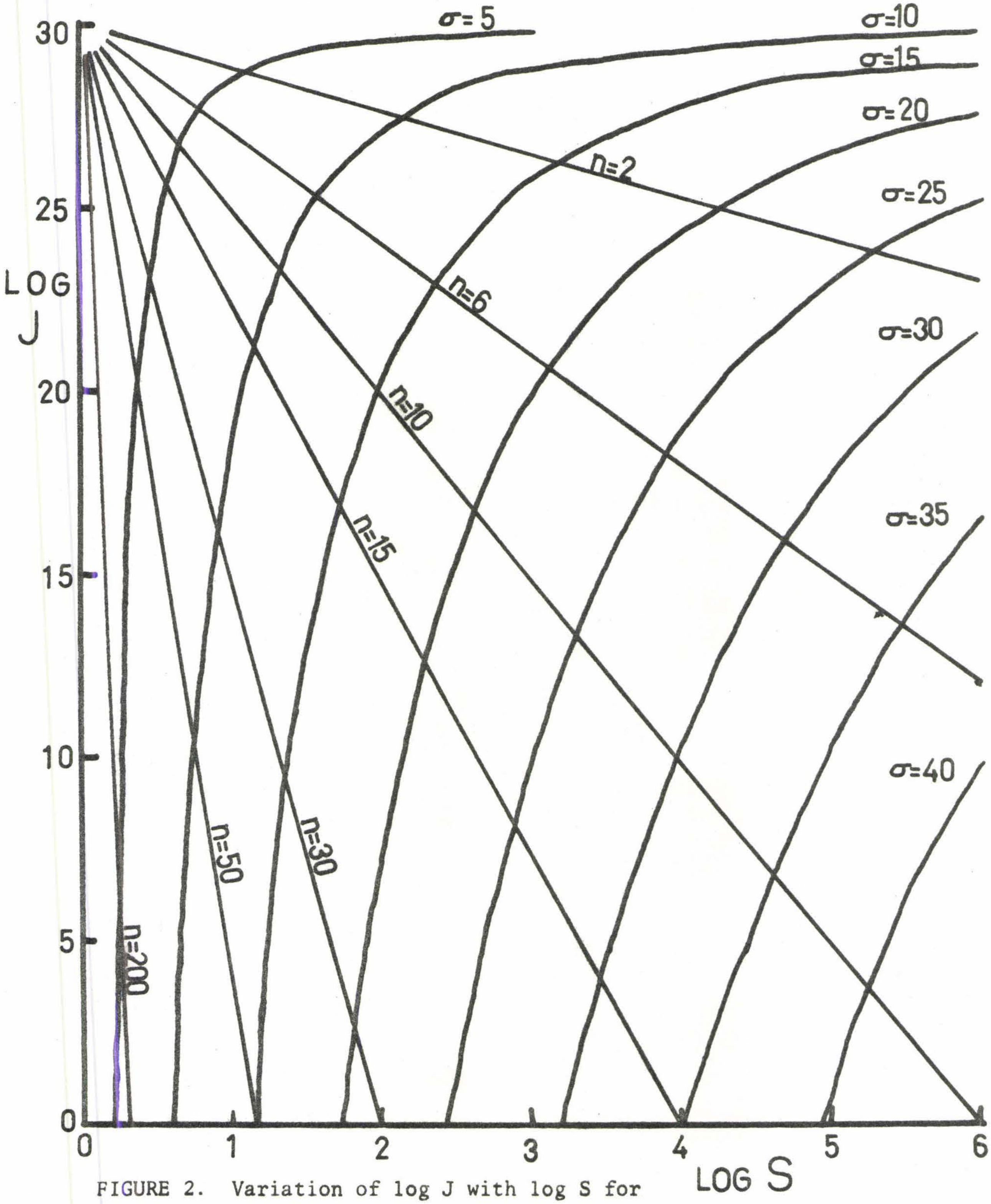

FIGURE 2. Variation of log J with log S for nickel dimethylglyoximate.

ments the critical supersaturation is measured and J is set equal to 1 at this supersaturation. In these experiments the variation of J with S is not measured.

A critical nucleus, once formed, may grow according to one of five mechanisms or a combination of them. The mechanisms and their linear rates of growth, dr/dt, are the following (59).

1. Screw Dislocation

$$\frac{dr}{dt} = \frac{DkTcg(\ln S)^2}{20\sigma} \qquad [19]$$

2. Mononuclear Layer Growth involving surface nucleation with one surface nucleus per molecularor ionic layer.

$$\frac{dr}{dt} = \frac{4Dr^2g}{v} \exp\left(\frac{-\Delta G'^*}{kT}\right) \qquad [20]$$

3. Polynuclear Growth (Surface nucleation with several intergrowing surface nuclei per layer.)

$$\frac{dr}{dt} = Dv^{1/3}(c-s)^{2/3}g \exp\left(\frac{-\Delta G'^*}{3kT}\right) \qquad [21]$$

4. Diffusion (the growth rate being controlled by the diffusional transport through the solution).

$$\frac{dr}{dt} = \frac{Dv(c-s)}{r} \qquad [22]$$

5. Convection (where the rate of diffusional growth is enhanced by convection).

$$\frac{dr}{dt} = \frac{F\ Dv(c-s)}{r} \qquad [23]$$

These equations for crystal growth may be used in conjunction with the theory of the rate of nucleation to predict the amount of reaction

α at any time t and also the size distribution of particles at that time. This is a useful tool for distinguishing between heterogeneous and homogeneous nucleation (a primary purpose in many experiments).

The relationship between the degree of reaction α and the time for all combinations of nucleation and growth laws is given by Nielsen (42,59,60). For heterogeneous nucleation the number of particles is assumed to be essentially constant. This leads to one way of distinguishing between heterogeneous and homogeneous nucleation. That is, for heterogeneous nucleation, increasing the supersaturation and thereby increasing the amount of material available for crystallization results in particles of a larger average size, as the number of particles has stayed essentially constant. Some authors (98) have pointed out, however, that the heterogeneous particles may have a range of nucleating abilities. This would result in an increase in the number of crystals formed with increasing supersaturation as less active heterogeneous particles catalyzed the nucleation process. For homogeneous nucleation, however, the particle number increases very rapidly with increasing supersaturation with the result that the average size of the particles becomes smaller with increasing supersaturation. This has been demonstrated by many authors.

(b) Experimental results

Several excellent reviews (87,79) have been written describing all aspects of precipitation from solution. Melia and Moffitt (62) have written that "the literature on the subject of crystal nucleation from aqueous solution is both extensive and confusing. Few reliable numerical data are available and many of the recorded conclusions are contradictory". This is undoubtedly true because most of the experiments reported in the literature have been concerned with heterogeneous nucleation on impurities present in solution no matter how carefully the solutions and containers have been cleaned. Experimental procedures must therefore be designed so that the effect of these impurities may be isolated from the process of true homogeneous nucleation. This has been effected in different ways. Several authors (62-66) have recently used the droplet technique in which the sample is dispersed as a large number of droplets in an immiscible oil. The number of droplets is assumed to be much greater than the number of impurities present so that in a majority of the droplets only homogeneous nucleation may take place. A second technique, used by Nielsen (67) and others, is to increase the supersaturation to a point where homogeneous nucleation competes effectively with any heterogeneous nucleation present. For supersaturations greater than this value homogeneous nucleation predominates. These supersaturations are initiated by a direct mixing technique.

Another technique widely used to produce supersaturation is precipitation from homogeneous solution. In this technique one of the precipitants is produced _in situ_ in the presence of the other precipitant. This has been successfully combined with the droplet technique by Hileman and Valazquez (63).

Most of the work done on the precipitation of crystals from solution has involved sparingly soluble ionic salts, e.g., $BaSO_4$. In general the work has been directed towards estimating the pre-exponential factor A, (Equation [15]), the "critical" supersaturation, the surface tension σ and the size of the critical nucleus. The value of $A = 10^{30}\ cm^{-3}\ sec^{-1}$ was calculated by Turnbull and Vonnegut (68) for the homogeneous nucleation of most crystals from their supercooled melts. This value, or a value close to it, has usually been assumed to apply to the nucleation of ionic salts from aqueous solution. The actual values of A found experimentally vary widely from this value. Melia and Moffitt (69) have reported values of A lying in the range $10^3 - 10^5\ cm^{-3}\ sec^{-1}$. Similar differences between the theoretical and experimental values of A have been found by Dunning for the nucleation of cyclonite from aqueous acetone solution (70) and for the nucleation of sucrose (71) from aqueous solution. Some typical values of A found experimentally are shown in Table 2.

Another problem is that the surface energy σ cannot be measured or calculated independently. Values of σ and critical supersaturations found for several classes of compounds are shown in Table 2. Attempts (42) have been made to relate the value of the interfacial energy to the Moh hardness scale without much success.

The size of the critical nucleus has also been calculated from experimental results (usually assuming $A = 10^{30}$). Some values for the size of critical nuclei for the different classes of compounds (i^* [number] or r^* [radius]) are shown in Table 2. The form of Equation [15] is such that the calculated values of σ and i^* are very insensitive to changes in the values of the pre-exponential factor A and the supersaturation S.

The values of these parameters (Table 2) vary widely, probably because in some cases heterogeneous rather than homogeneous nucleation

TABLE 2

Parameters for crystal nucleation from aqueous solution.

Compound	log A	σ	i*	r* (A°)	S*	Reference
$BaSO_4$		126		4.3	1000	67
		141	8	4.3	1090	78
	22.3	151				80
		135	15			59
$SrSO_4$		103	14	5.1	49	78
		52		7		82
		86		5.1	39	83
	11.8	70				80
		85	33			59
		84				84
$PbSO_4$		100	14	5.1	50	78
		79		5.3	78	83
	20.0	119				80
		100	20			59
			6			85
$PbCO_3$		81	23	5.7	10.8	78
		112		4.5	106	83
		125	24			59
$SrCO_3$		92		5	30	83
SrC_2O_4					2	83
$AgC\ell$		77		5.4	5.5	83
			5			86
CaF_2		114		4.3	21	83
	13.5	140				80
		140		9	80	87
		180				88
MgF_2		129		9	30	87
AgBr		56		15	37	87
Ag_2SO_4		62		14	19	87
$BaCrO_4$		120	15			59

TABLE 2 (cont.)

Compound	log A	σ	i*	r* (A°)	S*	Reference
$BaCO_3$		115	18			59
$BaMoO_4$		103	17			59
$BaWO_4$		94	16			59
$PbCrO_4$		170	9			59
		100				88
			5		136	89
$KC\ell O_3$		56			3.2	90
$NH_4C\ell$	3.27	35			1.5	90,69
		66	107	9.0	2.8	91
NH_4Br	2.96					69
KNO_3	5.31	57			3.4	90,69
NH_4I		15.4			1.21	92
$K_2Cr_2O_7$		72			12	90
		82	43	8.6	18.6	91
NH_4SCN		37	151	12.1	2.07	91
NH_4NO_3		47	141	10.5	2.33	91
$(NH_4)_2Cr_2O_7$		58	58	9.6	6.85	91
$(NH_4)_2C_2O_4 \cdot H_2O$		129	29	6.4	49.0	91
$Mg(OH)_2$		115	30		4	94
$CaPO_4$					2.3	95
$(CH_2(NH_2) \cdot COOH$		40		30	2.1	87
Cholesterol		17		28	1.3	87
Sucrose		6	100		1.6	96
$Pd(C_7H_{11}N_2O_2)_2$	6.7(a)	23	38	16	21	76
$Pd(C_6H_9N_2O_2)_2$	12.0(a)	36	19	12	249	76

TABLE 2 (cont.)

Compound	log A	σ	i*	r* (A°)	S*	Reference
$Ni(C_6H_9N_2O_2)_2$	8.0(a)	34	25	12	88	76
$Ni(C_7H_{11}N_2O_2)_2$	7.3(a)	29	30	14	46	76
$Ni(C_4H_7N_2O_2)_2$		40			500	77
$Ca(OH)_2$		65	55			93

(a) These values of log A were found experimentally. The theoretical value, log A = 30, was used to calculate the values of the other parameters in the table.

was being investigated.

Together with the references shown in Table 2 there exists a vast quantity of literature on other qualitative and quantitative aspects of the nucleation and growth of crystals. These studies include the effects of the age of solution, the effect of the previous history of solutions, the effect of added ions and seed crystals, on the number and morphology of the crystals formed.

1.E. Nucleation of Metal Chelates

In comparison with the work done on the nucleation and growth of ionic salts from solution the literature on the nucleation and growth of metal chelates is sparse, despite the fact that they might well be expected to show less anomalous behaviour because of their non-ionic character. As it is known (68) that the existence of heterogeneous nucleation depends to a large extent on the match of the lattices of the mote and growing crystal, then metal chelates may well be expected to be less susceptible to nucleation by a heterogeneous pathway.

The behaviour of metal chelates of analytical interest (e.g., metal dioximes) in aqueous solution is well known from purely analytical studies and so are the conditions under which the precipitate formed has various shapes and sizes of crystals. A study of the nucleation characteristics of metal chelates should therefore be of use in the elucidation of nucleation problems and also give a further insight into analytical conditions required to give precipitates with optimum characteristics.

The nucleation of nickel nioximate has been studied by Duke and Brown (72) using a direct mixing technique and visually counting the total number of particles formed. Several authors (73-75) have applied the technique of precipitation from mixed solvents to the study of the nucleation of metal chelates. These have been concerned mainly with crystal growth laws and none have investigated the validity of the theory for homogeneous nucleation or measured the parameters involved. A combination of the droplet method and the technique of precipitation from homogeneous solution has been used by Hileman and Velazquez (63,76) and Thompson and Gordon (64). The former authors have found that the pre-exponential factor varied from $10^{7.3}$ to 10^{12} cm^{-3} sec^{-1} for various nickel and palladium dioximates. The corresponding variation in σ and i^*, using a value of 10^{30} for the pre-exponential factor, was from 23 ergs cm^{-2} to 36 ergs cm^{-2} and from 19 to 38 molecules respectively. They also found that their data fitted the relationship between the logarithm of the rate of nucleation and the reciprocal of the square of logarithm of the supersaturation predicted by the classical theory of homogeneous nucleation.

Thompson and Walton have used a direct mixing technique and a visual counting method to study the nucleation of nickel and palladium dimethylglyoximates. They concluded that the nucleation step occurring was heterogeneous. From the upper limit of the supersaturations obtained they calculated that the value of the surface free energy was approximately 40 ergs cm^{-2}.

A precipitation system is only completely described by the variation of both the numbers of particles produced and their distribution with time. These parameters characterize the nucleation and crystal growth periods in the precipitation. Further, metal chelates seem to offer several advantages over ionic compounds in a study of the nucleation process. Metal chelates may possibly be less susceptible to heterogeneous nucleation than ionic compounds and the fundamental description of the nucleation step may be less complex.

The purpose of this thesis was therefore to develop methods to measure the variation with time of the size distributions of the particles precipitated for several metal chelates, in order to elucidate the type of nucleation and crystal growth laws occurring and to measure the parameters important in the classical theory of homogeneous nucleation.

2. EXPERIMENTAL

2.A. Apparatus and Reagents

2.A.1. Apparatus

Particle Counter

Particle sizes and numbers were measured using a Coulter Counter Industrial Model B and accessories supplied by Coulter Electronics Industrial Division. The counter was modified so that the voltage pulses after amplification and pre-amplification but before shaping could be fed to a multichannel analyser.

Multichannel Analyser

The pulses obtained from the counter were analysed by, and stored in the memory of, a multichannel analyser type ND 160 supplied by Nuclear Data Inc. Spectra of pulse sizes thus obtained were dumped onto magnetic tape using a magnetic tape unit MT36 supplied by the Potter Instrument Co. Inc. The tape was then read using an IBM 7040 computer.

Filtering Apparatus

Solutions were filtered through a PVC membrane filter, type MF10, of pore size 0.1 micron and diameter 47 mm. The filter was held in a stainless steel filter holder type 2220 supplied by the Gelman Instrument Company. The solutions were filtered, under pressure, from a 5-gallon stainless steel pressure cylinder supplied by the Cornelius Company Ltd. For small quantities of solution a 100 ml pressure filter holder supplied by Millipore Ltd. was used.

Spectrophotometric Measurements

Spectrophotometric measurements were made using a Spectronic 600 spectrophotometer supplied by Bausch and Lomb, Inc. and cells supplied by the Scientific Cell Company Ltd.

Standard Mono-sized Particles

Polystyrene spheres and ragweed pollen, both of known size and standard deviation were obtained from the Dow Chemical Company and Coulter Electronics Industrial Division.

Glassware

Pyrex glassware was used and calibrated pipettes and volumetric flasks used where applicable.

Microscope

For visual examination of both mono-sized particles and crystals obtained in precipitation experiments a Lumax microscope, model 24404, supplied by the Fisher Scientific Company Ltd., was used.

Constant Temperature Bath

A constant temperature bath, type 2073A, supplied by Forma Scientific Inc. was used to keep reactant solutions at constant temperature.

2.A.2. Reagents

Electrolyte solutions for use with the Coulter counter were made up from ammonium chloride of Analar quality supplied by the Fisher

Scientific Company, Ltd.

Nickel(II) solutions were made up using Analar quality nickel chloride supplied by B.D.H. Ltd.

Barium(II) solutions were made up using Analar quality barium chloride supplied by the Aldrich Chemical Company Inc.

Dimethylglyoxime was supplied by the Eastern Chemical Company.

1,2-Cycloheptanedioxime was supplied by K & K Laboratories Inc.

1,2-Cyclohexanedioxime was supplied by the Aldrich Chemical Company Inc.

2.B. Introduction

As indicated in Section 1.E. one of the purposes of this thesis was to determine experimentally the variation of the size distributions with time of growing crystals in a metal chelate precipitation system. Various methods have been used to measure the size distributions of precipitated crystals and also to count the total numbers of crystals formed in a precipitation experiment. These have included microscopic methods, sedimentation methods and methods involving particle counters. All of these methods are somewhat time-consuming. For example, they usually involve many separate precipitation experiments.

Particle counters, however, do appear to be most suitable for incorporation into a system which would give a rapid and reliable size distribution of crystals formed during the precipitation of a solid phase from aqueous solution. The basic principle of such a counter is as follows. Sample particles suspended in an electrolyte pass through an orifice in a wall separating two platinum electrodes. A D.C. voltage is applied between the two electrodes to give a specific and controlled constant current. The electrolyte chamber is in contact with a mercury manometer. Application of a vacuum to the electrolyte chamber causes the mercury to fall. When the vacuum is shut off the mercury rises drawing the suspension in the outer chamber through the orifice. The mercury, while moving up the manometer, passes two additional electrodes which are separated by a known volume. If signals from these electrodes are used to start and stop the measuring operation, particle counts can be made on a known volume of suspension.

The fluid in the orifice defines a volume of resistivity to the flow of current between the electrodes. When a particle passes through the orifice, the resistance temporarily increases. The resulting decrease in current causes the constant current source to generate a voltage pulse in a series resister. The magnitude of this pulse is linearly proportional to the volume of the particle for particles with diameters up to 40% of the diameter of the orifice. Normally, the number of pulses is recorded on a digital readout on the counter and size distributions are obtained by varying the voltage range to which the digital readout responds. This technique requires that many readings be taken at various combinations of different gate widths and lower threshholds. Also the size range of particles is such that this has usually to be repeated for many different amplifications of the original pulses. A typical particle counter operation is shown in schematic form in Figure 3.

In order to be able to obtain size distributions for a growing precipitate, ideally one would wish to make one instantaneous measurement and obtain a size distribution at that particular time and also to be able to repeat the measurement an instant later and obtain a new size distribution. In pursuit of this ideal it was decided to feed the amplified voltage pulses from the particle counter to a multichannel analyser. In order to free the analyser for immediate reception of another size distribution the spectrum from the analyser was dumped onto magnetic tape. The time taken for this was less than 0.5 seconds. The spectra were then to be retrieved later in either

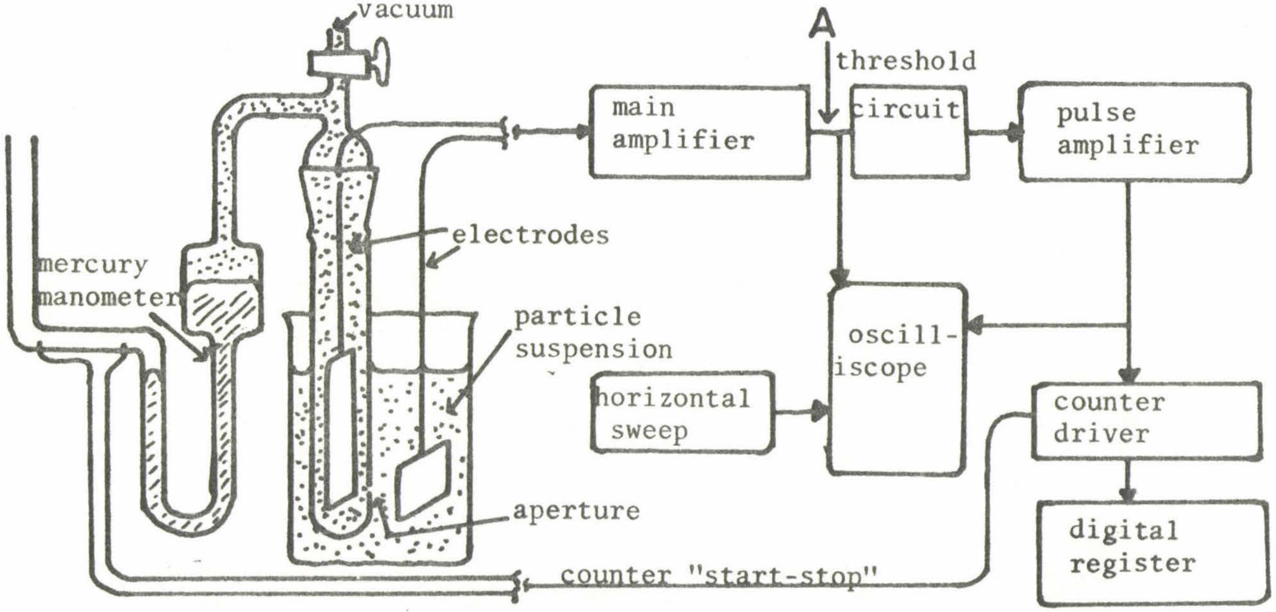

FIGURE 3. Schematic diagram of the Coulter counter.

graphical or tabular form by printout from a computer.

Acceptable pulses for the analyser, a Nuclear Data Model ND 161F, should have the following characteristics. The rise time should be not less than 1 microsecond and not greater than 5 microseconds, with a subsequent period of from a few tenths of a microsecond to a few microseconds in which the pulse should be essentially flat. The pulse should also be positive, either single ended or bipolar, and lie between 0-100 volts with the positive portion of the pulse carrying the energy information. These waveforms are recommended for maximum resolution and linearity but are not necessarily the only tolerable waveforms.

2.C. Procedures

The following procedures were devised from a study of the calibration and use of the particle counter and analyser as a system for the measurement of size distributions of both mono-sized particles and of particles produced in the precipitation of some insoluble compounds from aqueous solution. The procedures used to produce the supersaturation of the insoluble compounds are also described.

2.C.1. Preparation of electrolyte solutions

The electrolyte stock solution needed to provide a conducting solution for the particle counter was made up from ammonium chloride (1% w.v.) and filtered at least twice through a 0.1 μ PVC membrane filter and stored in glass vessels. The vessels were steam-cleaned by the method of Nielsen (102) and washed with filtered electrolyte before use. This electrolyte was used to make up all the other reagent solutions and was always checked before use to ensure that the background noise in the particle counter had a constant low value.

2.C.2. Preparation of calibration solutions

Calibration solutions of 1.099 μ, 3.49 μ, 11.7 μ and 18.8 μ diameter particles were made up by dispersing quantities of each size in electrolyte solutions by gentle stirring until all particles were individually dispersed and no agglomerates remained. For the smallest particles (1.099 μ diameter) this was difficult to achieve. Best results were obtained when a few drops of a 1% (v.v.) solution of Triton X·100 in electrolyte were added. The individual dispersion of particles was checked visually with a microscope. These solutions were then suitably diluted with electrolyte until each contained approximately 10^5 particles/ml. This dilution was required so as to minimize coincidence counting by the particle counter.

2.C.3. Calibration procedures

The Coulter counter probe was inserted into 100 mls of the calibration solution and the number of particles in 0.5 mls counted over the ten amplification settings of the instrument. Between each count the solution was manually stirred using a 10 ml hypodermic syringe. Other types of stirrers, magnetic and electrical, seriously increased the level of the background noise. The size distribution for each amplification setting was dumped onto magnetic tape. Later a complete size distribution was printed out by the computer. This procedure was carried out for each of the 1.099 μ, 3.49 μ, 11.7 μ and 18.8 μ diameter calibration particles and in addition for several particle counter aperture sizes.

2.C.4. Precipitation procedures

Two direct mixing procedures for producing supersaturated solutions were investigated. These were a continuous flow system and a stopped flow dilution system.

The apparatus used in the continuous flow system is shown in Figure 4. Equal amounts of reactants were mixed in a Roughton cell (A) by positive pressure on the storage vessels (B). The mixed solution in which precipitation and growth of crystals were occurring was sampled at various points along the precipitation tube (C). The Coulter counter probe (D) was welded to a small hole in the precipitation

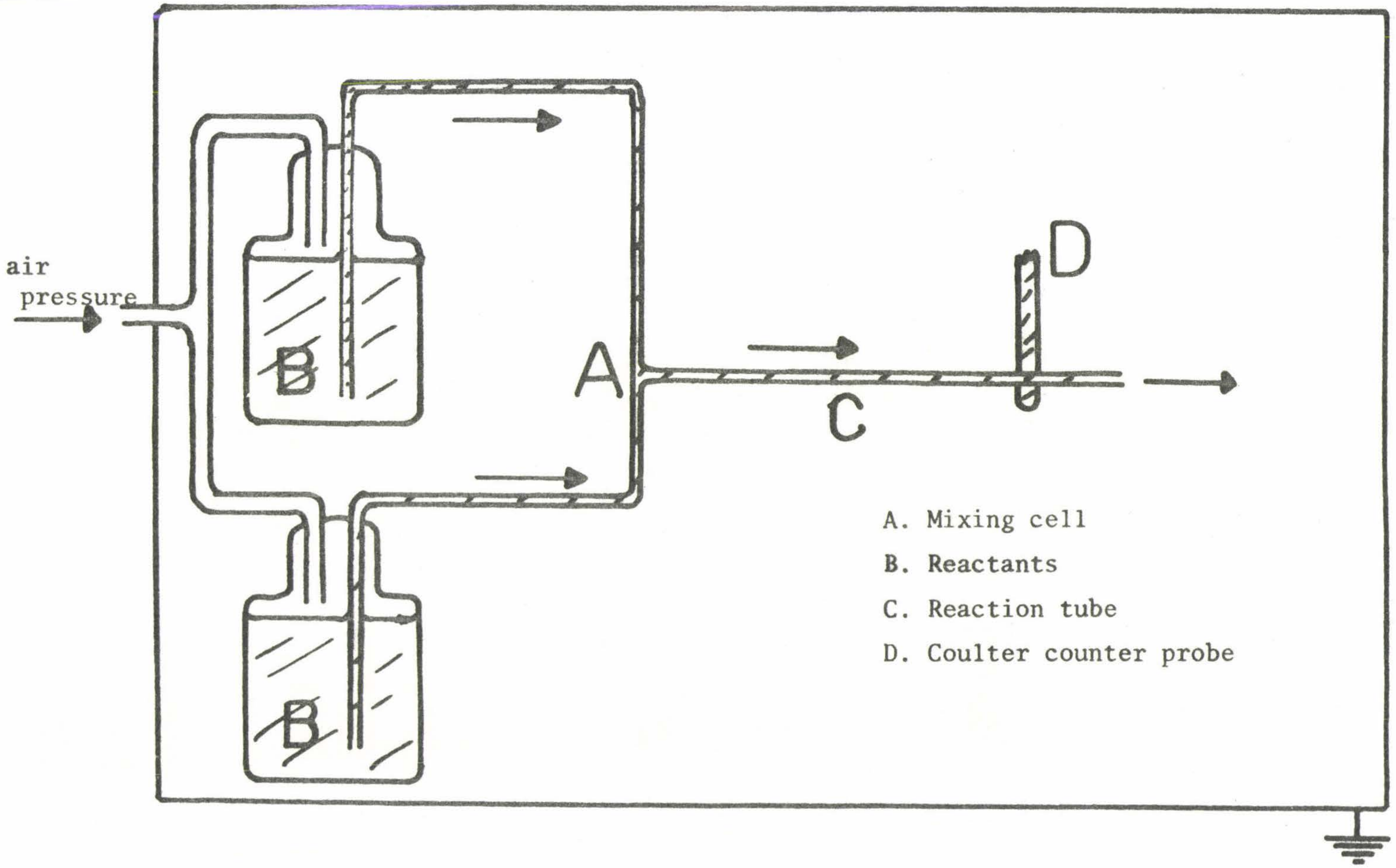

FIGURE 4. Schematic diagram of the continuous flow apparatus.

tube. The entire apparatus was enclosed in an earthed Faraday cage. This system was studied extensively with both mono-sized particles of known diameter and with barium sulphate, nickel dimethylglyoximate, nickel nioximate and nickel heptoximate as precipitating crystals to see if this method of mixing and size distribution determination would give reproducible results. The results obtained are described in Section 3.B. of this thesis.

The apparatus used in the stopped flow dilution method is shown in Figure 5. In this system the reactants were mixed with a Roughton cell directly into a clean container and the mixed solution was diluted suddenly with electrolyte after a given time. A and B are two 10 ml syringes which are forced down together so that mixing of reactants C and D occurs at E and the mixture then passes into syringe F. Each of the syringes A and B were cleaned thoroughly with the reactant which each was to contain. The Roughton cell E, the syringe F and connecting tubes were steam cleaned and dried. The solutions were kept in a constant temperature bath at 25°C and the experiment was carried out with the apparatus also at this temperature. After a noted time the solution in syringe F was transferred to a beaker containing enough electrolyte so that the resulting mixture gave approximately 10^5 counts/ml.

2.C.5. Measurement of size distributions of particles of barium sulphate

Crystals obtained in the precipitation of barium sulphate were dispersed in 100 mls of filtered electrolyte solution which had been saturated with barium sulphate. The size distributions were obtained as described in section 3.A.

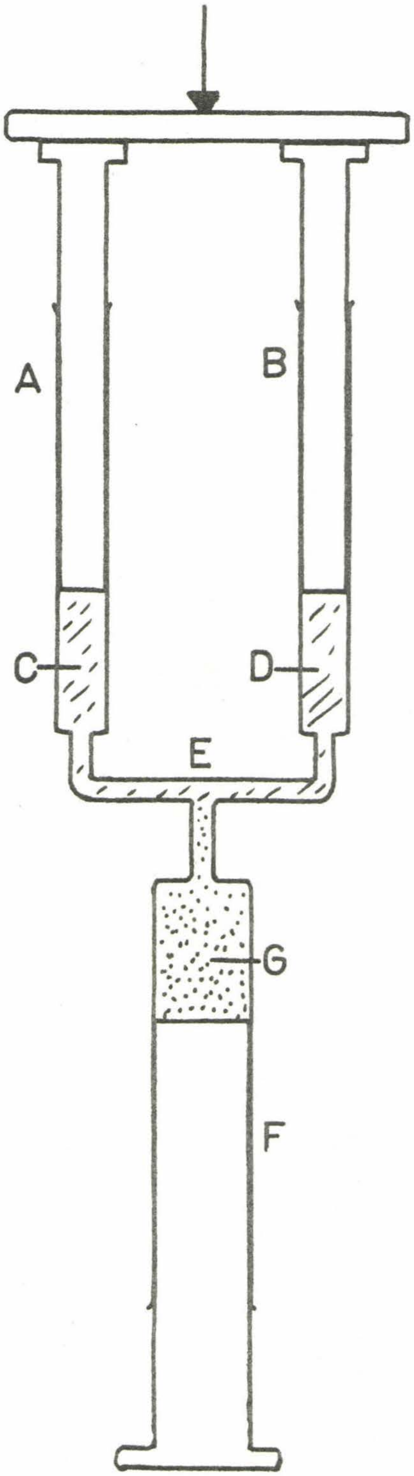

FIGURE 5. Schematic diagram of the stopped flow dilution apparatus.

2.C.6. Measurement of size distribution of crystals of nickel oximates

Crystals obtained in the precipitation of nickel oximates were dispersed in 100 mls of filtered electrolyte solution. The size distributions were obtained as described in Section 3.A.

2.C.7. Nucleation and crystal growth experiments

The procedures for mixing and counting described in Sections 2.C.3. and 2.C.4. were used to measure the size distributions of particles obtained in the precipitation of barium sulphate, nickel nioxime, nickel dimethylglyoxime and nickel heptoxime.

Solutions of barium^{2+} (0.1 M) and nickel (0.1 M) were prepared by dissolving their respective chlorides in the standard electrolyte solution. Stock solutions of dimethylglyoxime (3×10^{-3} M), nioxime (1.0×10^{-2} M) and heptoxime (1.0×10^{-2} M) solutions were each made up in 1% electrolyte solution. All other concentrations were prepared from these stock solutions by dilution with the standard electrolyte solution. Before use, each solution was filtered at least twice through 0.1μ PVC membrane filters. The background count was checked to ensure that it was nearly the same constant low value as for the pure electrolyte alone. Barium sulphate precipitations were carried out at pH 7.0, nickel dimethylglyoxime precipitations at pH 7.0, nickel heptoxime precipitations at pH 3.28 and nickel nioxime precipitations at pH 2.8.

2.C.8. Measurement of the nickel dioximate solubilities.

The solubilities of the nickel dioximates were determined spectrophotometrically as follows. The same procedure was followed for each dioximate. A weighed amount of the dioximate was dissolved in electrolyte solution (1% NH_4Cl) at pH 0-1. This solution was diluted with electrolyte to give calibration solutions of appropriate dioximate concentrations for construction of a Beer's law plot. A 200 ml portion of each of these solutions was then extracted at pH 7 with three 5 ml aliquots of chloroform. For each solution the three extracts were combined and reduced to 5 mls. The absorbance of each of these chloroform solutions was measured at 375 mμ and a linear Beer's law plot drawn.

An excess of the dioximate was then added to 200 mls of the electrolyte at the pH used in the nucleation studies (Section 2.C.7.). This suspension was shaken for three days, filtered through a 0.1μ PVC filter, shaken for another three days and filtered again. The filtrate was extracted with three 5 ml aliquots of chloroform at pH 7. The combined extracts were reduced to 5 mls. The absorbance at 375 mμ was measured. The solubility for each dioximate was then read from the appropriate calibration curve.

3. RESULTS AND DISCUSSION

3.A. Calibration of the Apparatus for Measuring Size Distributions

The "Coulter counter" circuitry was interrupted at point A, Figure 3, so that the amplified pulses could be fed to the multichannel analyser. The pulse sizes and shapes obtained at this point in the circuitry using standard sized particles of known size and standard deviation, were examined with an oscilloscope to determine how closely the pulse shapes agreed with the limits set for the analyser. Figure 6a shows typical pulse shapes and sizes for standard particles of 3.49 μ diameter. The pulses have an average total length of about 10 microseconds with a rise time of 4 or 5 microseconds. The pulse is never actually flat on top but does remain close to its maximum value for approximately 1-3 microseconds. The characteristics of most of the pulses fall approximately within or close to those recommended for best resolution and linearity. Having shown that the pulse shapes produced by spherical mono-sized particles were approximately the correct shape it was then necessary to ascertain if the pulse shapes obtained with particles from a real precipitation system, e.g., nickel dimethylglyoximate, were similar to those obtained for spherical mono-sized particles. An example of the shapes obtained are shown in Figure 6b. The pulses, which varied in height, were of the same general shape and time duration as those of the mono-sized particles. These results indicated that the spherical mono-sized particles could be used as calibration standards to relate the analyser channel number to size and, further, that these calibration curves could be used to measure the size distribution of particles obtained in the precipitation of metal chelates.

Before setting up calibration curves, the values of the resistance of the electrolyte in the aperture and of the current between the electrodes were first optimised. These variables affected the size of the pulses, the signal to noise ratio and determined the smallest pulse which could be distinguished from the background. It was found in these investigations that for apertures of all sizes (except the 30 μ diameter aperture) an electrolyte concentration of 1% (w.v.) ammonium chloride and a current of 8 milliamps were suitable. For the 30 μ diameter aperture currents greater than 4 milliamps caused the amplifier to be overloaded and spurious pulses were obtained.

Having shown that the voltage pulses from the particle counter could be fed to the analyser and size distribution spectrum obtained, then, in order to completely calibrate the system, it was necessary to do the following three experiments:

(i) Show that reproducible calibration curves which related analyser channel number to size could be prepared.

(ii) Determine the standard deviation of mono-sized particles of known dispersion.

(iii) Measure the size distribution obtained for a mixture of various mono-sized particles.

Spherical mono-sized particles of diameter 1.099 μ, 3.49 μ, 11.7 μ, and 18.8 μ particles were used to calibrate the particle counter-multichannel analyser combination. This was done by using the visual readout onto an oscilloscope and recording the channel number of the analyser at which the maximum number of pulses occurred. The known diameter of the particles was then plotted against channel number. Because the voltage pulses are proportional to the volume of the particles their magnitude varies widely as the particle diameter increases from 1.099 microns to 18.8 microns. It was, therefore, necessary to use different signal amplifications so that the peak would fall within the 1024 channels available and not in the electrical noise at low channel numbers or off scale at high channel numbers. Consequently for each aperture, there was a series of calibration curves. Each one corresponded to a different signal amplification. Such a set of calibration curves for the 30 μ diameter aperture is shown in Figure 7. Similar curves were constructed for 100 μ and 200 μ apertures. Since the 30 μ diameter was found to have the highest sensitivity it was used almost exclusively in subsequent work. Because of the size range of calibration particles and the rapid change of signal height with particle diameter only a few points fell on each calibration curve. As a result it was difficult to set up a completely empirical calibration curve. If the channel number which corresponded to zero volts was carefully chosen, the calibration curves could be set up so that they were accurately described over a range of 4 to 5 microns by Equation [24]

$$P = \frac{V}{I.A.K} \qquad [24]$$

where P is the channel number corresponding to the diameter d of a particle,

V is the volume of the particle of diameter d, I is the current between the electrodes, and

K is a constant calculated from the empirical data for the mono-sized particles.

Using Equation [24] and the empirical calibration points found using mono-sized particles accurate calibration curves, such as those shown in Figure 7 were constructed.

It is a relatively simple matter to obtain these channel number-diameter calibration curves. If the method is to be useful, however, the resolution of one particle size from another must be assessed. The standard deviations of several sizes of particles were calculated from the experimental data for several amplifications and compared with the standard deviations quoted by the supplier (where available). These results are shown in Table 3. For the 1.099 μ diameter particles, where a quoted resolution was available, the poorer resolution is probably due to the fact that all pulses from one particle size are not in fact identical because of interference effects at the aperture. These effects were minimized by using a sufficiently dilute suspension. In subsequent studies, which were carried out using the 30 μ diameter aperture, most of the particle sizes fell within the diameter range 1 to 4 microns where the standard deviation was found to be from 0.03 to 0.09 μ. Table 4 shows the size ranges covered for each amplification setting for the 30 μ diameter aperture, at an aperture current of 4 milliamps. The size range covered for each amplification setting is small especially for small sizes (high amplifications).

Preliminary investigations with nickel dimethylglyoximate showed that crystal diameters were likely to fall in the range 0 to 5 microns

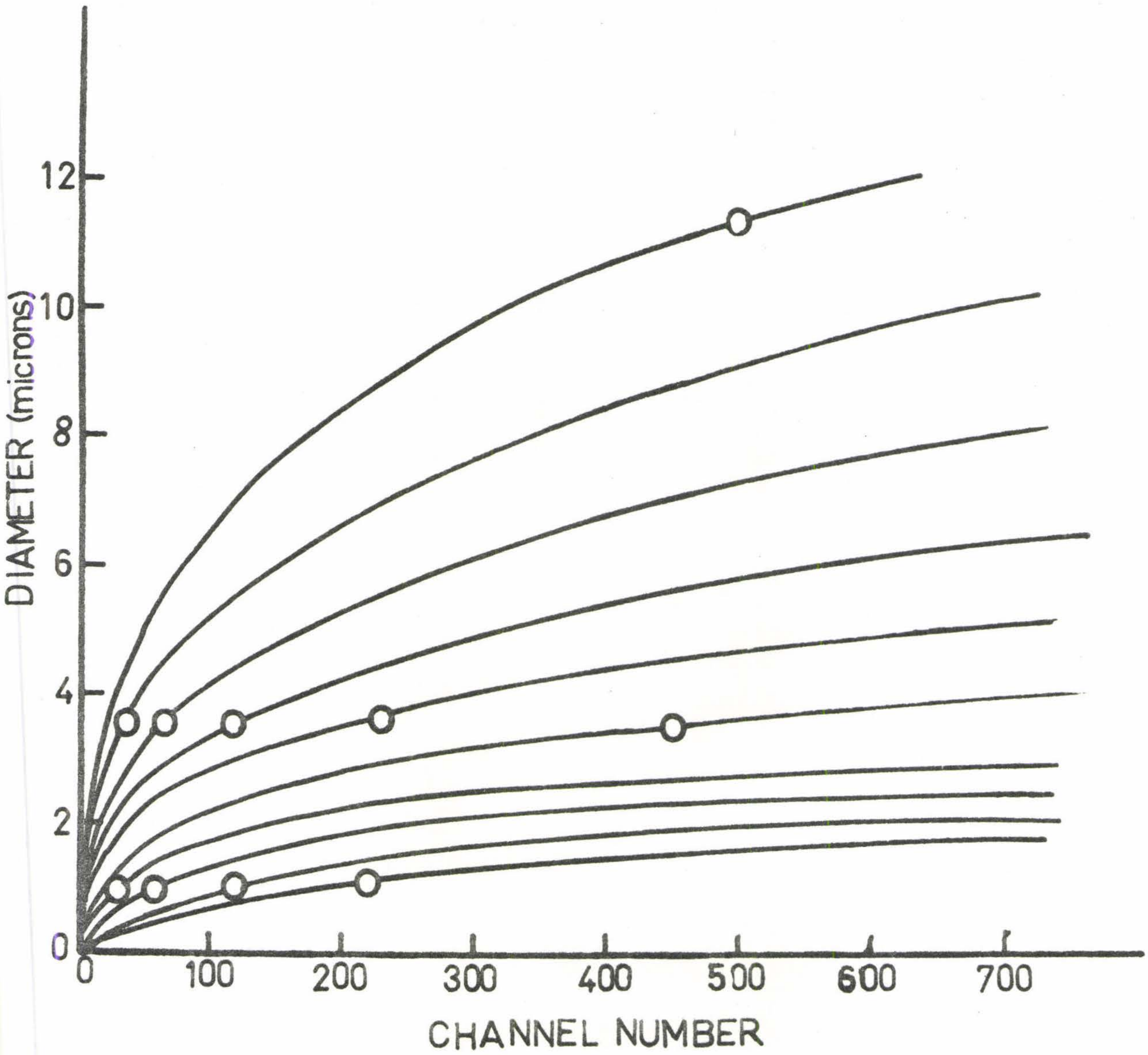

FIGURE 7. Calibration curves relating channel number to diameter for mono-sized spherical particles.

TABLE 3

Standard deviations found for standard-sized particles.

Aperture Diameter (μ)	Particle Size (μ)	Amplification Setting	σ Found μ	σ Quoted μ
30	1.099	1/4	0.060	0.0059
		1/2	0.047	
		1	0.036	
	3.49	2	0.068	Not available
		4	0.065	
		8	0.097	
	11.7	64	0.47	Not available
70	1.099	1/8	0.39	0.0059
	11.7	8	0.89	Not available
		16	0.79	
		32	0.72	
		64	0.66	
	18.8	32	0.67	Not available
		64	0.64	

TABLE 4

Size ranges for each amplification setting.

Amplification setting	Size range
1/8	0 - 1.8 μ
1/4	0.5 - 2.0 μ
1/2	1 - 2.6 μ
1	1.5 - 3.5 μ
2	2 - 4.2 μ
4	3 - 5 μ
8	4 - 6.5 μ
16	5.2 - 8 μ
32	7 - 10 μ
64	8.5 - 12 μ

sig figs?

and would have distributions wider than the range covered by any one of the amplification settings. Consequently, for one aperture size, it was necessary to measure over the ten amplification ranges of the particle counter to produce a complete size distribution. The size distribution spectra from the ten different amplification ranges were dumped onto magnetic tape. The tape was read by computer and the number of counts in each channel printed out for each amplification.

A computer programme was written which manipulated the data in the following manner. From the calibration curves channel numbers were identified with particle diameters and the number of pulses calculated for 0.1 μ increments over the whole size range of the amplification setting. This was done for each amplification and gave ten overlapping spectra of the number of particles per 0.1 μ versus diameter. The overlapping parts were averaged and then a composite spectra from 0 to 12 μ was printed out in increments of 0.1 μ in either graphical or tabular form. The computer programme to accomplish this is shown in Appendix I.

Figure 8 shows a composite size distribution spectrum obtained for a mixture of two sets of mono-sized particles, of diameter 1.099 μ and 3.49 μ. A schematic diagram of the entire apparatus is shown in Figure 9.

It was found early in the investigation that it was essential to have all solutions as clean as possible because blocking of the aperture whilst a measurement was being taken was a major problem. All electrolyte solutions and reactant solutions were therefore filtered, under pressure, through 0.1 μ membrane filters. A second reason for thorough

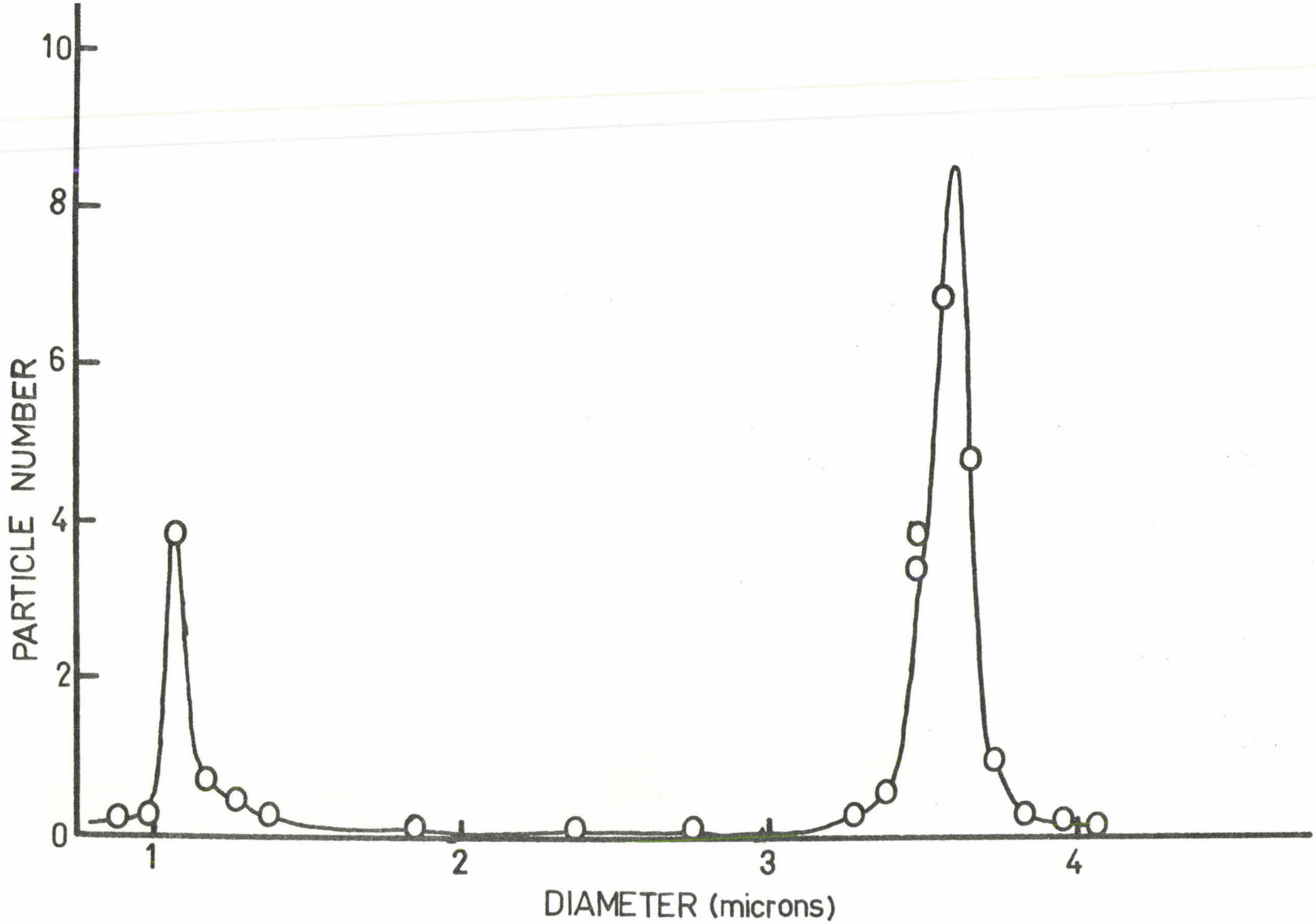

FIGURE 8. Size distribution for two sizes of spheres.

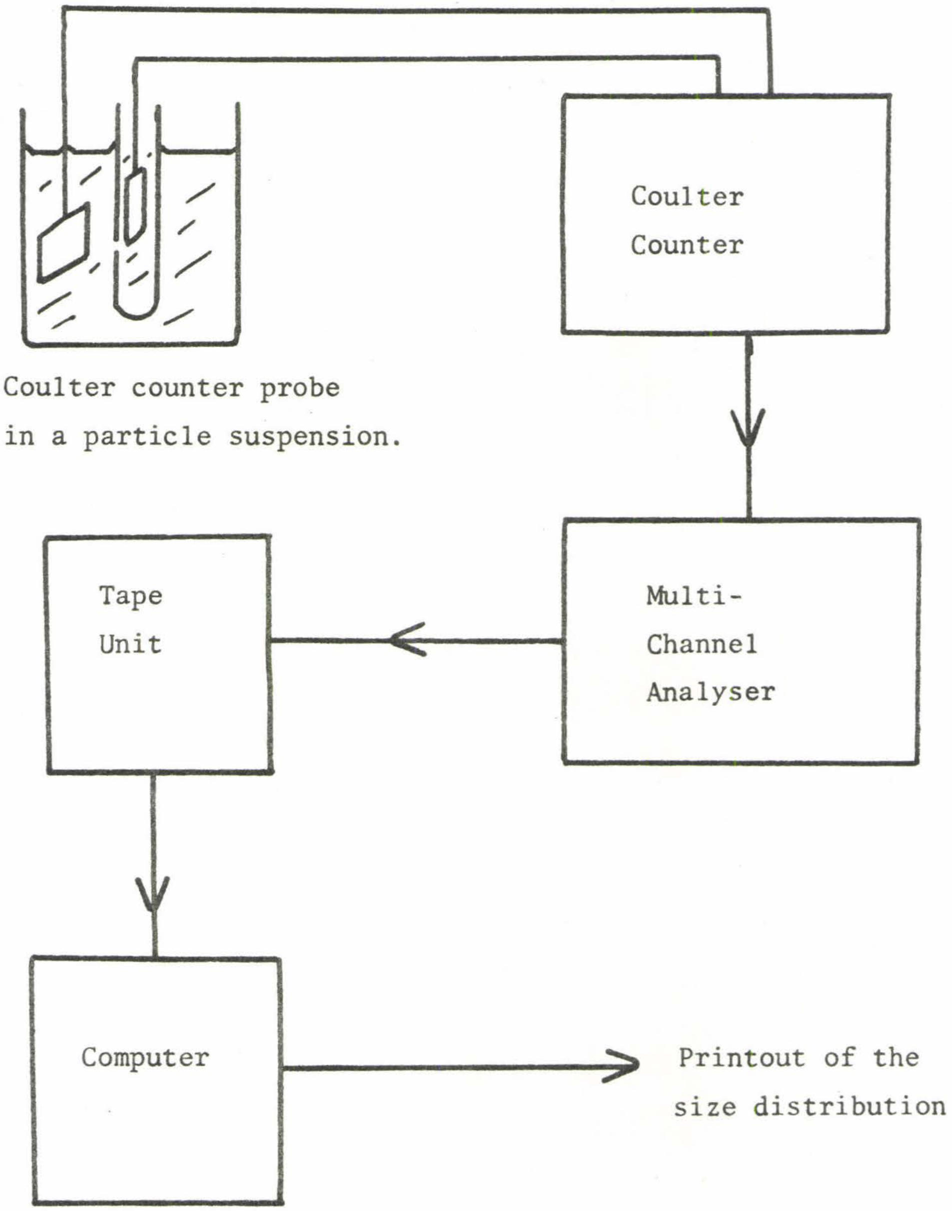

FIGURE 9. Schematic diagram of the apparatus for measuring size distributions.

cleaning of solutions was to keep the signal to noise ratio as high as possible. After two filtrations the electrolyte solutions registered a count of 10^3 particles/ml with diameter greater than 0.7 μ. Below this size electrical noise swamped all other signals. Further filtrations failed to reduce the background count which was therefore probably due to electrical noise rather than foreign particles present in the solution. These low background counts and high signal to noise ratios also enabled the size distributions of dilute crystal suspensions to be measured. It was necessary to use suspensions as dilute as possible in order to minimize coincidence counting. A further advantage of filtering the solutions was that the possibility of heterogeneous nucleation of the metal dioximates was reduced. Every effort was made to reduce the electrical noise by putting electrical filters in the high voltage supply line and adequately grounding the counter.

For the mono-sized calibration particles the length of time taken to measure the size distribution and the length of time taken between measurements were not important. When growing crystals were involved these times were important and were kept as low as possible. To minimize the time taken for measurement the volume of solution was kept as small as was consistent with adequate statistical counting. For the 30 μ diameter aperture the minimum volume was 0.05 mls. Approximately 30 seconds were required for this volume to pass through the aperture. To minimize the time taken between measurements a magnetic tape unit was used in conjunction with the multichannel analyser. This enabled the dumping of the spectra onto the magnetic tape to be performed in less than 0.5 seconds. It could then be stored on tape until its subsequent retrieval at will using computer methods.

3.B. Mixing Methods

3.B.1. Continuous flow method

Numerous problems were encountered with this method. The main problem was that the electrolyte, required in the counting cell, acted as an antenna and picked up enough electrical noise to completely swamp the small voltage pulses generated by the passage of the particles through the aperture. This background was reduced to a tolerably low level by enclosing the mixing cell, stock solutions and counting cell in a Faraday cage. The electrical noise could also be minimized by using the shortest tube which was compatible with a measurable flow of reactants, so that the size distribution measurement took place close to the mixing site. Under these conditions, when particles of known size were dispersed in the electrolyte size distributions corresponding to those taken in a static solution were obtained.

A total count of less than 2×10^5 counts/ml of suspension was required so that coincidence counting by the counter and the analyser could be neglected. Preliminary experiments with barium sulphate and several nickel dioximes showed that for most concentrations of reactants the number of crystals produced was much in excess of 2×10^5/ml. As a result, therefore, the coincidence counting was very high and the size distributions obtained were meaningless. Only in the case of low initial concentrations of reactants were the number of particles produced low enough to reduce the coincidence counting to a negligible level. At these concentrations, however, a very long reaction tube was required even at low flow rates. To overcome the problem of excessive coincidence counting it was attempted to set up a second mixing cell, at various distances along the precipitation tube, in which the suspension was diluted with electrolyte. The dilution required was, however, 100-200 to 1 (v.v.) and was very irreproducible. The method also used vast quantities of electrolyte.

The third problem encountered with the continuous flow system was that growth of the precipitate occurred on the walls of the precipitation tube, on the counter probe and in the probe aperture. Large crystals broke off from the growth on the walls and blocked the aperture.

The continuous flow method because of the above difficulties was used only in a very few instances, for example early in a fast precipitation where the supersaturation was high and few particles had appeared.

3.B.2. Stopped flow dilution method

The difficulties with the continuous flow method indicated that in order to make a meaningful measurement of size distribution three conditions would have to be satisfied.

(i) The precipitation suspension would have to be diluted so as to minimize coincidence counting.

(ii) The counter probe should not be in a suspension of growing particles.

(iii) The volume of solution should be kept as small as possible so as to minimize electrical noise.

A stopped flow dilution method (described in Section 2.C.4.) which satisfied these conditions was therefore used in most of the experiments subsequently carried out. In this method samples were taken at various times after mixing and crystal growth stopped by dilution of the sample with electrolyte.

For this method to be successful the following additional conditions had to be met.

(i) The method of mixing and transference to a counting chamber should in itself give rise to no increase in background count.

(ii) The dilution, which was sufficient to give a reasonable number of particles above the background, should also be sufficient to stop the growth of crystals, or at least to slow the growth down enough so that no detectable size distribution change would occur within the time of measurement of the size distribution.

(iii) The time of mixing should be as short as possible so that all particles would stop their growth at the same time.

In experiments to test (i) above, first one reactant and then the other were run through the mixing procedure and diluted. No detectable change in the background reading was noted.

To test the truth of (ii) above, that the dilution necessary to give a reasonable counting rate also stopped the crystal growth, the following experiments were carried out. After dilution, the size distribution of a precipitate suspension was immediately measured. The measurement was repeated many times in succession over a period of hours. The suspension was manually stirred using a syringe before each count. The results showed that no detectable difference occurred in the size distribution over a long period of time. As the size distribution was measured immediately upon dilution and no change occurred thereafter it was reasonable to suppose that the size distribution measured was that of the original solution.

The time taken to mix the reactants [(iii) above] is made up of the time taken to physically mix the solutions and the time taken for each component to distribute itself homogeneously throughout the solution. It has been shown (105) that for this method of mixing using a Roughton tube the latter time is less than 10^{-3} sec. The former time was observed to be less than 0.5 sec.

The method used to dilute the sample, was to inject it from syringe F (Figure 5) into 200 mls of diluting electrolyte. This operation required less than 0.5 sec. [(iii) above] so that all the crystals stopped growing at the same time.

3.C. The Nucleation of Barium Sulphate

The nucleation and crystal growth properties of barium sulphate have been widely studied by a large number of investigators (67,103, 78,80,59). As a result a large amount of experimental data exists in the literature regarding its precipitation by both direct mixing techniques and techniques in which the sulphate ion is produced _in situ_. Barium sulphate was therefore chosen as a precipitation system on which both the mixing methods and the entire apparatus for measurement of size distributions, described earlier, could be tested. Comparisons between the results obtained by the methods described in this thesis and those reported by other investigators could then be made. If agreement was found between the results obtained and those reported in the literature then the methods used for producing precipitation and measuring size distributions could be applied with some degree of confidence to the investigation of the nucleation and crystal growth of some nickel dioximates.

It was attempted to measure the size distributions of the precipitates obtained when barium^{2+} and sulphate^{2-} were directly mixed using the mixing procedures described in Section 2.C.4.

In the method of continuous flow it was found that it was impossible, for most of the precipitations studied, to measure the size distribution of the precipitated barium sulphate because of the very high number of particles produced. Also for those cases where the particle number may have been sufficiently low it was found that the crystals nucleated and grew on the walls of the precipitation tube "upstream" from the counting probe and in the probe itself.

Any size distribution analysis was therefore impossible. The stopped flow dilution method was therefore used to measure the final size distributions of barium sulphate crystals obtained for various initial concentrations of barium^{2+} and sulphate^{2-} ions. The precipitations were carried out at pH 7. Solutions of barium^{2+} and sulphate^{2-} ions were made up from $BaC\ell_2$ and $(NH_4)_2SO_4$ in 1% $NH_4C\ell$ solution. This solution was buffered to pH 7 and filtered so that the background count was as low as possible.

The main qualitative features of the size distributions obtained are as follows.

(1) The total number of particles formed varies from $10^6 \rightarrow 10^7$ particles/ml of solution in the concentration range studied.

(2) The particles of barium sulphate showed wide variation in their size distributions but in general varied from 1 μ to 7 μ in diameter.

(3) The average size of the particles formed got larger as the supersaturation increased.

(4) At a definite supersaturation the number of particles rose drastically, the induction period shortened drastically and the size of the particles went below the lowest size which the instrument could measure. The presence of these particles was indicated by the large number of coincidence counts recorded by the instrument.

Table 5 shows the variation of the total number of particles formed with the initial barium sulphate supersaturation. In Figure 10 the total number of particles formed is plotted against the initial supersaturation.

TABLE 5

Variation of the total number of barium sulphate crystals formed with initial supersaturation.

Total Number N	log N	c_o (moles litre^{-1})	S	log S
0.9×10^6	5.96	5.00×10^{-4}	2.37×10^1	1.36
1.29×10^6	6.11	7.50×10^{-4}	3.55×10^1	1.55
1.61×10^6	6.20	1.25×10^{-4}	5.91×10^1	1.77
5.67×10^6	6.75	2.50×10^{-4}	1.18×10^2	2.07
7.03×10^6	6.8	5.00×10^{-3}	2.37×10^2	2.43
8.32×10^6	6.92	7.50×10^{-3}	3.55×10^2	2.55
10.0×10^6	7.00	1.00×10^{-2}	4.74×10^2	2.67
12.1×10^6	7.08	1.50×10^{-2}	7.11×10^2	2.85
$>> 10^8$		2.00×10^{-2}	9.49×10^2	2.97

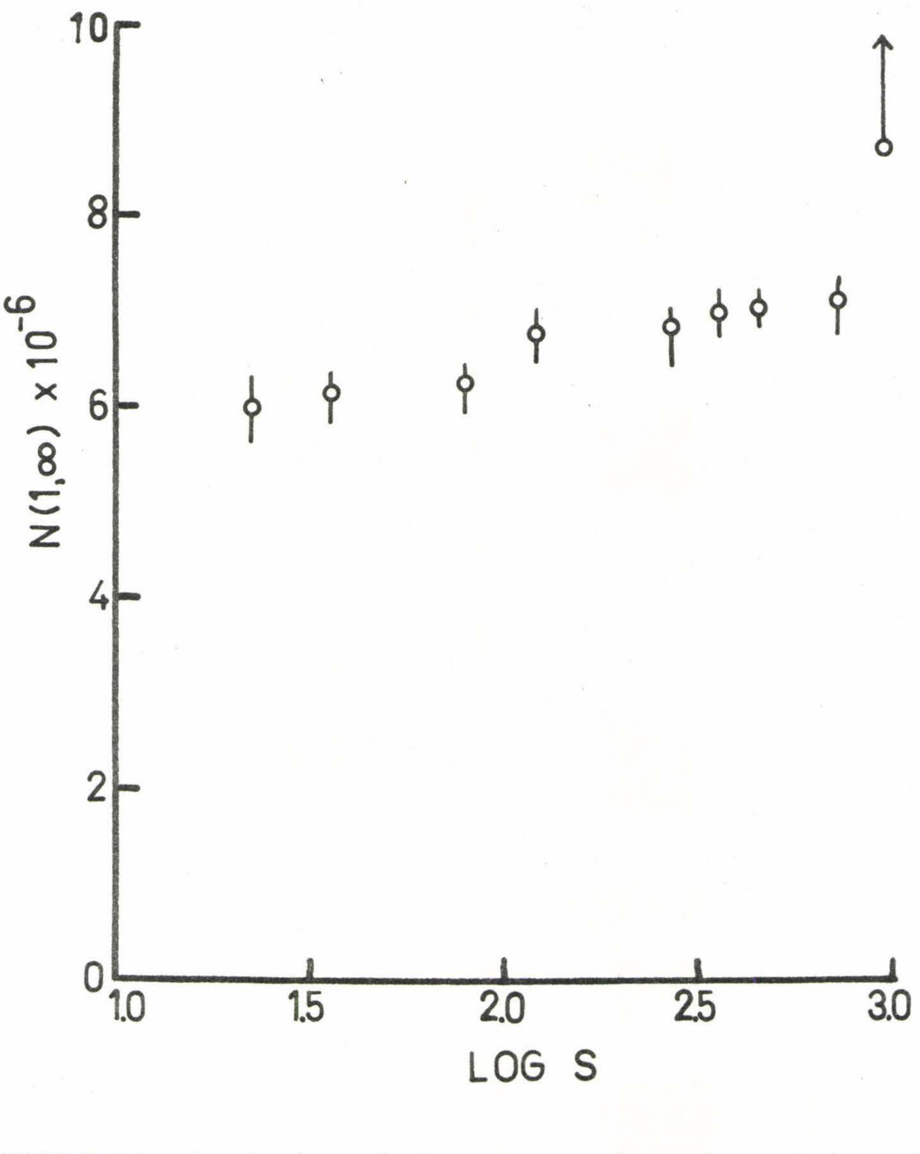

FIGURE 10. Variation of the total number of precipitated barium sulphate crystals with supersaturation.

The size distributions obtained can be interpreted in terms of the initial nucleation event being either homogeneous or heterogeneous. If homogeneous nucleation were occurring the rate of nucleation and hence the total number of crystals formed should increase exponentially with increase in the initial supersaturation. The dependence found in the present study, as shown in Figure 10, is such that the total number formed increases only slowly with increasing supersaturation. On Figure 10, the range of values found for each concentration is shown. These ranges are sufficiently wide that all points almost lie within the same range. For the numbers corresponding to the lowest supersaturations a substantial unknown proportion of them lie below the limit of detection of the instrument. This relationship between the total number of particles formed and the initial supersaturation is indicative that nucleation was occurring on a practically constant number of heterogeneous sites. The slight increase can be explained by postulating that some impurities are more efficient nucleators than others. Then, as the supersaturation increases, the less efficient sites catalyse the nucleation process. The result that the average size of the particles produced increases with increasing supersaturation also indicates that heterogeneous nucleation is occurring at supersaturations below $10^{2.85}$.

The fourth feature of the study indicates that at a well-defined supersaturation the number of particles formed rises drastically with a slight increase in supersaturation. In this investigation no study of this dependence was possible because the particles produced were below the lower limit of detection of the instrument. Other authors have shown that this dependence of number of particles formed with supersaturation is consistent with the Volmer-Becker-Doring theory of homogeneous nucleation. From this study, identifying the marked change in number with the onset of homogeneous nucleation then it can be concluded that homogeneous nucleation predominates at supersaturations above $10^{2.85}$. Putting the rate of nucleation = 1 at log S = 2.85 and using the relation

$$J = A\ e^{-\frac{16\pi\sigma^3 v^2}{3K^3T^3(\ln S)^2}} \qquad [15]$$

the surface tension σ may be calculated assuming a spherical nucleus. The value of A used commonly in the literature and here is 10^{30}. The volume of a barium sulphate molecule (calculated from the density and formula weight) used is $4.30 \times 10^{-23}\text{cm}^3$. The value of σ calculated in this way is 130 ergs cm^{-2} which is in good agreement with that quoted by Nielsen (67) for the surface tension of the barium sulphate nucleus. The number of ions in the nucleus was also calculated from the same equation and found to be 21 (see Table 2).

The results found in this study are both qualitatively and quantitatively in agreement with those for barium sulphate in the literature. This indicates that even though it was very difficult to reproduce individual size distributions some degree of confidence could be placed in the trends shown in the size distributions and on the calculations made on the averages of many measurements. The counting and mixing techniques were therefore used in a more complete study of the nucleation and growth of several nickel dioximates.

3.D. Nucleation of Nickel Dioximates

The procedures described in section 2.C. were used to measure the size distributions of the crystals formed when bis(1,2-butanedione-dioximate)nickel(II), bis(1,2-cycloheptanedione-dioximate)-nickel(II), and bis (1,2-cyclohexanedione-dioximato)nickel(II) were precipitated from aqueous solution. Hereinafter, the chelates will be referred to by their more common names of nickel dimethylglyoximate, nickel heptoximate and nickel nioximate respectively. The size distributions obtained were used to elucidate whether the type of process controlling the nucleation step in the precipitation of each of the above chelates was homogeneous or heterogeneous.

The results were evaluated in terms of the classical theory of homogeneous nucleation and were used to determine the parameters of importance in equation [15].

$$J = A \exp \left(- \frac{\beta\sigma^3 v^2}{k^3 T^3 (\ln S)^2}\right) \qquad [15]$$

These parameters were the pre-exponential factor A, the value of the surface free energy σ and the number of molecules i* in the critical nucleus. To evaluate these parameters it was necessary to experimentally measure the dependence of the rate of nucleation J on the supersaturation S and to measure the size distribution of the precipitated particles at various times. The variables, J and S, and the variation of size distributions with time and with supersaturation were measured for the three nickel dioximates mentioned earlier. The validity of the measurements of J and S and the assumptions involved will be discussed later.

The size distributions of the crystals obtained were recorded in terms of the distribution of diameters of the crystals. All of the nickel dioximates studied crystallize in the form of long thin needles. This raises the important question as to whether differences in pulse heights due to the particles passing through the aperture of the counter are a result of different orientations of the crystal in the aperture. Fortunately, however, due to the viscous flow of the suspension through the aperture of the counter cell, all of the crystals pass through it with their long axis perpendicular to the plane of the aperture. This was confirmed by visual observation, with a microscope, of the crystals in a suspension moving along a tube. The length of the voltage pulse obtained was not substantially affected by the varying lengths of the crystals. This was due to the fact that the electrical field around the aperture extended to several of its diameters on either side and the voltage pulses were initiated when the crystals enter this force field and end when they left the force field. The size distributions measured were thus diameter distributions.

The particle size distribution may be expressed in terms of the size distribution function $N(d,t)$, the number, per unit volume, of those crystals whose size is greater than d at time t. Thus $N(0,\infty)$ is the total number of particles formed at the end of a precipitation (neglecting agglomeration and aging effects). Also the rate of nucleation J can be expressed as

$$J = dN(0,t)/dt = (\partial N/\partial t)_{d=0} \qquad [25]$$

All size distributions in this thesis are recorded in terms of the first derivative of the size distribution function. The size distributions, at various times t, are therefore plots of $(\partial N/\partial d)_t$ against the diameter d. Experiment actually gives a histogram of the number of crystals in diameter intervals of 0.1 μ. As the diameter interval is small and the number of intervals is large, this histogram can be replaced by the continuous function $(\partial N/\partial d)_t$.

3.D.1. The nucleation of nickel dimethylglyoximate

The crystal and molecular structures of nickel dimethylglyoximate have been studied (101). It has been assigned a square planar structure with a strong nickel-nickel bond between molecules. The crystal structure has shown the unit cell to have the dimensions a = 16.88, b = 10.44, c = 6.49 and Z = 4. From this data the density may be calculated to be 1.70 giving a molecular volume of 2.97×10^{-22} cm^3. The evaluation of the volume is of importance in the final determination of the surface free energy σ and the size of the critical nucleus i^*.

In the present investigation solutions of nickel chloride and dimethylgloxime were made up as described in Section 2.C.7., buffered to pH 7 with ammonium hydroxide and mixed in stoichiometric amounts using the direct mixing procedures described in Section 2.C.4. These are the conditions (except for stoichiometry) used in the analytical precipitation of nickel using dimethylglyoxime as the precipitating agent. Preliminary investigations showed that these conditions would give particles of a suitable final size for measurement using the counter-analyser system described earlier. That is, for the period of the reaction in which the greater part of the crystal growth occurred the crystals were larger than 0.9 microns in diameter. The concentrations of the nickel dimethylglyoximate in solution after mixing were 1.0×10^{-3} M, 5.0×10^{-4} M, 2.5×10^{-4}M, 1.0×10^{-4} M, 5.0×10^{-5} M and 2.5×10^{-5} M.

After direct mixing the suspension was sampled at various times and diluted so as to give a count of approximately 5000 to 10000/0.05 mls. To obtain the optimum dilution factor required several trial and error experiments. The variation of the size distributions with time so obtained for an initial nickel dimethylglyoximate concentration of 10^{-3} M is shown in Figure 11. These are typical size distributions obtained. The size distributions were recorded many times for each run and while the actual positions of the peaks at particular times were difficult to reproduce exactly the trends shown in Figure 11 were reproducible. Similar representative variations of the size distributions obtained for the other concentrations of nickel dimethylglyoxime quoted above are shown in Figures 12 to 15 inclusive.

One of the most important aspects of this series of size distributions is that the average size of the particles decreases with increasing supersaturation. That is, even though the total mass of material available for precipitation is increasing, the total number of particles increases more rapidly. Several authors (67,103) have used this effect as a criteria for distinguishing between homogeneous nucleation and heterogeneous nucleation. Homogeneous nucleation, if described by the classical theory, should give rise to a rapidly increasing number of particles as the supersaturation is increased.

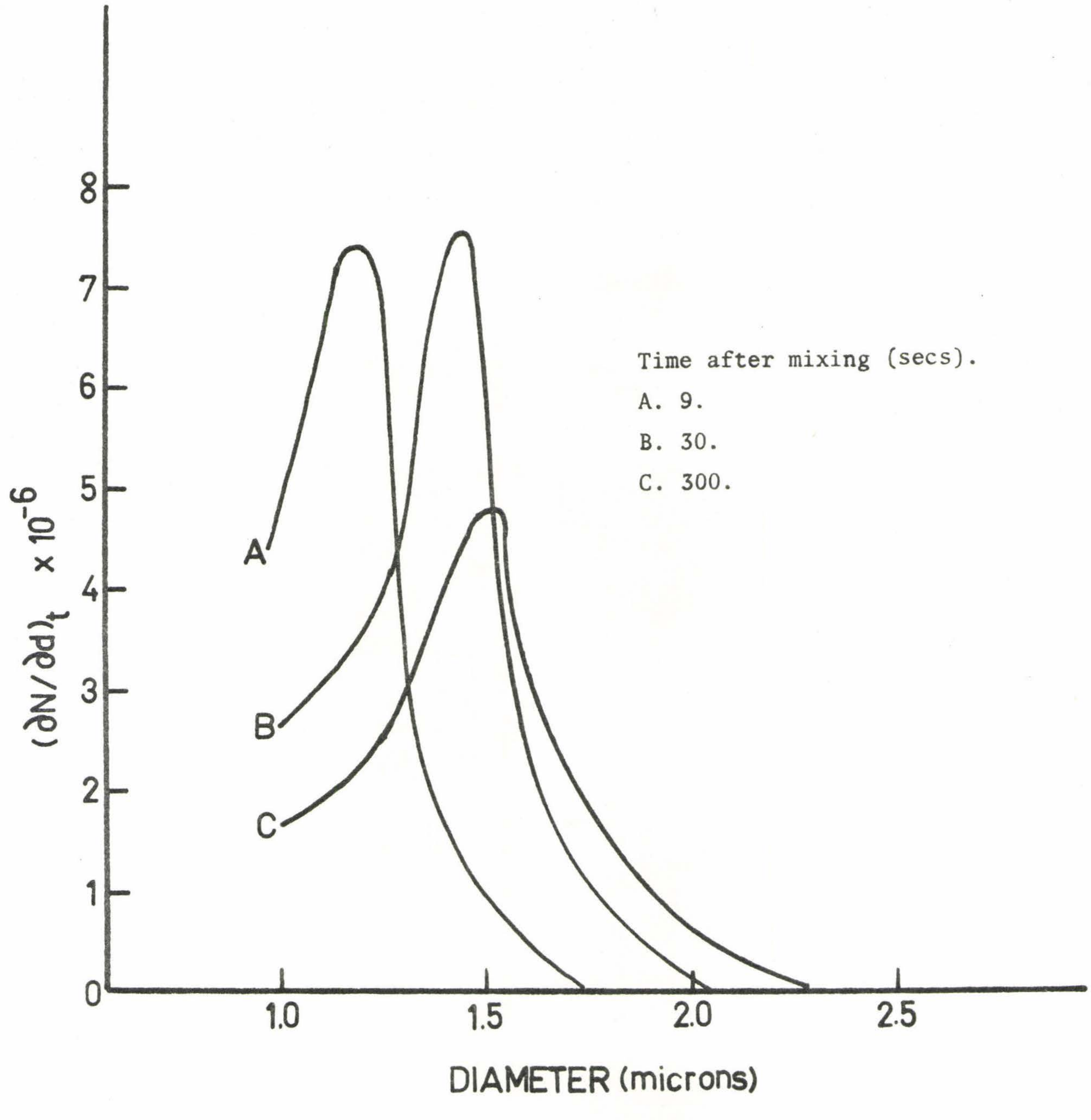

FIGURE 11. Nickel dimethylglyoximate size distributions ($c_0 = 1.0 \times 10^{-3}$M).

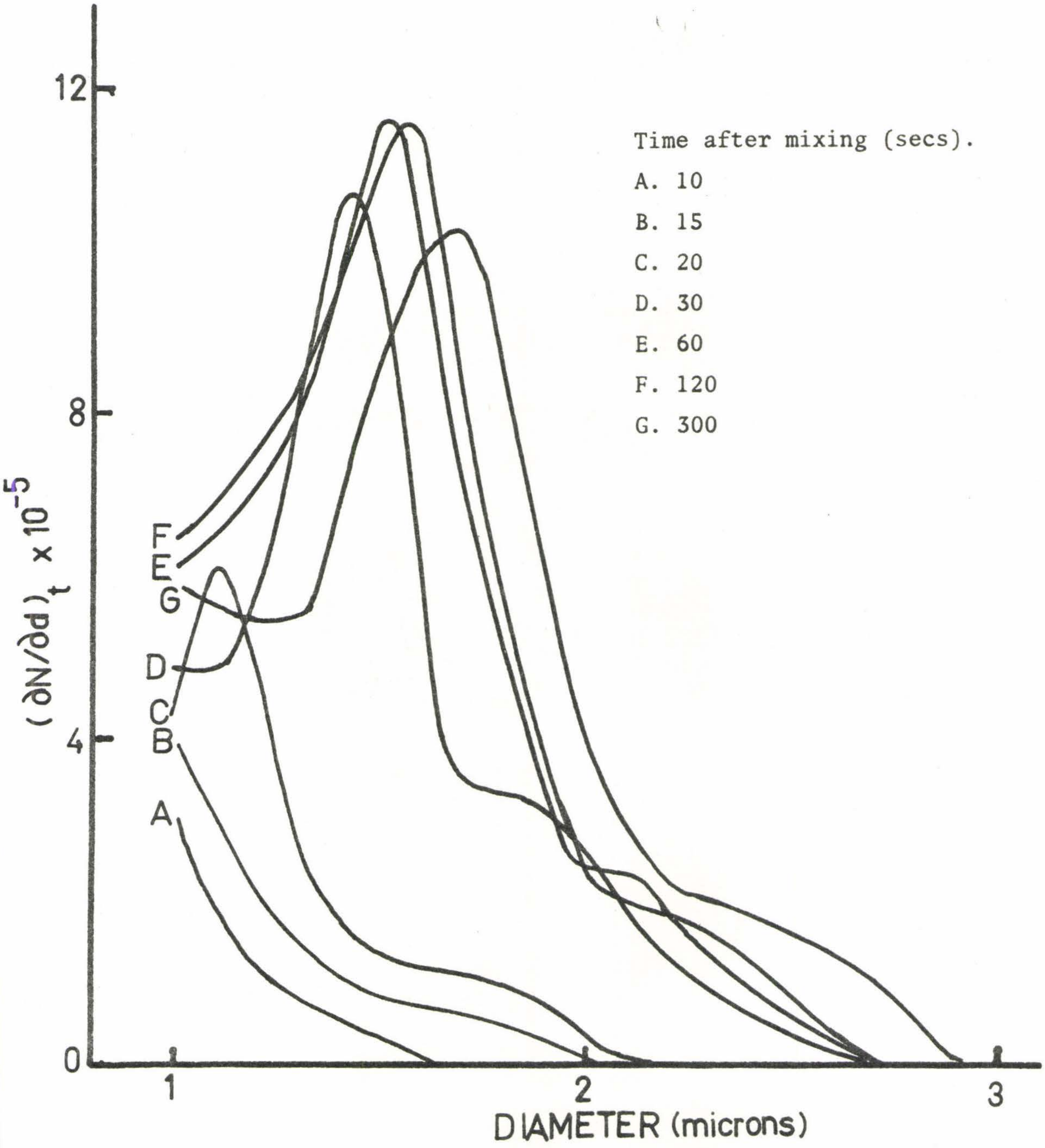

FIGURE 12. Nickel dimethylglyoxime size distributions ($c_0 = 5.0 \times 10^{-4}$M).

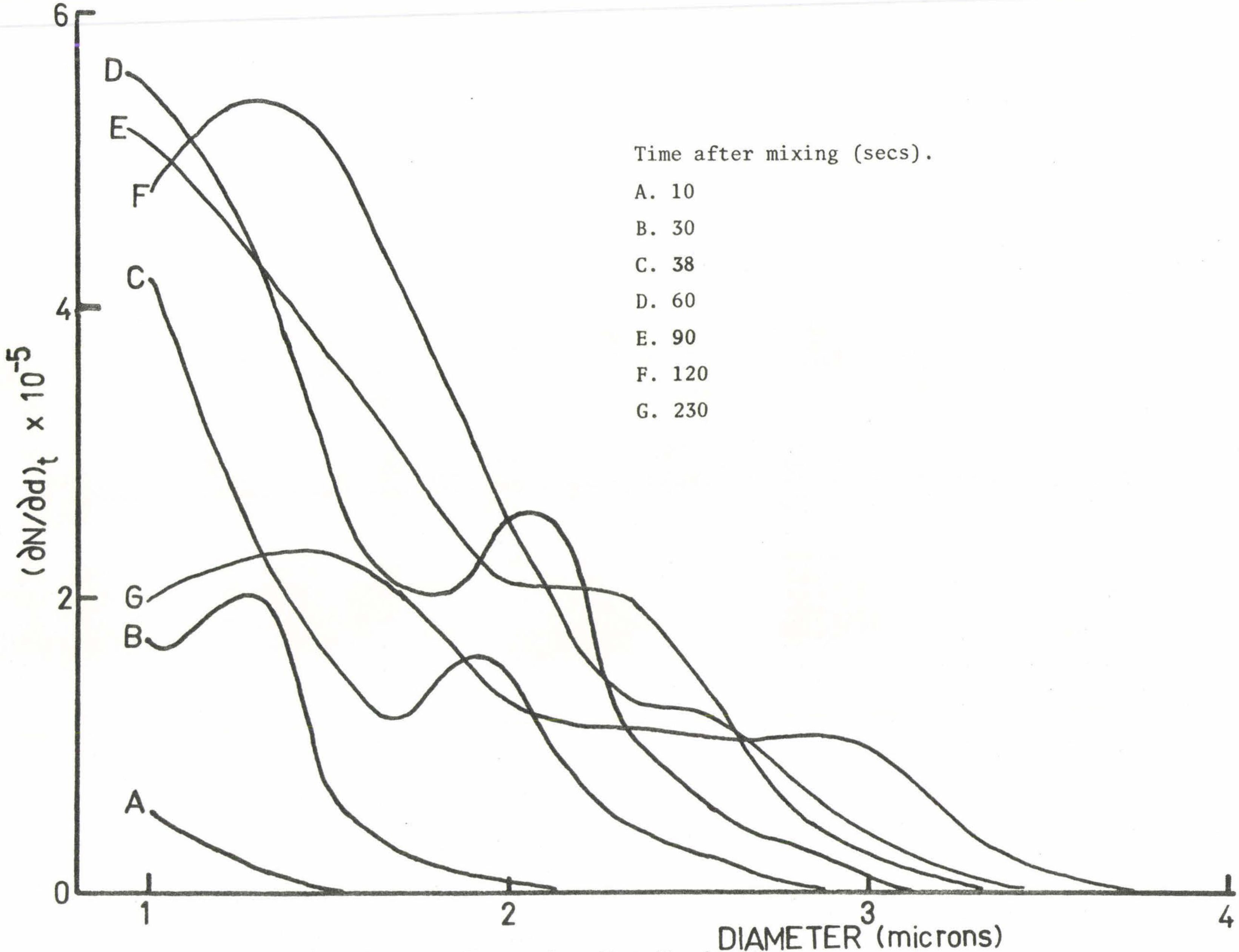

FIGURE 13. Nickel dimethylglyoximate size distributions ($c_0 = 2.5 \times 10^{-4}$M).

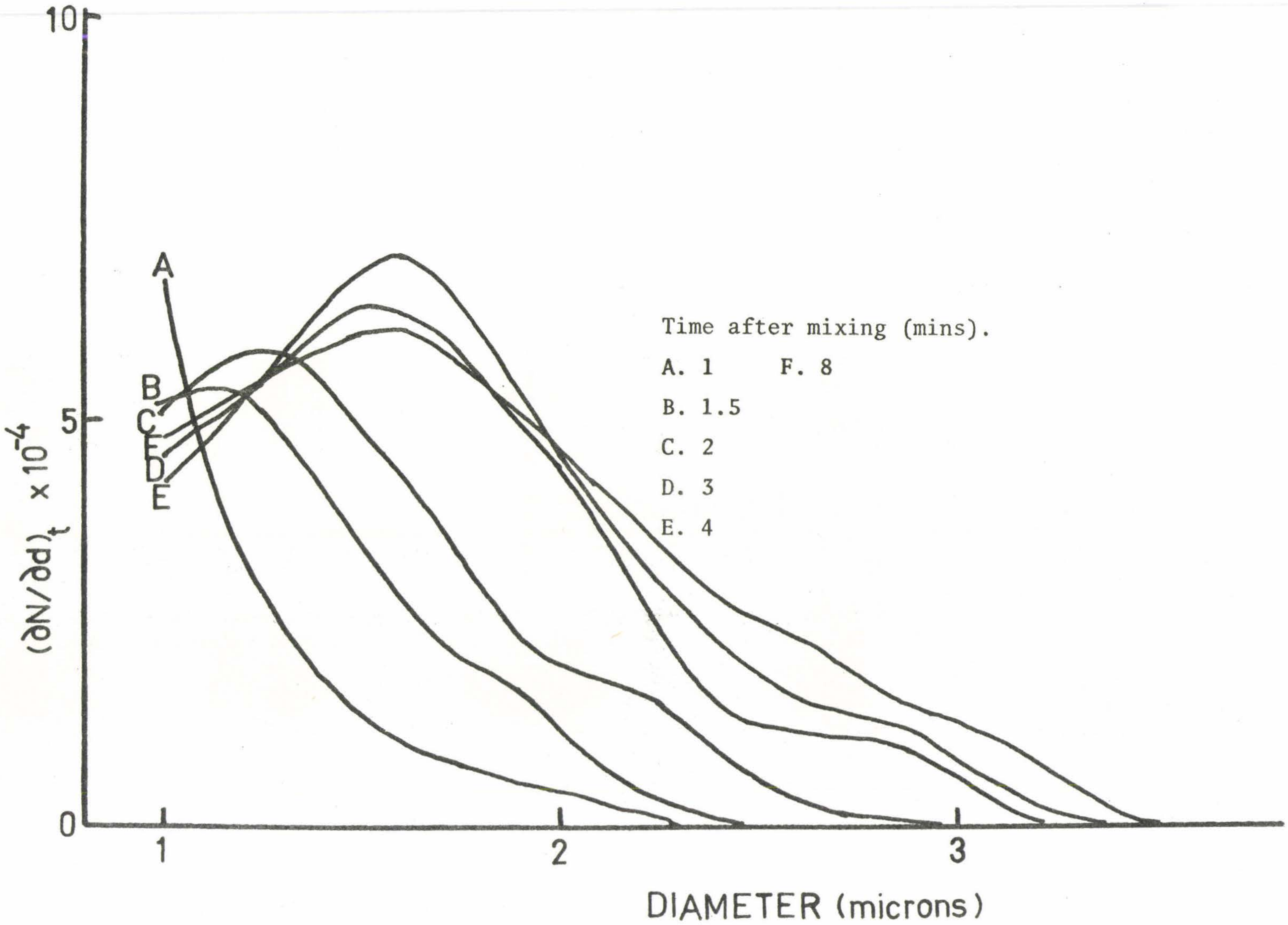

FIGURE 14. Nickel dimethylglyoximate size distributions ($c_0 = 1.0 \times 10^{-4}$M).

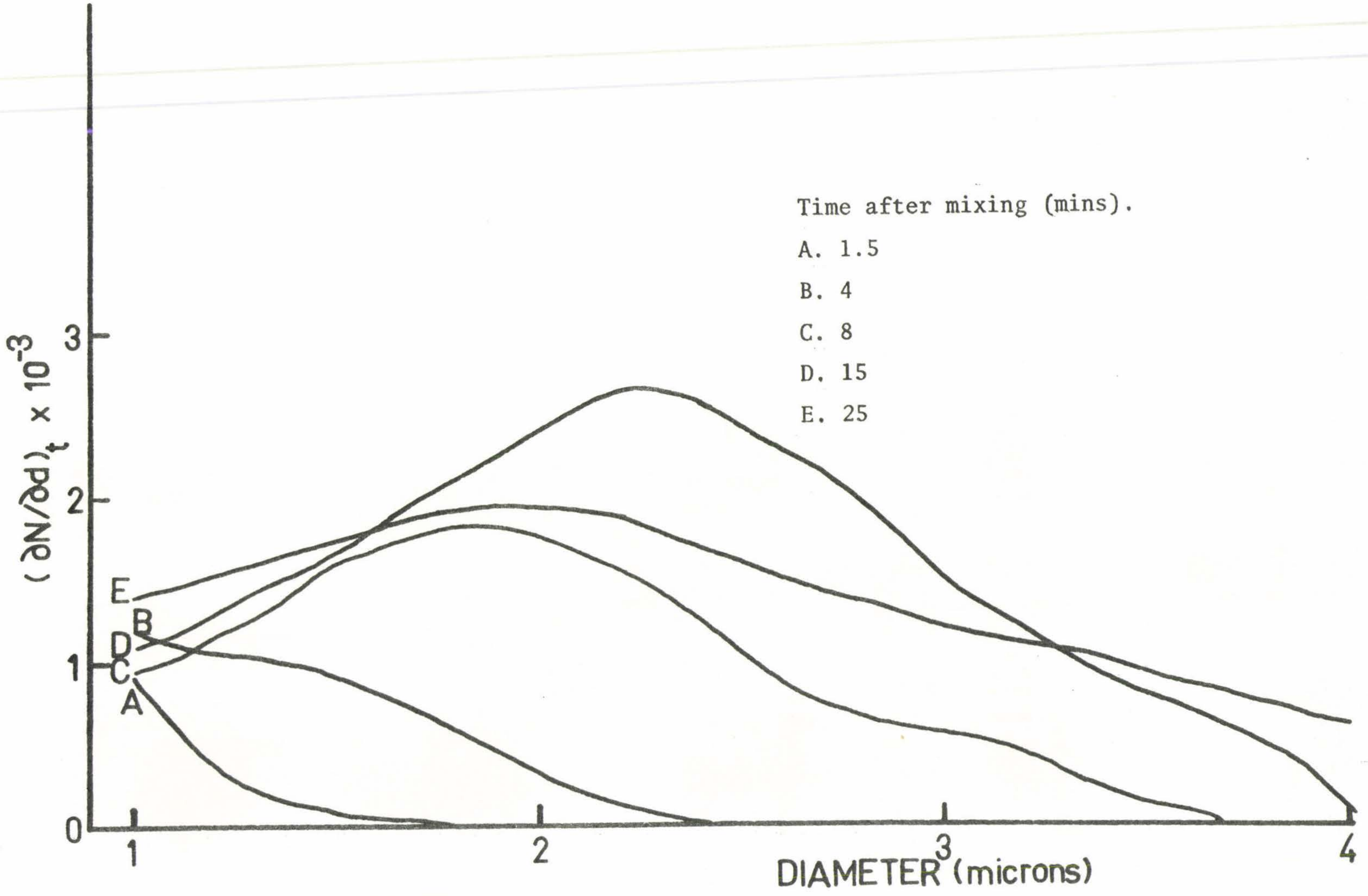

FIGURE 15. Nickel dimethylglyoximate size distributions ($c_0 = 5.0 \times 10^{-5}$M).

The end result should be less mass per particle and a resultant decrease in average final particle size with increasing supersaturation. In the concentration range studied here nickel dimethylglyoximate shows the same trends as above. Consequently, these trends indicate that homogeneous nucleation of nickel dimethylglyoximate is taking place. Heterogeneous nucleation, on the other hand, may be expected to take place on a constant number of foreign particles. This should result in an increase in the final crystal size as the supersaturation is increased. Some authors (98) have postulated that heterogeneous nucleation could occur on particles of different nucleating abilities resulting, as for homogeneous nucleation, in an increase in the number of particles formed. While particles of different nucleating abilities undoubtedly exist, it would seem unlikely that they would have exactly that range of nucleating abilities necessary to give the increase in numbers expected assuming a homogeneous nucleation mechanism.

The other main qualitative aspects of the Figures 11 to 15 inclusive are as follows.

(i) The size distributions move through 1 μ, the position of the peak moving to larger diameters with time. This shows that the crystal growth is occurring at measurable rates and that crystals do not appear visibly immediately after the nucleation event.

(ii) All of the size distributions show at least one maximum (except for those taken early in the precipitation where the maximum is below the level of detection of the instrument). For those precipitations carried out at high supersaturations there is a single maximum of narrow diameter range (Figure 11). For a lower supersaturation, i.e., Figure 12, the single peak has broadened slightly and has a shoulder on the high diameter side. In Figure 13 two distinct peaks are visible early in the precipitation and the distribution has broadened considerably. At later times in this same precipitation the maxima broaden further and the larger diameter maximum becomes a plateau (Figure 13). At even lower supersaturations (Figures 14 and 15) the maxima broaden further and more, large particles are formed.

(iii) It was found that it was very difficult to reproduce the actual position of the maxima from experiment to experiment. The trends shown by the sizes distributions were however quite reproducible within any particular experiment.

(iv) The total number of particles formed varied widely for different initial supersaturations.

For each of the size distributions in Figures 11 to 15 inclusive a total number against time plot was drawn. The total number of crystals formed at any time t is given by the equation

$$N(0,t) = \int_0^\infty \left(\frac{\partial N}{\partial d}\right)_t dd \qquad (26)$$

As the apparatus used had a lower limit of accurate detection of just less than 1 μ, it was not possible to measure directly N(0,t). The total number of particles above 1 μ at time t, N(1,t), was therefore used instead of N(0,t). Plots of N(1,t) versus t for the initial concentrations quoted above are shown in Figures 16 to 20 inclusive. Tables 6 to 8 inclusive show the variation of N(1,t) with time for various initial concentrations.

All of these plots show the same general characteristics. N(1,t)

TABLE 6

Variation of the total number of nickel dimethylglyoximate crystals formed with time.

$c_o = 1.00 \times 10^{-3}$ M		$c_o = 5.00 \times 10^{-4}$ M	
Total Number $\times 10^{-7}$	Time (secs)	Total Number $\times 10^{-6}$	Time (secs)
0.61	6	0.71	10
1.8	9	0.36	10
2.9	15	1.03	15
3.2	30	0.85	15
3.6	30	2.2	20
3.8	60	6.4	30
2.4	120	4.9	30
2.9	120	10.1	60
3.2	120	10.3	60
2.7	210	9.1	60
2.3	210	9.2	120
2.2	300	8.5	120
2.2	300	5.9	300
2.9	300	8.4	300
		7.8	300

TABLE 7

Variation of the total number of nickel dimethylglyoxinate crystals formed with time.

$c_o = 2.5 \times 10^{-4}$ M

Total Number $\times 10^{-5}$	Time (secs)	Total Number $\times 10^{-5}$	Time (secs)
0.89	10	22.0	90
0.62	10	23.7	90
1.8	20	20.1	120
3.0	20	20.6	120
4.1	30	21.1	120
6.2	30	18.8	210
8.1	38	18.1	210
12.8	60	14.5	300
15.3	60	16.5	300
10.7	60	15.9	300

TABLE 8

Variation of the total number of nickel dimethylglyoximate crystals formed with time.

$c_o = 1.0 \times 10^{-4}$ M		$c_o = 5.0 \times 10^{-5}$ M	
Total Number $\times 10^{-5}$	Time (mins)	Total Number $\times 10^{-5}$	Time (mins)
2.4	1	0.15	1.5
1.8	1	0.49	2
4.3	1.5	0.61	2
2.7	1.5	0.91	4
6.3	2	2.7	8
8.9	3	3.1	8
9.8	4	4.6	15
11.3	4	5.4	15
9.5	8	4.2	25
9.9	8	4.0	30

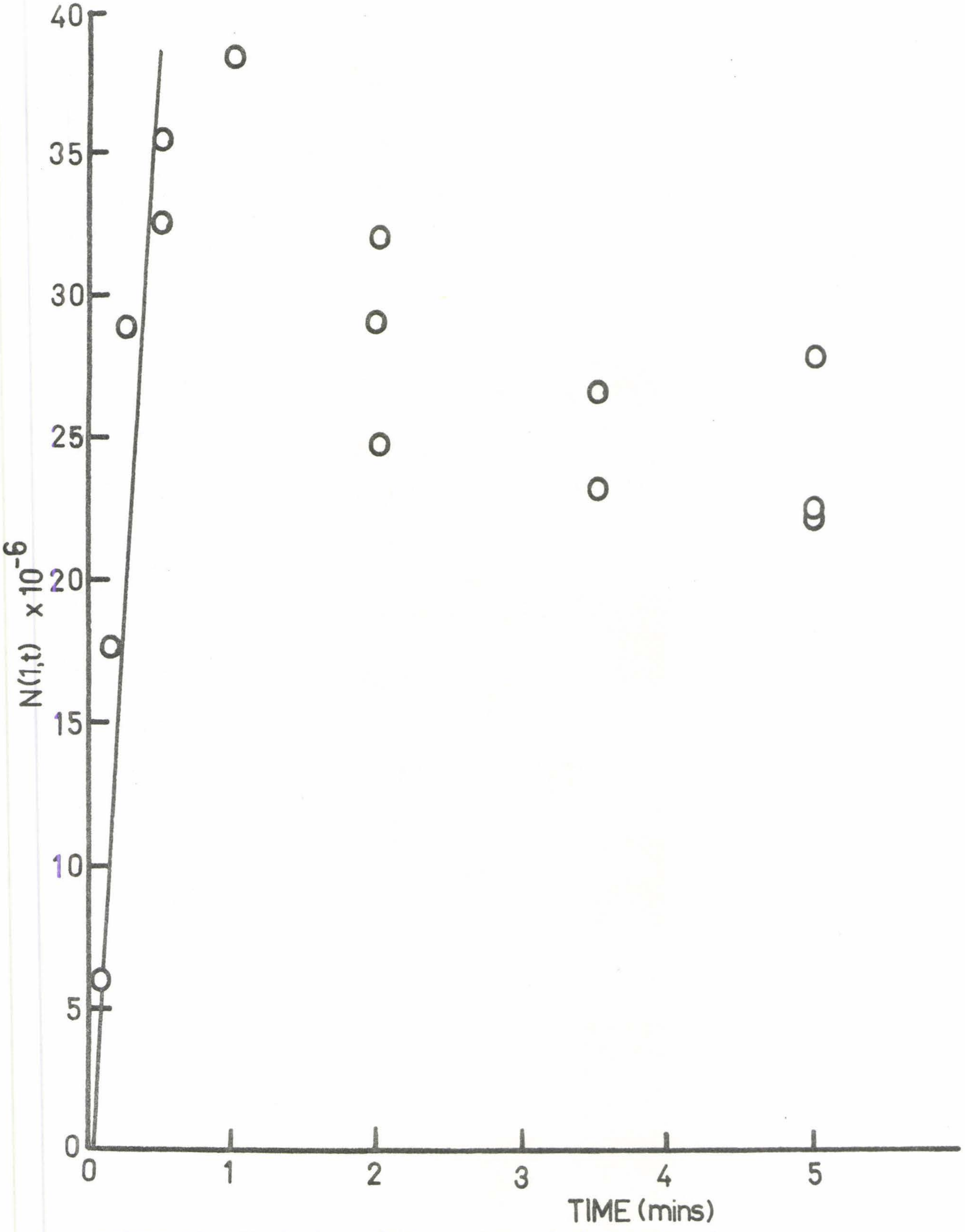

FIGURE 16. Variation of the number of nickel dimethylglyoximate crystals with time ($c_0 = 1.0 \times 10^{-3}$M).

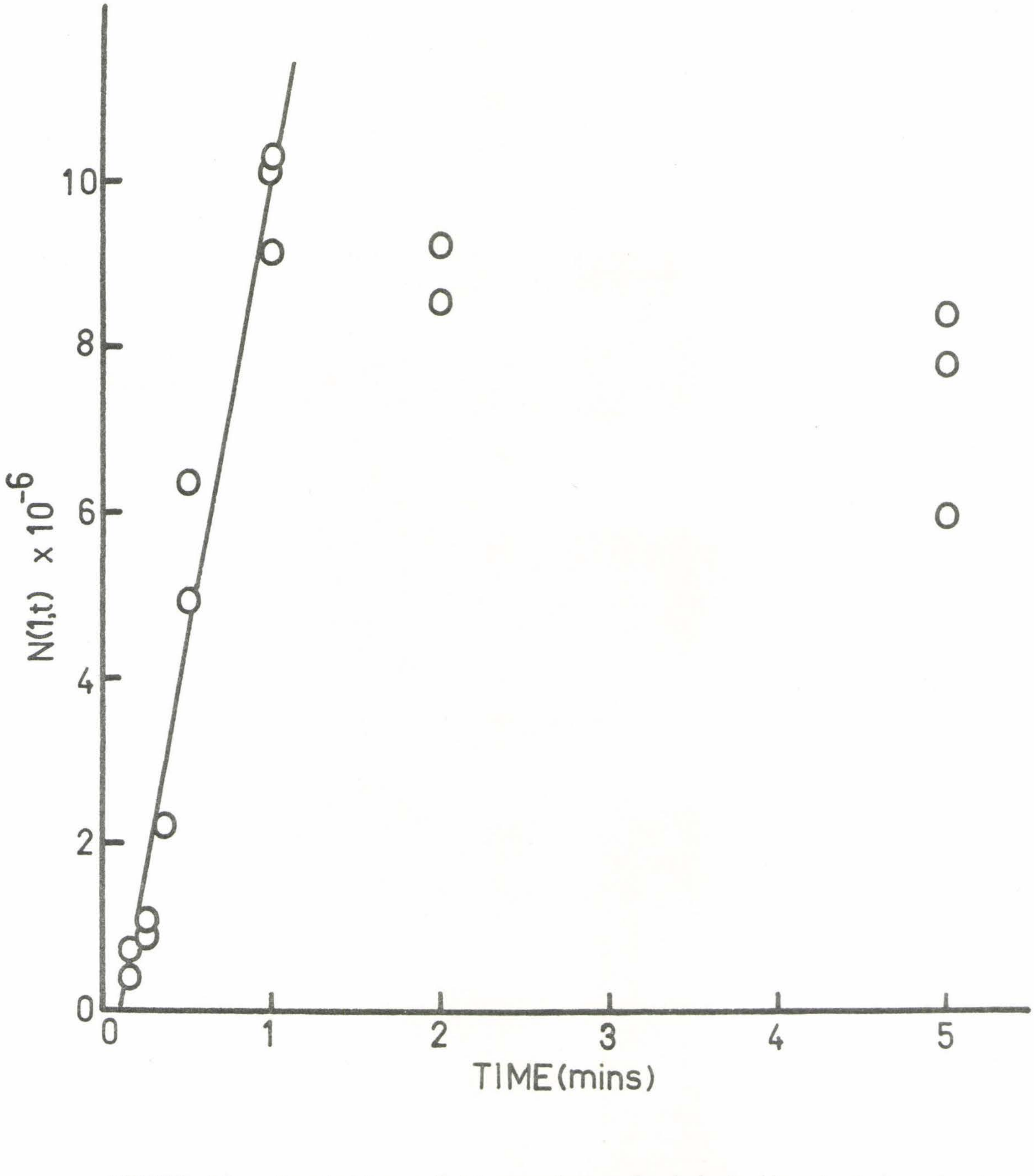

FIGURE 17. Variation of the number of nickel dimethylglyoximate crystals formed with time (c_0= 5.0 x 10^{-4}M).

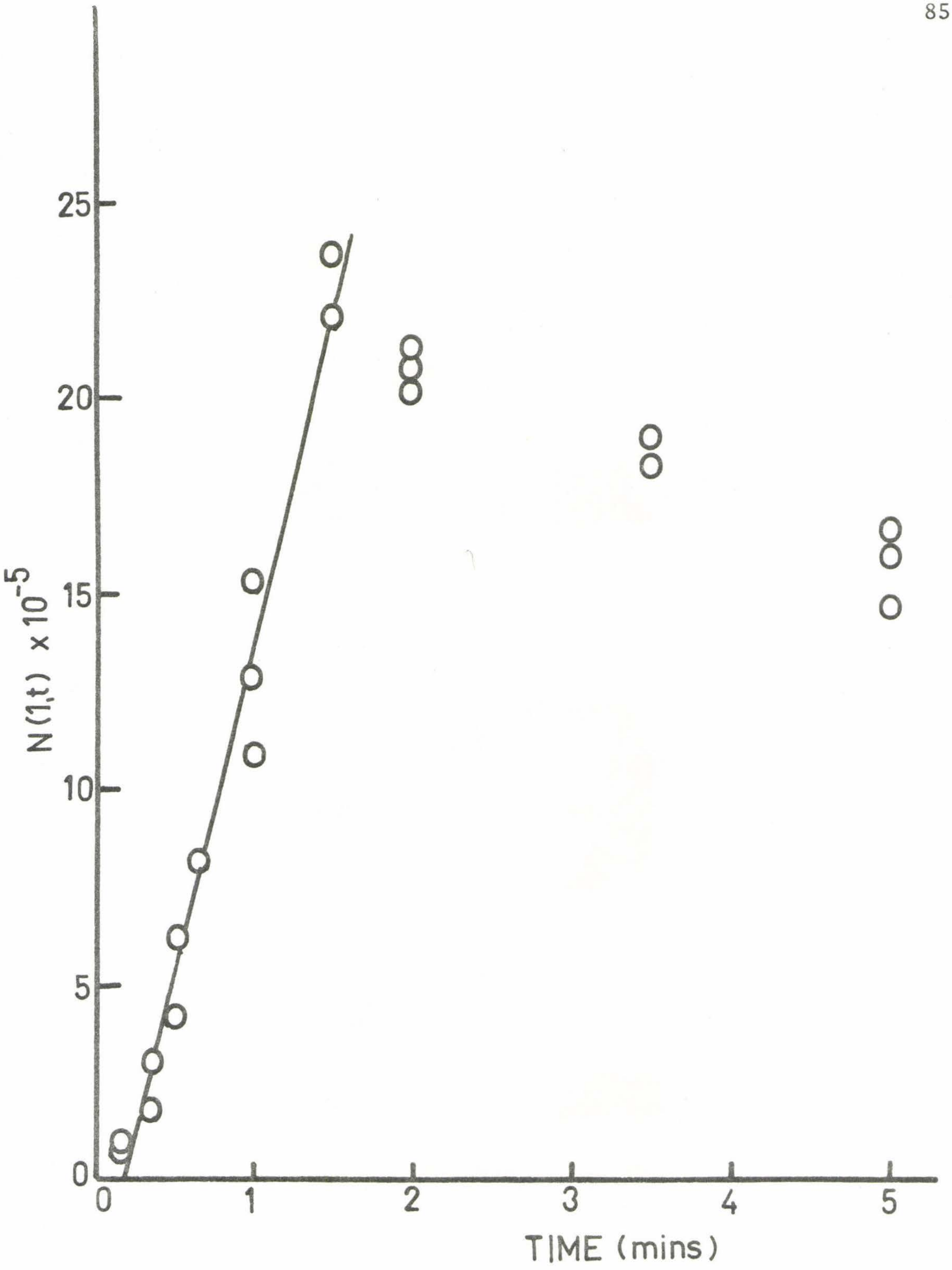

FIGURE 18. Variation of the number of nickel dimethylglyoxime crystals formed with time ($c_0 = 2.5 \times 10^{-4}$M).

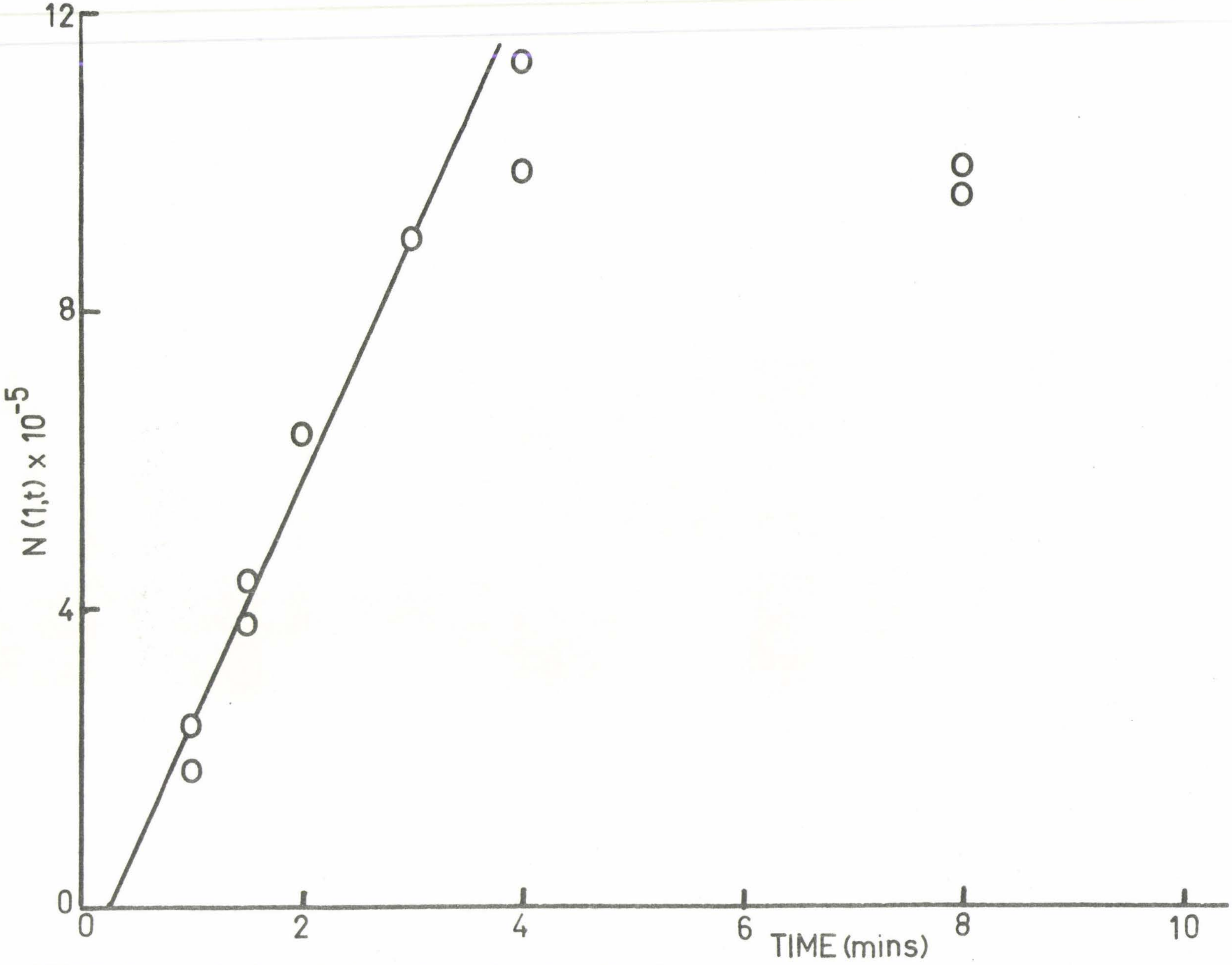

FIGURE 19. Variation of the number of nickel dimethylglyoximate crystals with time ($c_0 = 1.0 \times 10^{-4}$M).

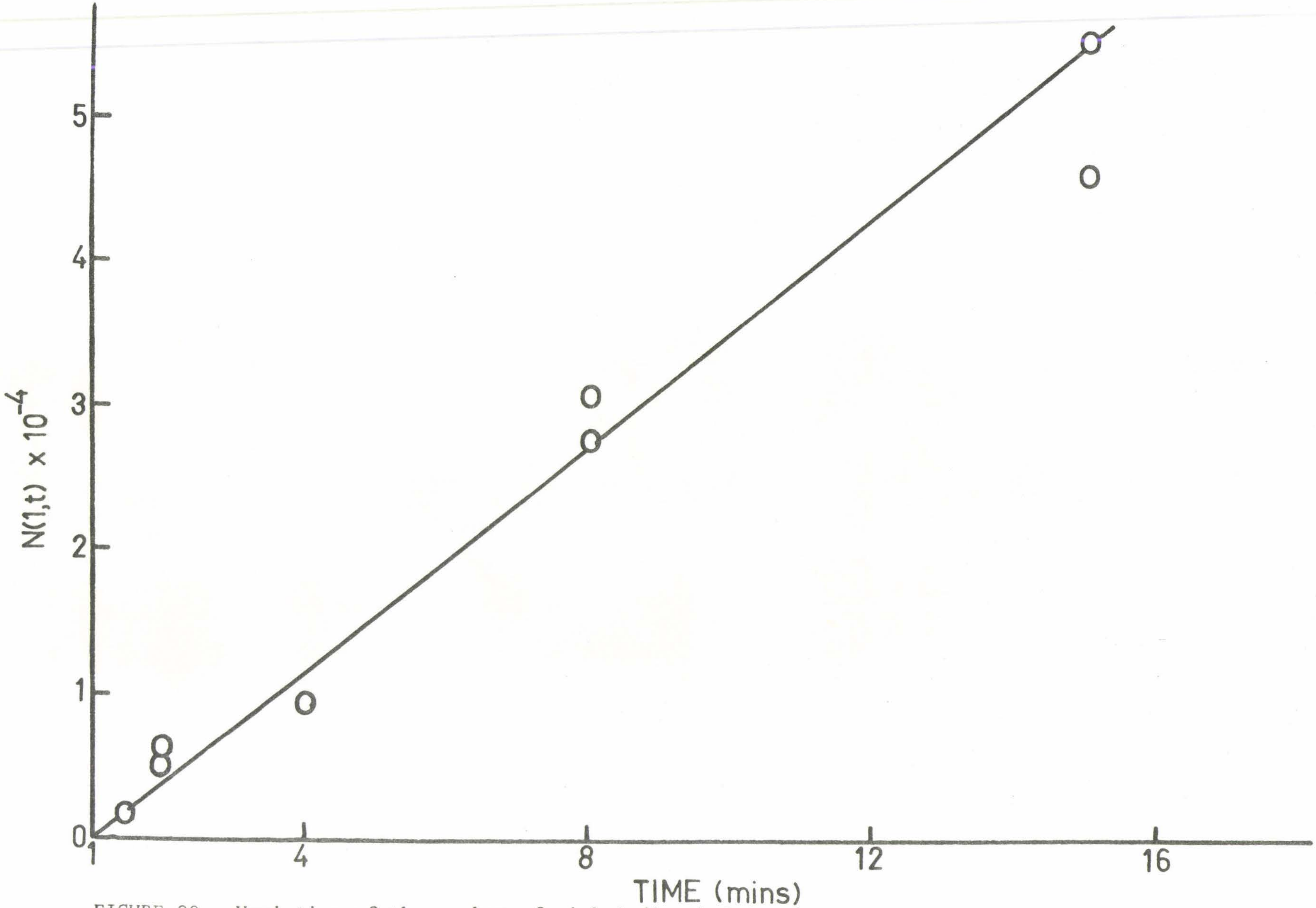

FIGURE 20. Variation of the number of nickel dimethylglyoxímate crystals formed with time ($c_0 = 5.0 \times 10^{-5}$M).

rises almost linearly to a maximum and then decreases slightly. This decrease is most pronounced for higher initial supersaturations. This effect is probably due to agglomeration of the smaller particles. This is indicated by the increase in the number of large particles and the decrease in the number of smaller particles as shown by the size distribution curves corresponding to the longest times in Figures 11 to 15 inclusive. That the effect is not due to sedimentation was demonstrated by the fact that the size distributions did not change when the solutions were stirred more vigorously.

The rate of nucleation $J = (\frac{\partial N}{\partial t})_{d=0}$ was equated with the rate of appearance of crystals to the counter, i.e., $(\frac{\partial N}{\partial t})_{d=1}$. The rate of appearance of particles to the counter was taken as the slope of the linear portion of the total count versus time plots. The validity of these assumptions will be discussed later.

Figure 21 shows on the same scale the final size distributions for three different initial supersaturations. This figure indicates that errors, due to poor reproducibility of size distributions and the assumption that J is equal to the rate of appearance of crystals, are small compared with the relative magnitudes of J obtained for different initial supersaturations. The values of J calculated in this fashion for each supersaturation are shown in Table 9 together with the corresponding values of S, log J, log S and $(\log S)^{-2}$. The supersaturation is calculated by dividing the initial concentration of nickel dimethylglyoximate by its molar solubility, under the conditions of the precipitation, as found in Section 2.C.8.

This supersaturation has been calculated without taking into

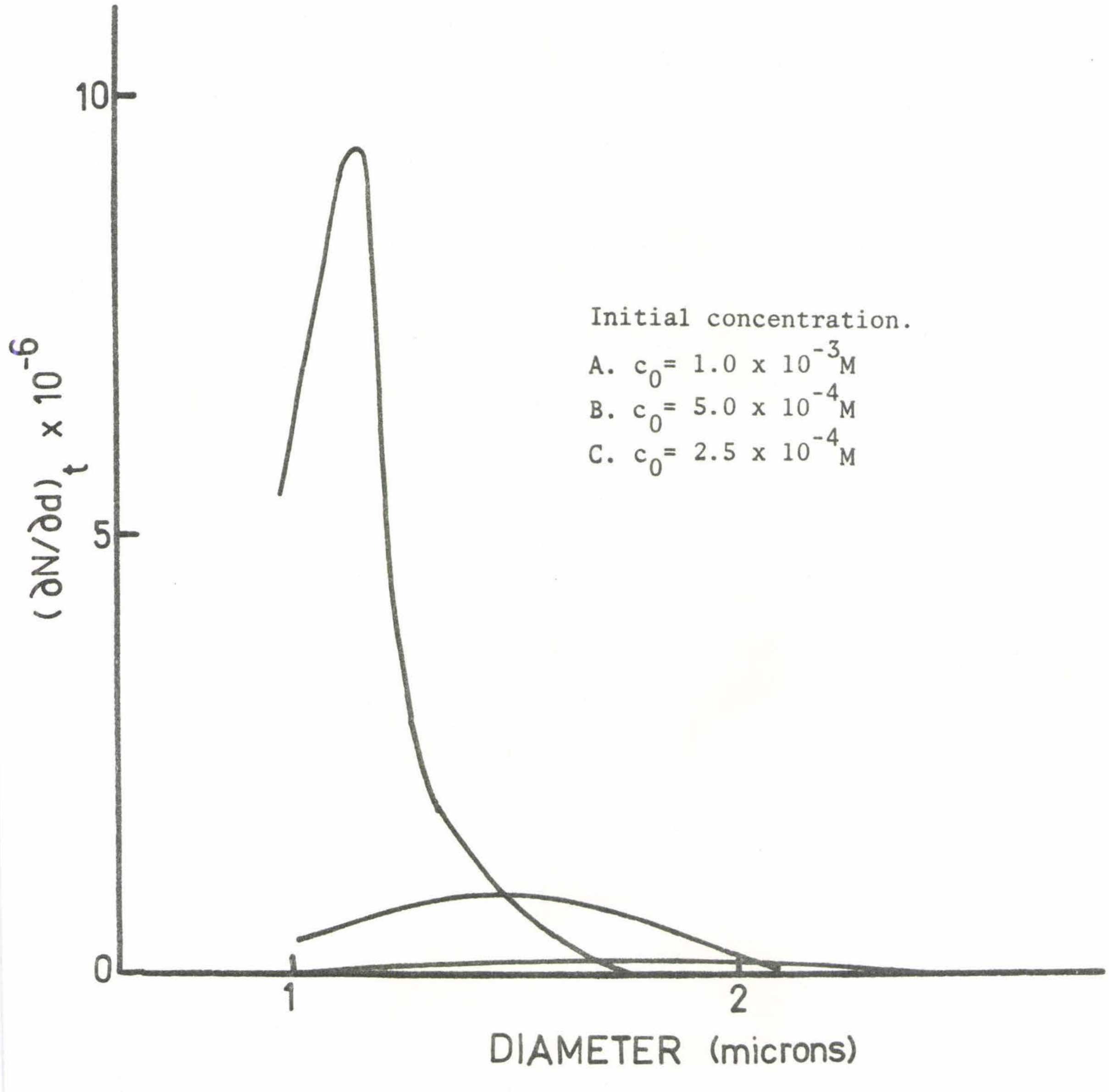

FIGURE 21. Final size distributions for three initial supersaturations of nickel dimethylglyoxime.

account the activities of the monomers in solution. Banks and Anderson (101) have shown that the equilibrium constant for the reaction

$$Ni^{2+} + 2HD^- \rightleftharpoons Ni(HD)_2$$

(where HD^- represents a singly ionized dimethylglyoxime molecule) is 10^{17}. Nickel dimethylglyoximate exists therefore predominantly as the molecular species in solution. The activity may therefore be equated with its concentration and the effect of the high ionic strength may be neglected. The high ionic strength will, however, lower the solubility due to solvation effects.

A plot of log J versus log S is shown in Figure 22 which can be compared with the theoretical diagram shown in Figure 2 for nickel dimethylglyoximate. It is immediately seen that the dependence of log J on log S found experimentally for nickel dimethylglyoximate is qualitatively consistent with the theoretical dependence predicted by equation [15].

Perhaps the most theoretically reliable criteria for determining whether experimental results are consistent with the theory of homogeneous nucleation is a plot of log J versus $(\log S)^{-2}$. This should be a straight line with an intercept on the log J axis of log A. A plot of log J versus $(\log S)^{-2}$ for nickel dimethylglyoximate is shown in Figure 23. This linear relationship indicates that homogeneous nucleation is occurring in the supersaturation range studied. The intercept found by extrapolation to $(\log S)^{-2} = 0$ gives the value of log A to be 9.4.

The value of the surface free energy may be calculated from the

TABLE 9

Variation of the nucleation rate with supersaturation for nickel dimethylglyoximate.

c_o (moles litre^{-1})	S	J ($\text{cm}^{-3}\text{sec}^{-1}$)	log J	log S	$1/(\log S)^2$
1.0×10^{-3}	6.90×10^{2}	1.31×10^{6}	6.12	2.84	0.124
5.0×10^{-4}	4.05×10^{2}	1.96×10^{5}	5.29	2.61	0.147
2.5×10^{-5}	2.38×10^{2}	2.76×10^{4}	4.43	2.38	0.177
1.0×10^{-4}	1.18×10^{2}	5.55×10^{3}	3.74	2.07	0.233
5.0×10^{-5}	6.91×10^{1}	6.03×10^{1}	1.78	1.84	0.295
2.5×10^{-5}	4.06×10^{1}	1	0	1.61	0.386

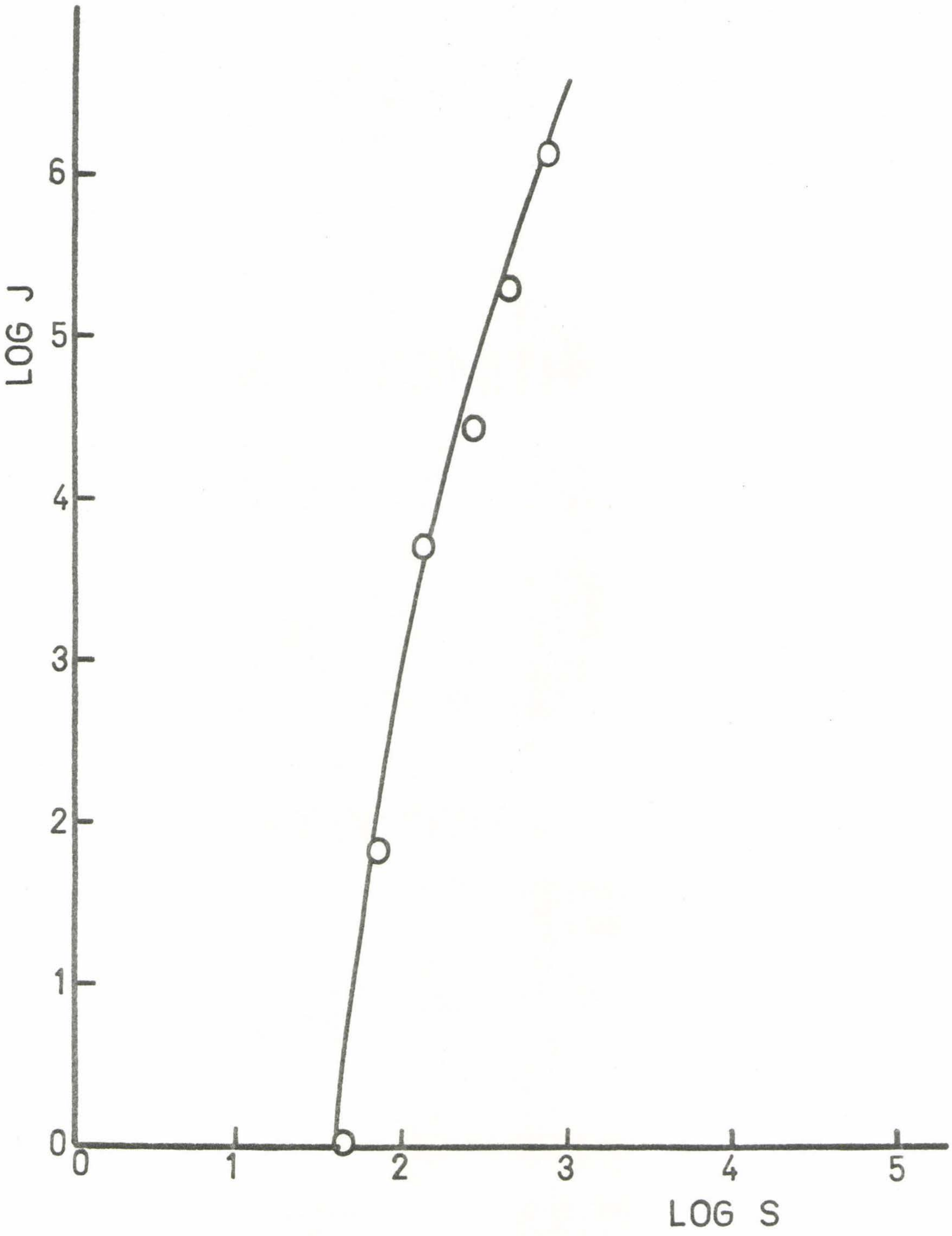

FIGURE 22. Variation of log J with log S for nickel dimethylglyoxime.

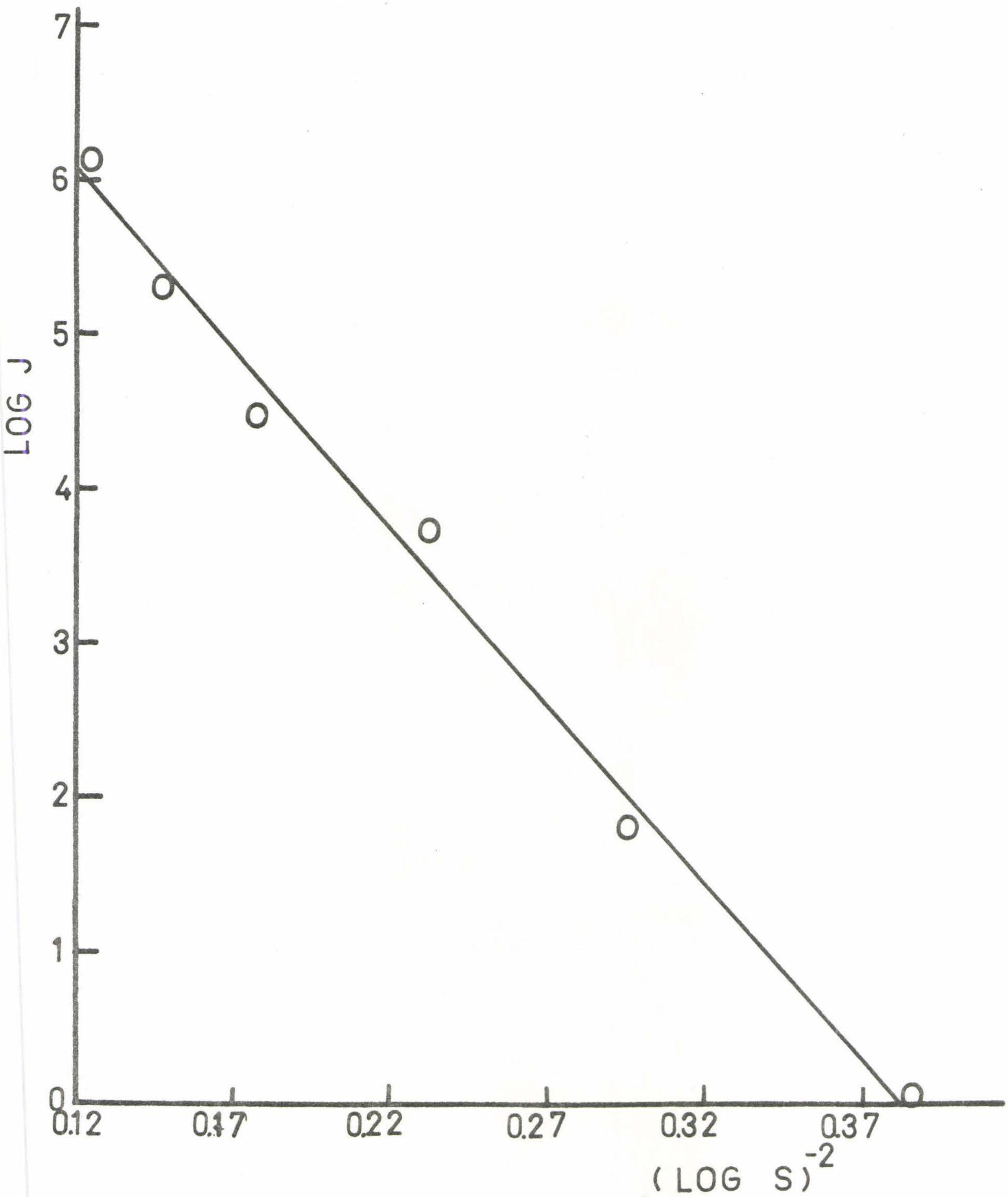

FIGURE 23. Variation of log J with (log S)$^{-2}$ for nickel dimethylglyoxiamate.

slope of the straight line. From Equation [15] the slope is given by

$$\frac{d \log J}{d[(\log S)^{-2}]} = -\frac{\beta\sigma^3 v^2}{(2.303\ kT)^3}$$

from which $\sigma = [\frac{(2.303\ kT)^3}{\beta\cdot\ {}^{2}} \times \text{slope}]^{1/3}$

where the shape factor β equals 109 for a rod 1 × 1 × 10 1 and equals 16.7 for a sphere (42). The molecular volume v is 2.97×10^{-22} cm^3. The surface free energy for nickel dimethylglyoximate, assuming that the nucleus is rod-shaped (1 × 1 × 10 1), is found to be 13 ergs cm^{-2}. If a spherical nucleus is assumed the surface free energy is found to be 24 ergs cm^{-2}.

The size of the critical nucleus is predicted from Equation [13] to vary with supersaturation and the value most often quoted is that corresponding to a critical supersaturation where J = 1 and log J = 0. Under these conditions

$$i^* = \frac{2\beta\sigma^3 v^2}{(2.303\ kT)^3 (\log S)^3}$$

from Figure 23 log J = 0 at log S = 1.6 (i.e., S* = 77). This gives i* = 12 molecules for nickel dimethylglyoximate.

3.D.2. The nucleation of nickel heptoximate

For nickel heptoximate the sequence of experiments and calculations was the same as that already described (Section 3.D.1.) for nickel dimethylglyoximate. That is, the counting and mixing techniques described in Sections 2.C.3. and 2.C.4. were used to measure the variation of the crystal size distribution with time and initial supersaturation.

It was not possible to carry out the precipitations at pH 7 because the crystals formed were much too small to be detected by the counter. Banks and Anderson (101) have measured the solubility product and intrinsic solubility for nickel heptoximate and found that, at pH 7, it is much less soluble than nickel dimethylglyoximate. This means that for a given supersaturation there is much less mass of material available for the crystal growth of the former chelate than the latter. Consequently, if equal numbers of crystals are formed, the nickel heptoximate crystals will be much smaller and undetectable by the counter. The mass available for crystal growth can be increased by increasing the initial concentration of the reactants. The theory of homogeneous nucleation, however, predicts that the number of crystals will increase more rapidly than the increase in mass available and consequently the final precipitate crystals will be smaller still. If the nucleation occurring is heterogeneous then the final precipitate crystals should be larger. The former situation was the one found experimentally by visually examining the precipitate with a microscope. The solubility of the metal chelate and consequently the mass available for crystal growth was increased by lowering the pH to 3.28. At this pH the solubility was 4.0×10^{-6} M. As in the case of nickel dimethylglyoximate the change in the activity of the chelate, due to ionic strength, was neglected and its activity equated with its concentration. The initial concentrations of the nickel heptoximate studied were 1.25×10^{-3} M, 1.00×10^{-3} M, 0.75×10^{-3} M, 0.50×10^{-3} M, 0.38×10^{-3} M and 0.25×10^{-3} M. The variation of the size distributions with time was measured for each of the above initial concentrations. Also, as in the case of nickel dimethylglyoximate the individual size distributions were not very reproducible but the trends shown in the size distributions in Figures 24 to 28 inclusive were reproducible.

These size distributions showed the same qualitative features as those obtained with nickel dimethylglyoximate. In particular the average size of the particles produced increased with decreasing supersaturation and the shoulder on the main peak was again present at low initial supersaturations. At high initial supersaturations a substantial number of the crystals were below the limit of detection of the instrument. Tables 10 to 12 inclusive and Figures 29 to 33 inclusive show the variation of the total numbers of crystals, above the level of the detector, with time. These are plots of N(1,t) versus t and again for reasons to be discussed later the slope of the initial portion of this curve $(\frac{\partial N}{\partial t})_{d=1}$ is equated with $(\frac{\partial N}{\partial t})_{d=0}$, the rate of nucleation, J. The final size distributions at various initial supersaturations bear a similar relationship to each other as do those shown in Figure 21 for nickel dimethylglyoximate.

Table 13 lists J, S, log J, log S and $(\log S)^{-2}$ for nickel heptoximate. A plot of log J versus log S is shown in Figure 34. This plot can be compared with the theoretical diagram (Figure 2). This comparison is only qualitative as Figure 2 is constructed for nickel dimethylglyoximate whose molecular volume is 2.97×10^{-22} cm^3. The volume of the nickel heptoximate molecule could only be estimated as the exact unit cell dimensions were not known. The molecule will be only slightly larger than the nickel nioximate molecule whose

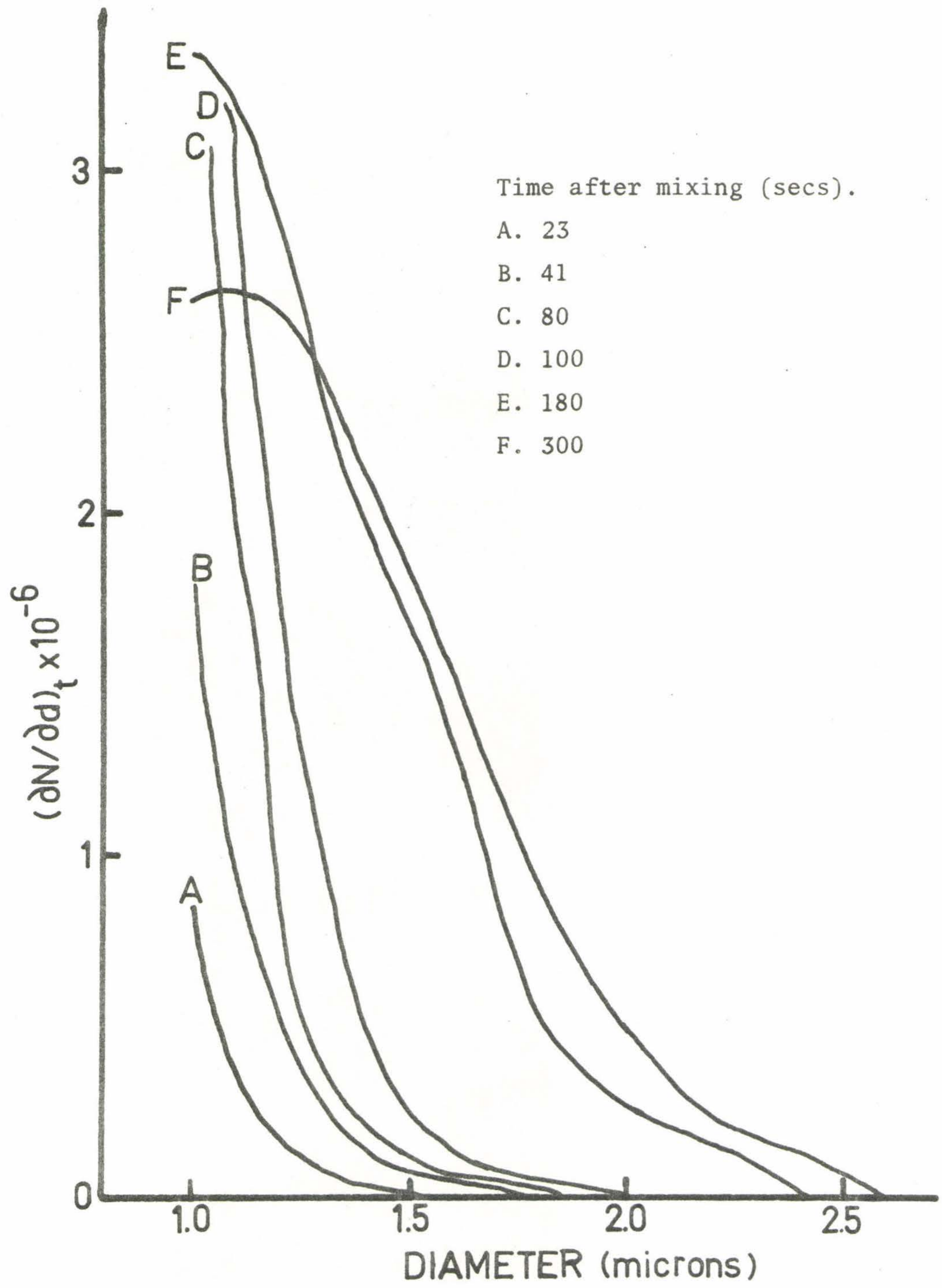

FIGURE 24. Nickel heptoximate size distributions ($c_0 = 1.25 \times 10^{-3}$M).

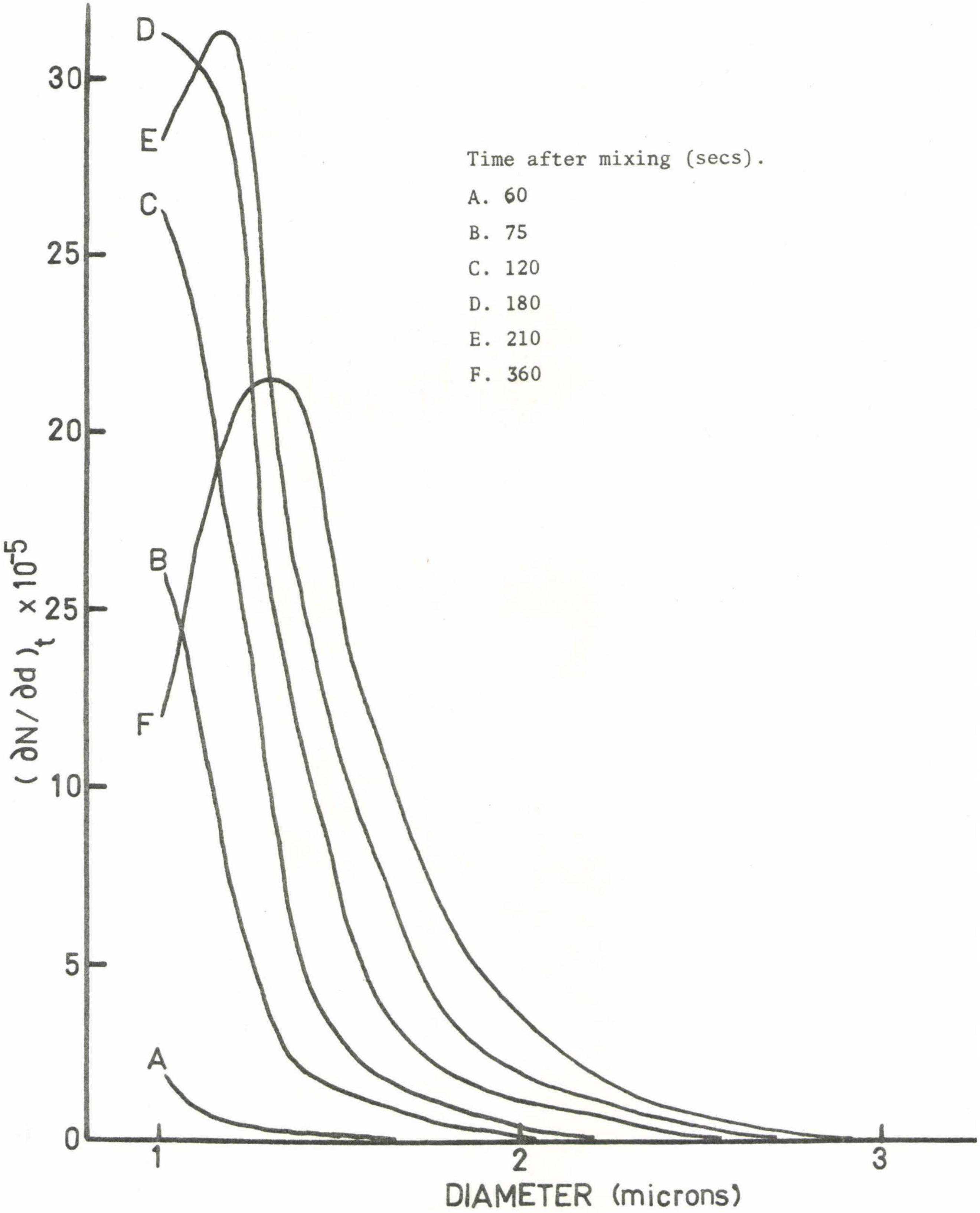

FIGURE 25. Nickel heptoximate size distributions ($c_0 = 1.0 \times 10^{-3}$M).

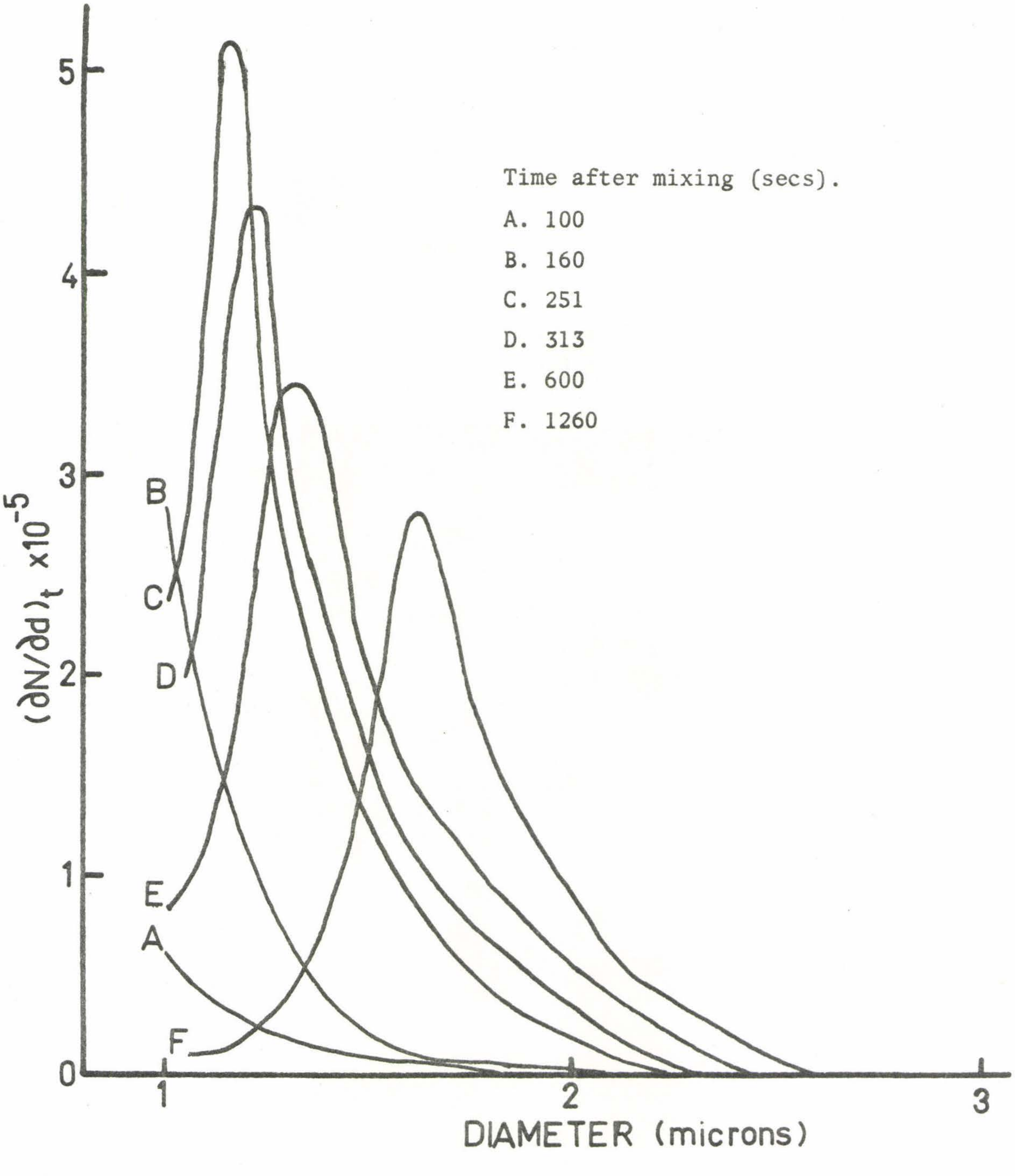

FIGURE 26. Nickel heptoximate size distributions ($c_0 = 7.5 \times 10^{-4}$M).

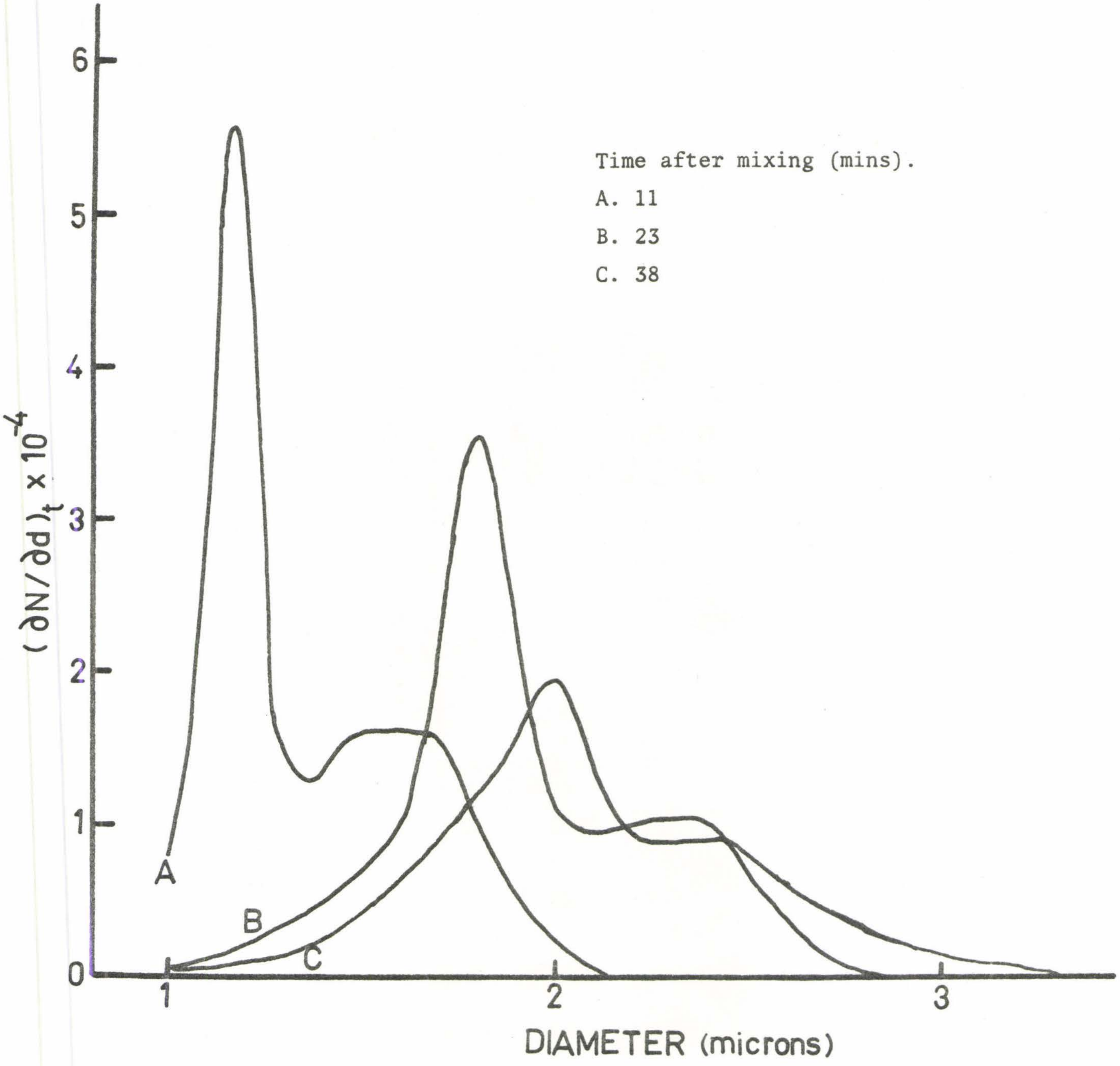

FIGURE 27. Nickel heptoximate size distributions ($c_0 = 5.0 \times 10^{-4}$M).

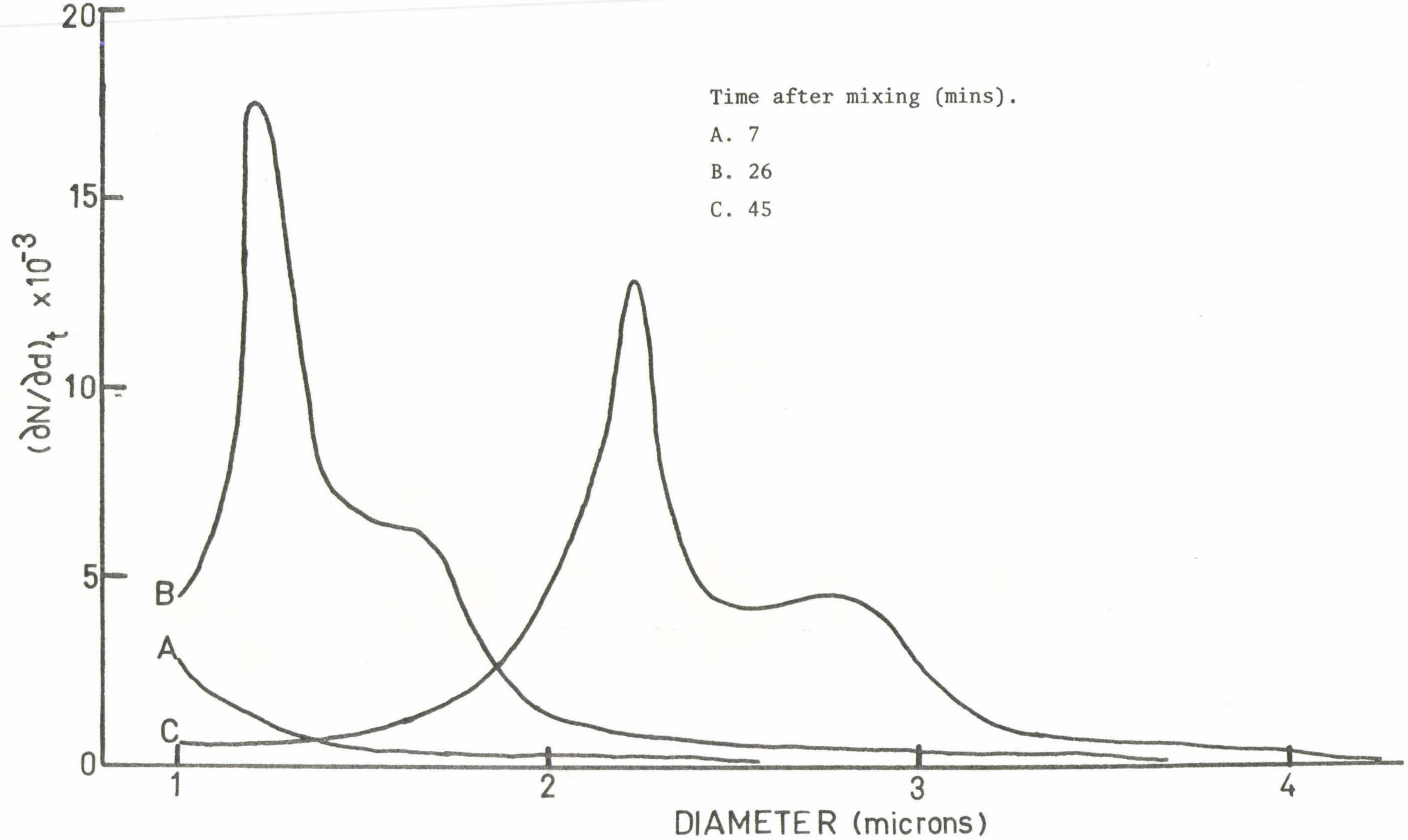

FIGURE 28. Nickel heptoximate size distributions ($c_0 = 3.75 \times 10^{-4}$M).

TABLE 10

Variation of the total number of nickel heptoximate crystals formed with time.

$c_o = 1.25 \times 10^{-3}$ M		$c_o = 1.0 \times 10^{-3}$ M	
Total Number $\times 10^{-6}$	Time (secs)	Total Number $\times 10^{-6}$	Time (secs)
1.5	23	0.11	45
4.9	41	0.23	60
5.5	60	3.2	90
7.2	60	4.9	90
9.2	80	6.9	120
17.6	100	7.6	150
33.8	180	11.2	180
34.8	300	12.8	180
		14.2	210
		13.5	270
		11.4	300
		11.2	360
		13.6	360

TABLE 11

Variation of the total number of nickel heptoximate crystals formed with time.

$c_o = 7.5 \times 10^{-4}$ M		$c_o = 3.75 \times 10^{-4}$ M	
Total Number $\times 10^{-4}$	Time (secs)	Total Number $\times 10^{-4}$	Time (mins)
1.6	100	0.11	2
2.8	140	0.40	4
5.4	160	0.75	7
8.2	180	1.5	9.5
12.5	210	3.4	12
17.7	251	3.6	15
17.1	313	5.9	20
16.7	600	7.8	26
10.9	1260	7.7	45

TABLE 12

Variation of the total number of nickel heptoximate crystals formed with time.

$c_o = 5 \times 10^{-4}$ M

Total Number $\times 10^{-4}$	Time (mins)	Total Number $\times 10^{-4}$	Time (mins)
1.4	2.0	33.4	9.75
4.7	3.75	33.5	11.0
8.7	4.65	33.4	11.8
14.4	5.3	26.6	18.0
19.9	6.3	30.6	23.0
30.6	7.4	28.7	31.0
32.7	8.2	27.3	38.0

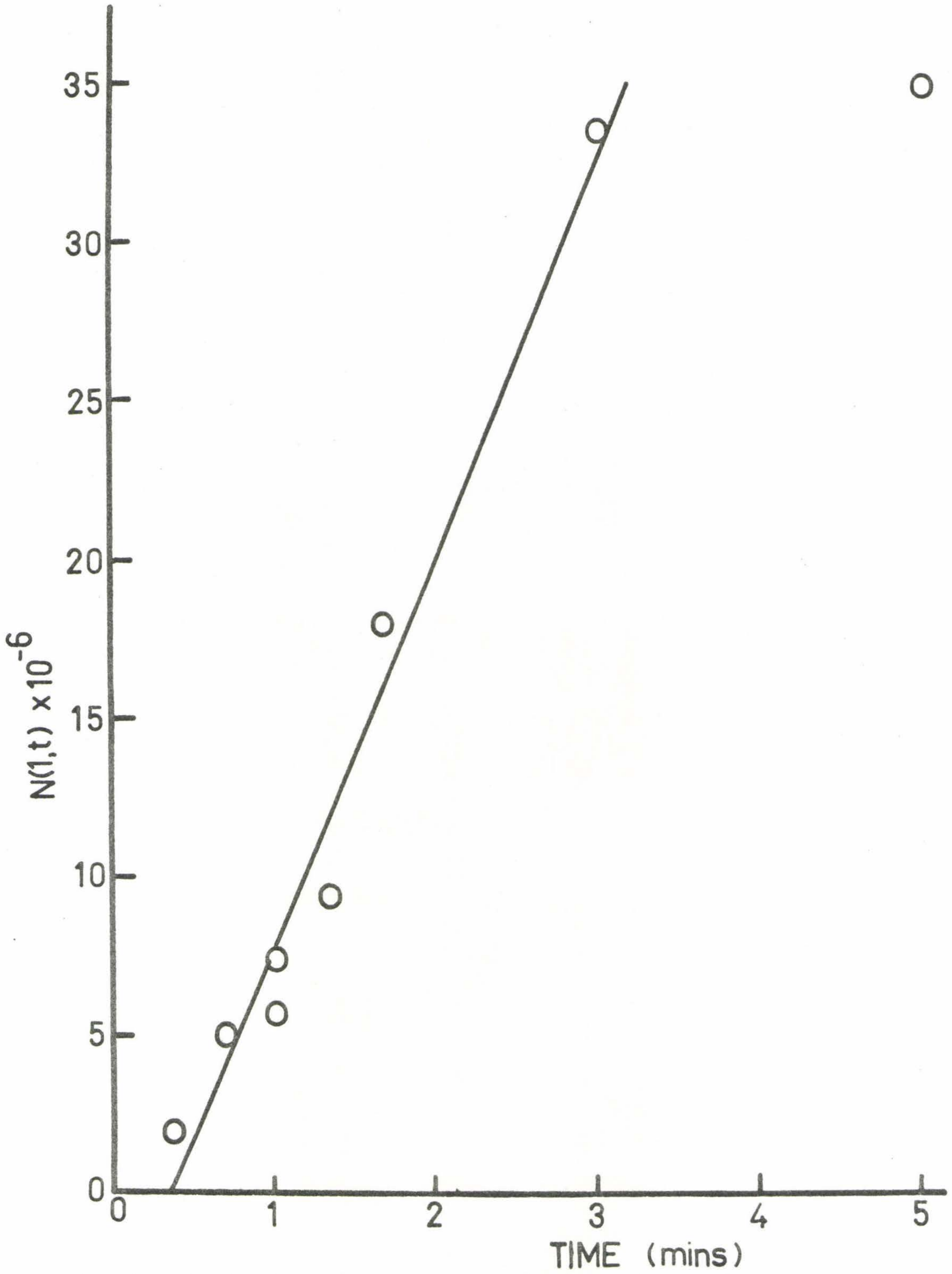

FIGURE 29. Variation of the number of nickel heptoximate crystals formed with time ($c_0 = 1.25 \times 10^{-3}$M).

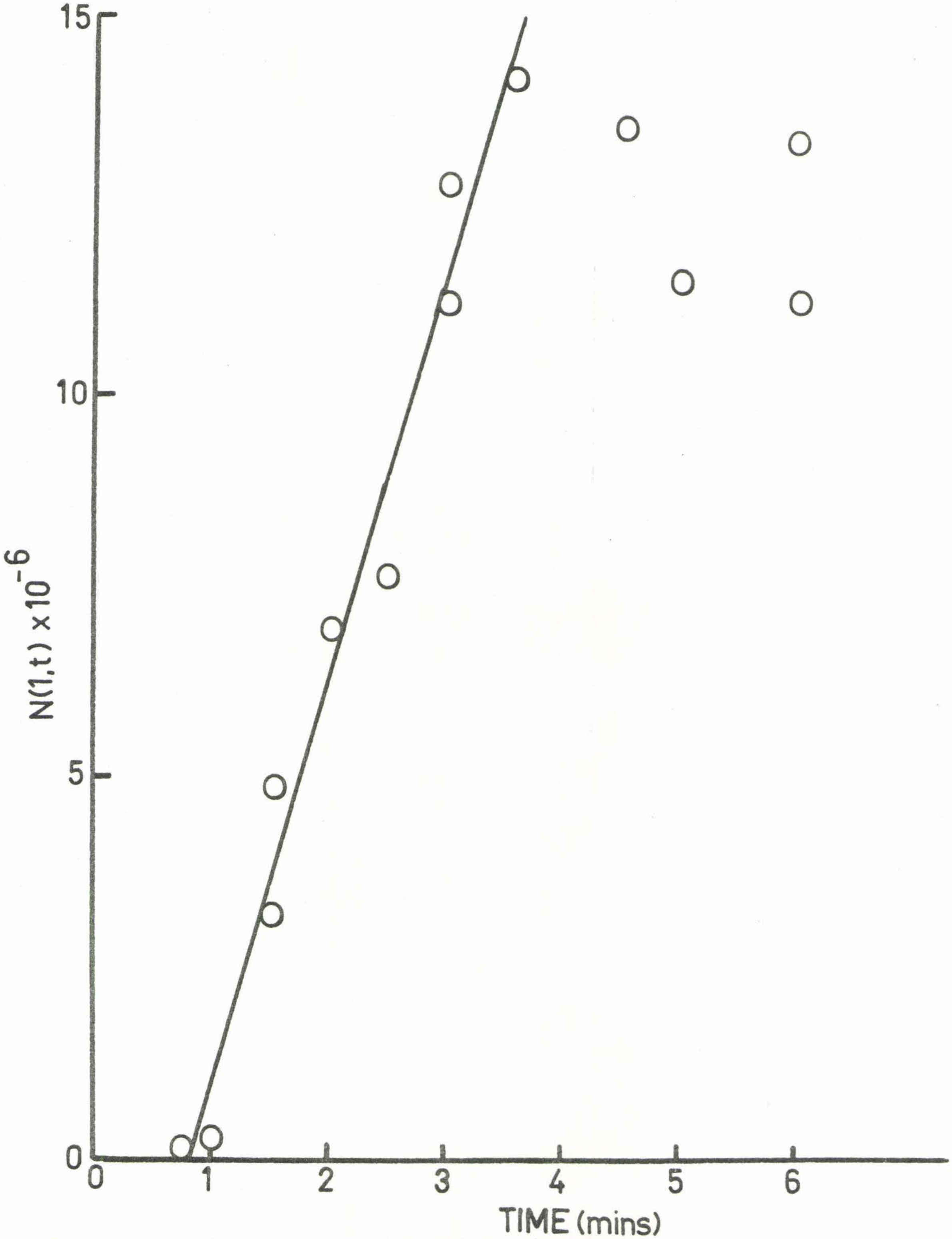

FIGURE 30. Variation of the number of nickel heptoximate crystals formed with time (c_0= 1.0 x 10^{-3}M).

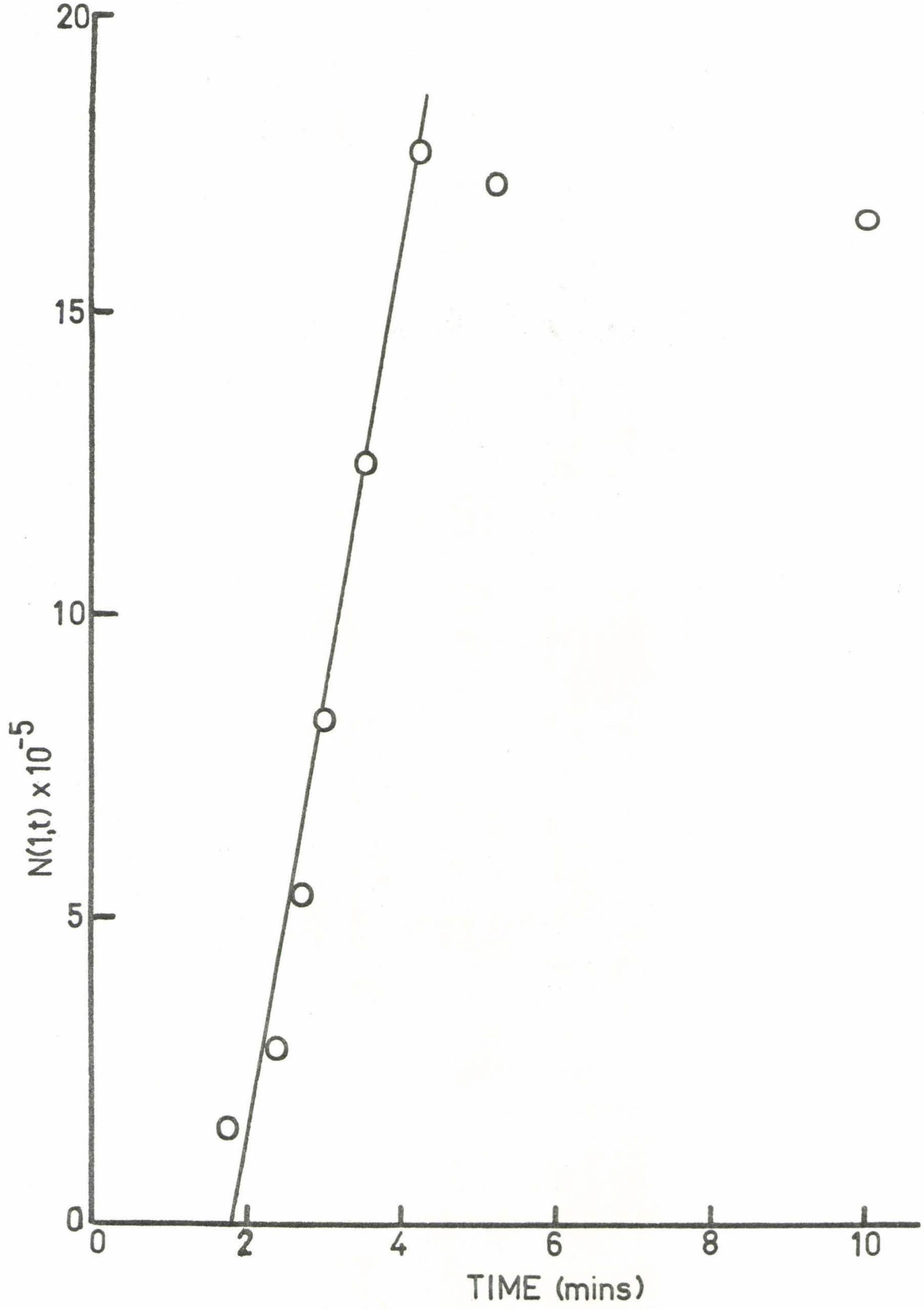

FIGURE 31. Variation of the number of nickel heptoximate crystals formed with time ($c_0 = 7.5 \times 10^{-4}M$).

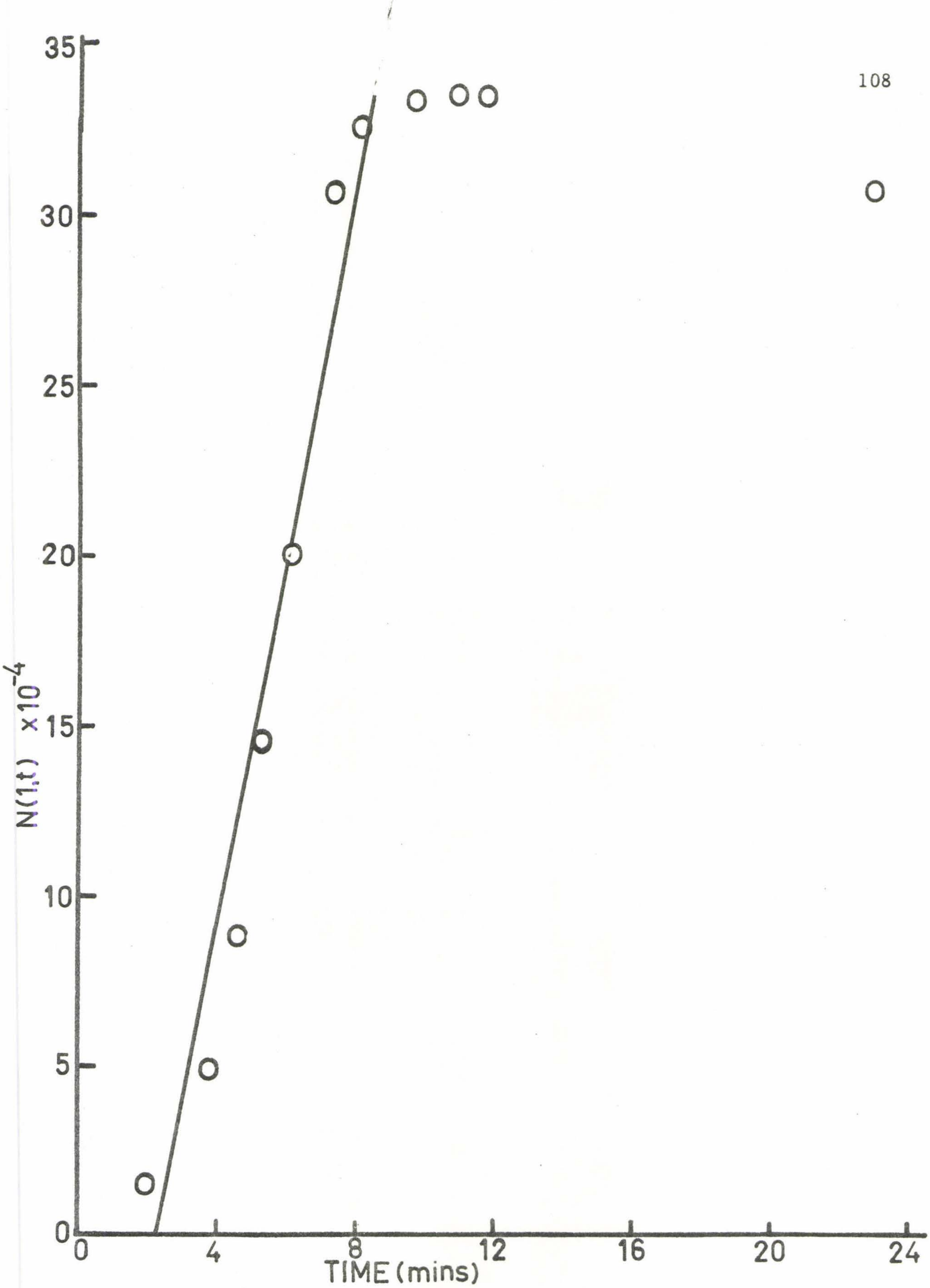

FIGURE 32. Variation of the number of nickel heptoximate crystals formed with time ($c_0 = 5.0 \times 10^{-4}$M).

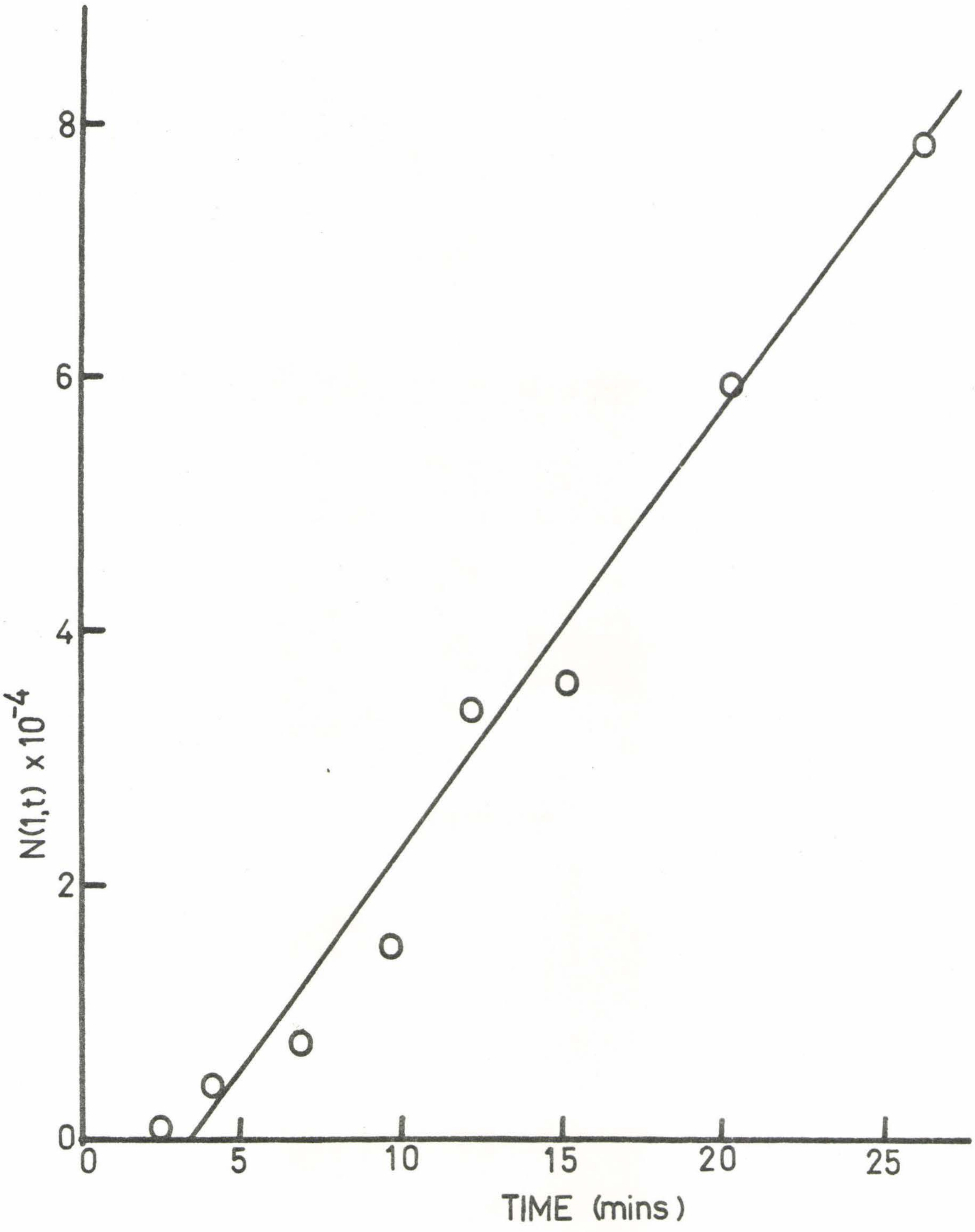

FIGURE 33. Variation of the number of nickel heptoximate crystals formed with time ($c_0 = 3.75 \times 10^{-4}$ M).

TABLE 13

Variation of the nucleation rate with supersaturation for nickel heptoximate.

c_o (moles litre^{-1})	S	J ($cm^{-3}sec^{-2}$)	log S	log J	$1/(\log S)^2$
1.25×10^{-3}	3.12×10^2	2.12×10^5	2.49	5.32	0.161
1.00×10^{-3}	2.50×10^2	9.34×10^4	2.39	4.97	0.174
0.75×10^{-3}	1.87×10^2	1.13×10^4	2.27	4.05	0.194
5.00×10^{-4}	1.25×10^2	9.08×10^2	2.09	2.96	0.227
3.75×10^{-4}	9.33×10^1	5.89×10^1	1.97	1.77	0.257
2.50×10^{-4}	6.16×10^1	1	1.79	0	0.310

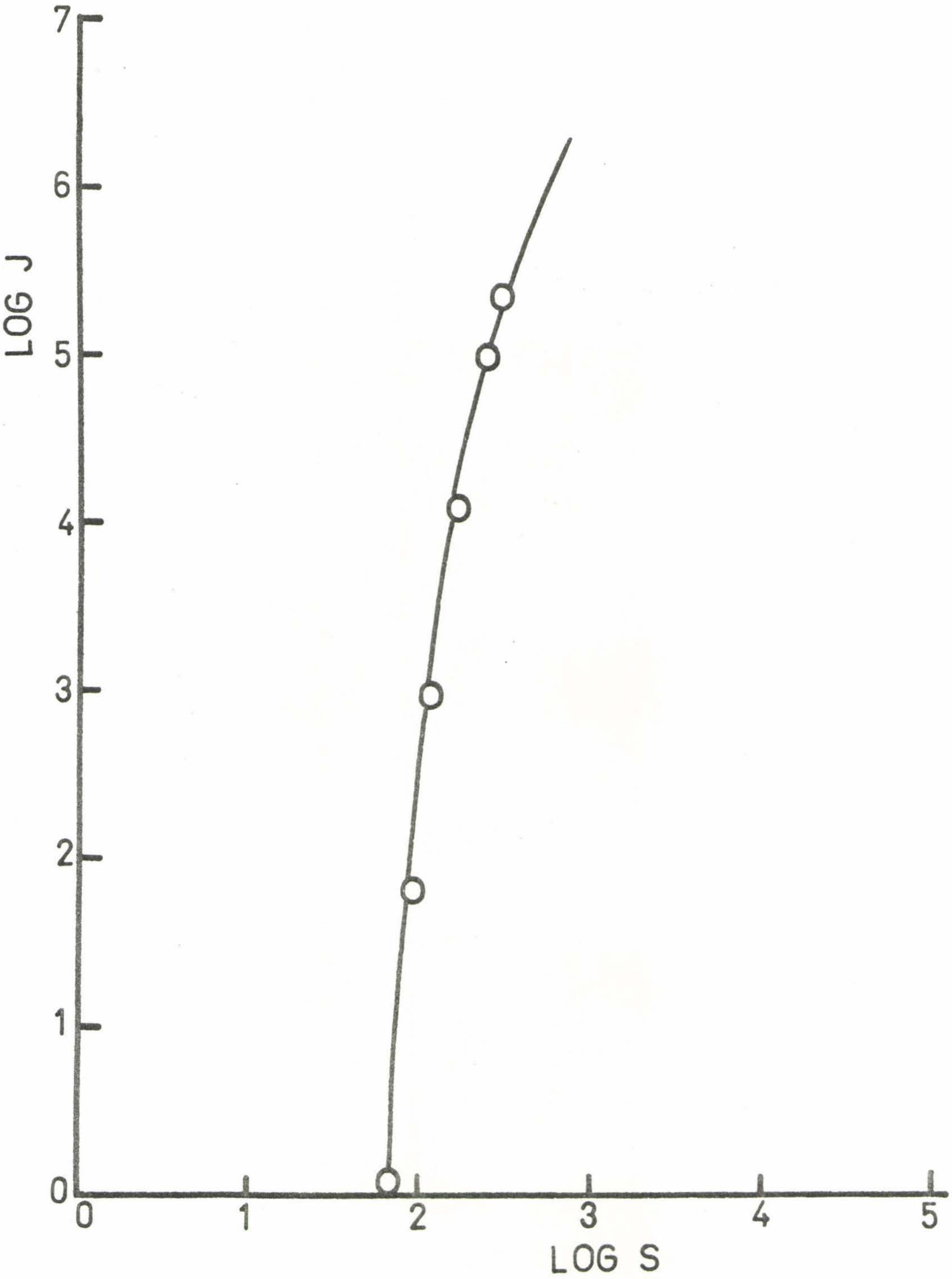

FIGURE 34. Variation of log J with log S for nickel heptoximate.

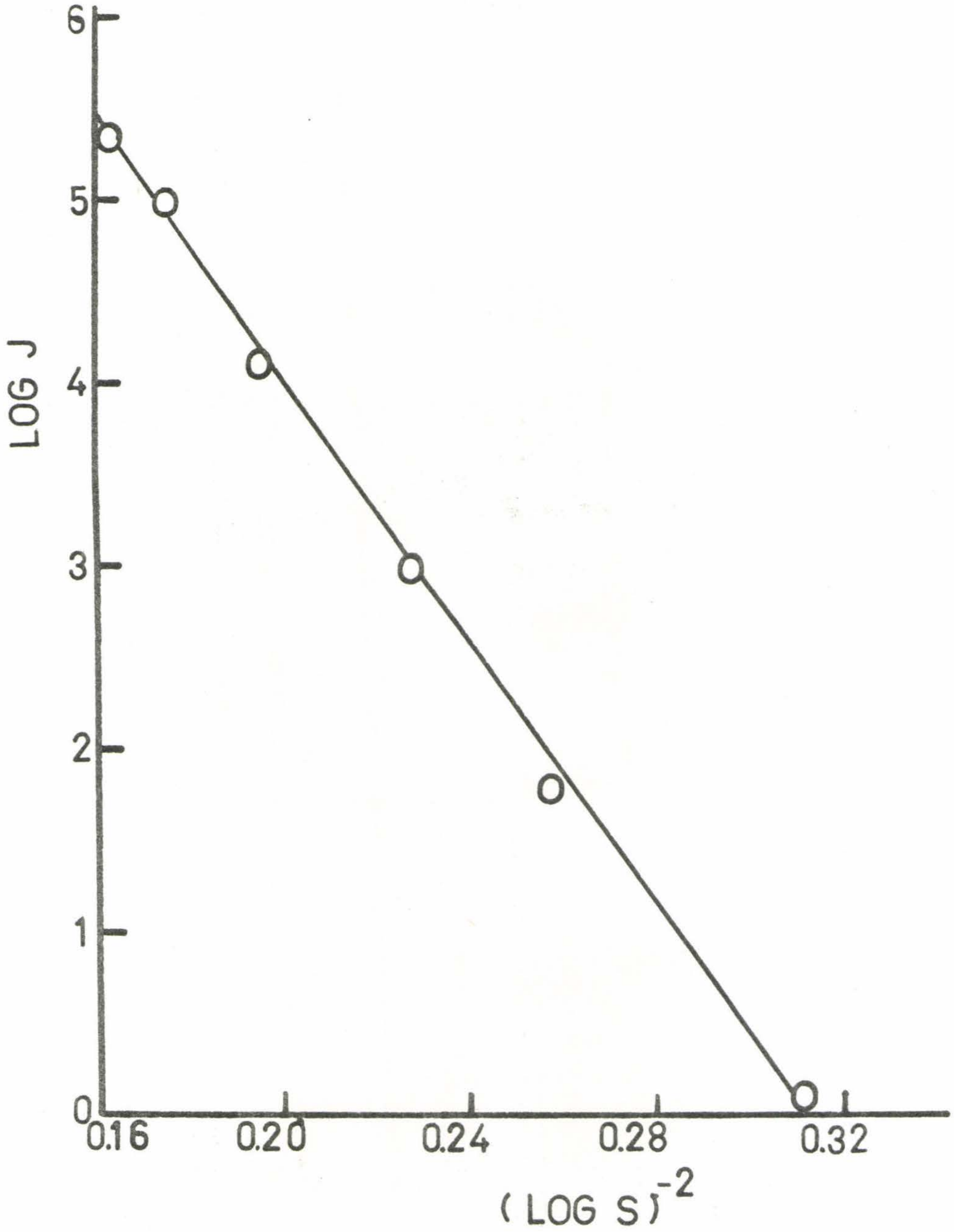

FIGURE 35. Variation of log J with $(\log S)^{-2}$ for nickel heptoximate.

volume, calculated from the unit cell dimensions, is 3.31×10^{-22} cm^3. The molecular volume used in subsequent calculations for nickel heptoximate was 3.5×10^{-22} cm^3.

Figure 35 is a plot of log J versus $(\log S)^{-2}$ for nickel heptoximate. The relationship is linear satisfying the equation relating J to S for homogeneous nucleation. The logarithm of the pre-exponential factor, A, obtained by extrapolation of the straight line to $(\log S)^{-2} = 0$ is 11.26. The values of the surface free energy and the number of molecules in the nucleus calculated from the slope of the line and Equation [15] are 13.2 $ergs/cm^2$ and 13 molecules respectively. The surface free energy is calculated assuming that the shape of the nucleus is a rod of dimensions 1 × 1 × 10 1. If a spherical nucleus is assumed the surface free energy is found to be 24 ergs cm^{-2}.

3.D.3. The nucleation of nickel nioximate

The sequence of experiments carried out with nickel nioximate was the same as in the cases of the two chelates already discussed (Sections 3.D.1. and 3.D.2.). Firstly, as in the case of heptoxime, crystals formed at pH 7 were too small to be detected by the counter. Banks and Anderson (101) have measured the solubility product and intrinsic solubility of nickel nioximate. At pH 7 they are $10^{-28.80}$ and 10^{-11} respectively, i.e., much less soluble than nickel dimethylglyoximate at pH 7. Using a microscope crystals of nickel nioximate formed in a precipitation at pH 7 were seen to behave similarly to those of nickel heptoximate. Namely, the number of crystals increased and their size became smaller as the initial supersaturation was increased. This behaviour indicated that homogeneous nucleation was taking place. Subsequent precipitations were carried out at pH 2.8, the crystals formed at this pH were just large enough to be detected by the counter. The solubility at this pH was 1.5×10^{-6} M (Section 2.C.8.). This value was used to calculate the supersaturation S. As in the case of the two previous chelates studied, the activity of nickel nioximate was taken to be the same as its concentration. The initial concentrations of nickel nioximate were 5.00×10^{-4} M, 3.75×10^{-4} M, 2.50×10^{-4} M, 2.00×10^{-4} M and 1.25×10^{-4} M.

The variation of the size distributions of the crystals formed with time was measured for each of these initial concentrations. The size distributions obtained are shown in Figures 36 to 39 inclusive. The features of these distributions are not as clear as those of the previous two chelates studied because for most initial concentrations a substantial proportion of the crystals were not detectable by the counter. Tables 14 and 15 and Figures 40 to 43 inclusive show the variation with time of the total numbers of crystals above the level of the detector. These are plots of N(1,t) versus t and the slope, $(\frac{\partial N}{\partial t})_{d=1}$, of the linear portions of curves is equated with $(\frac{\partial N}{\partial t})_{d=0}$, the rate of nucleation J.

Table 16 lists the values of J, S, log J, log S and $(\log S)^{-2}$. Figure 44 shows the variation of log J with log S. The values of log J at the highest supersaturation is probably low because of the inability of the counter to detect all of the crystals formed.

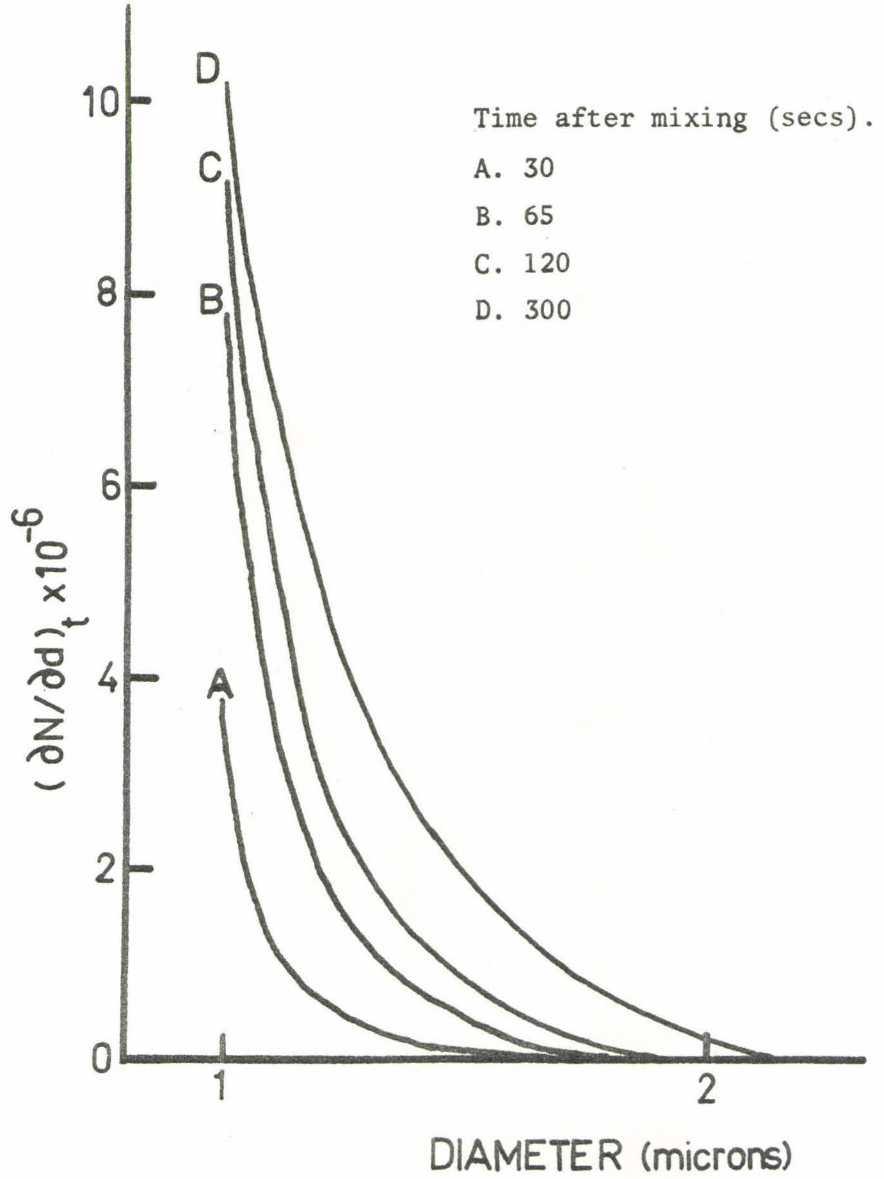

FIGURE 36. Nickel nioximate size distributions ($c_0 = 5.0 \times 10^{-4}$M).

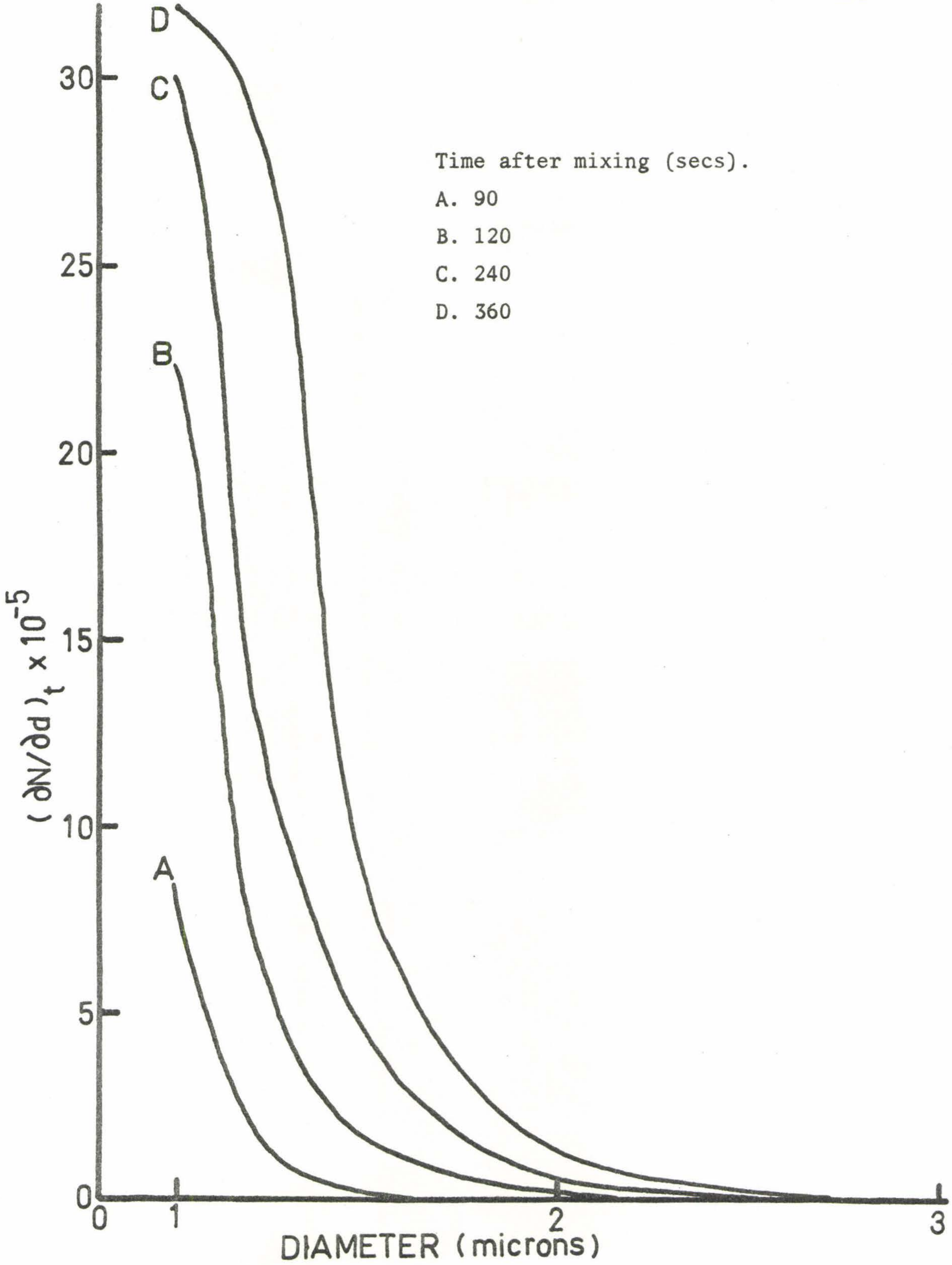

FIGURE 37. Nickel nioximate size distributions ($c_0 = 3.75 \times 10^{-4}$M).

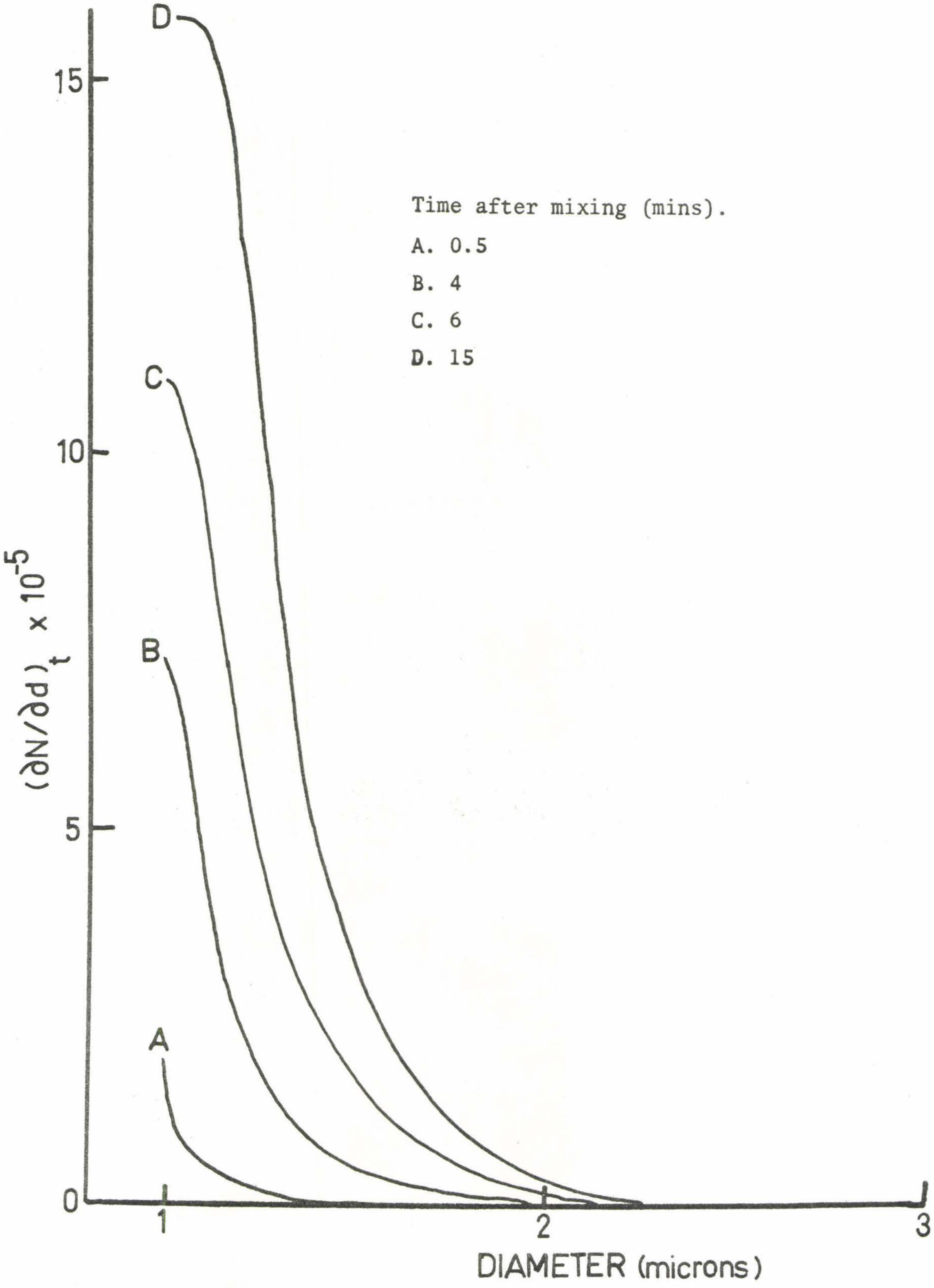

FIGURE 38. Nickel nioximate size distributions ($c_0 = 2.5 \times 10^{-4}$M).

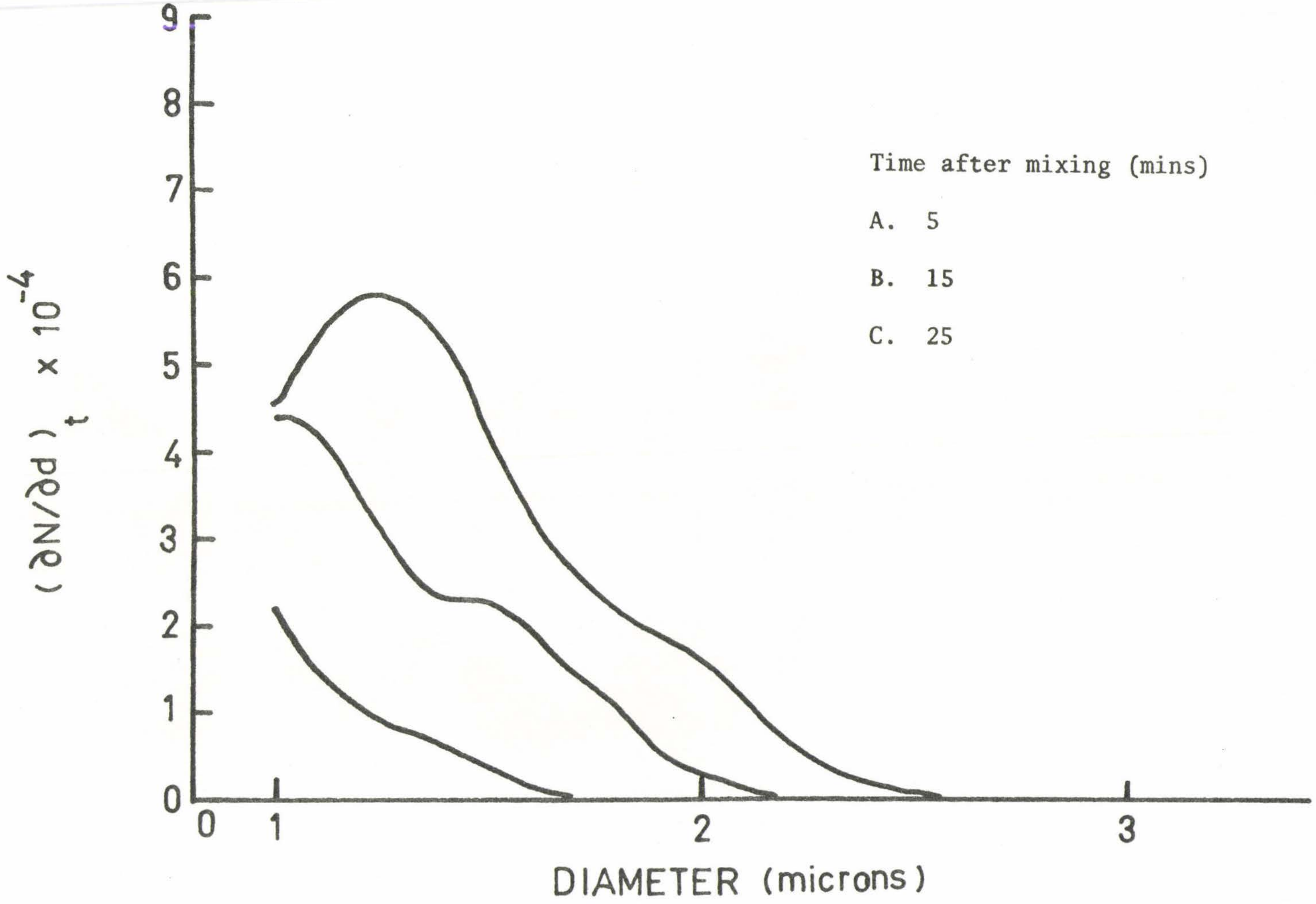

FIGURE 39. Nickel nioximate size distributions ($c_0 = 2.0 \times 10^{-4}$M).

TABLE 14

Variation of the total number of nickel nioximate crystals formed with time.

$c_o = 5.0 \times 10^{-4}$ M		$c_o = 3.75 \times 10^{-4}$ M	
Total Number $\times 10^{-6}$	Time (secs)	Total Number $\times 10^{-6}$	Time (secs)
1.43	15	0.22	30
3.1	30	0.53	60
9.9	65	1.2	90
14.2	120	2.9	120
22.1	150	4.3	120
22.9	300	7.4	180
23.3	510	8.3	240
		10.6	270
		13.7	300
		14.2	360

TABLE 15

Variation of the total number of nickel nioximate crystals formed with time.

$c_o = 2.5 \times 10^{-4}$ M		$c_o = 2.0 \times 10^{-4}$ M	
Total Number $\times 10^{-5}$	Time (mins)	Total Number $\times 10^{-4}$	Time (mins)
3.4	3	0.7	2
2.5	3	2.1	4
8.1	4	2.6	5
13.6	6	4.9	7
14.8	7	10.5	10
24.5	9	19.1	12
49.8	15	20.4	14
43.2	16	25.1	17.5
41.6	30	34.2	20
		37.9	24
		38.8	26

TABLE 16

Variation of the nucleation rate with supersaturation for nickel nioximate.

c_O (moles litre^{-1})	S	J (cm^{-3}sec^{-1})	log S	log J	1/(log S)^2
5.0×10^{-4}	3.33×10^2	1.43×10^5	2.52	5.16	0.157
3.75×10^{-4}	2.49×10^2	5.13×10^4	2.39	4.71	0.174
2.5×10^{-4}	1.66×10^2	5.89×10^3	2.22	3.77	0.202
2.0×10^{-4}	1.33×10^2	2.88×10^2	2.12	2.46	0.221
1.25×10^{-4}	8.32×10^1	1	1.92	0	0.271

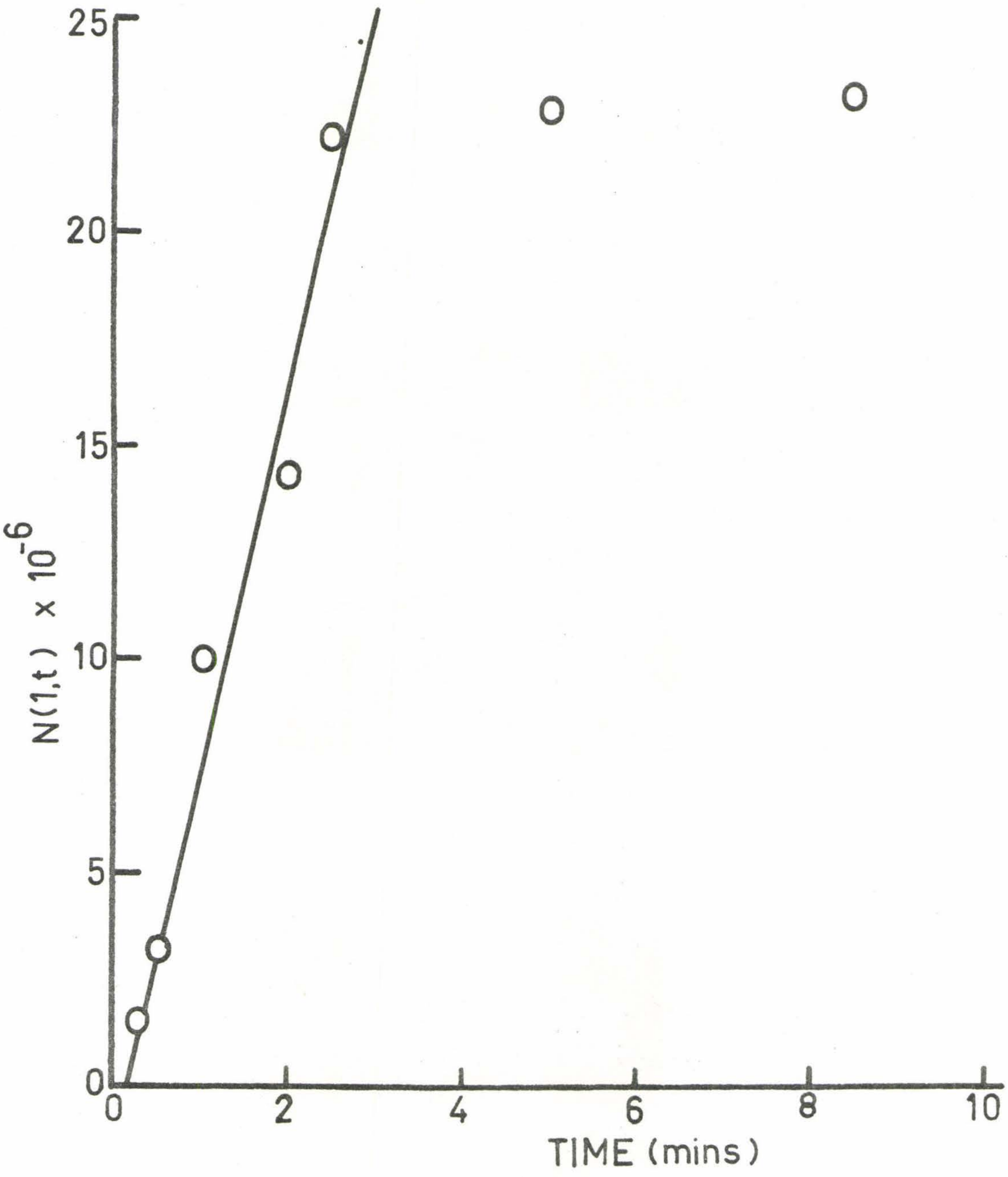

FIGURE 40. Variation of the number of nickel nioximate crystals formed with time ($c_0 = 5.0 \times 10^{-4}$M).

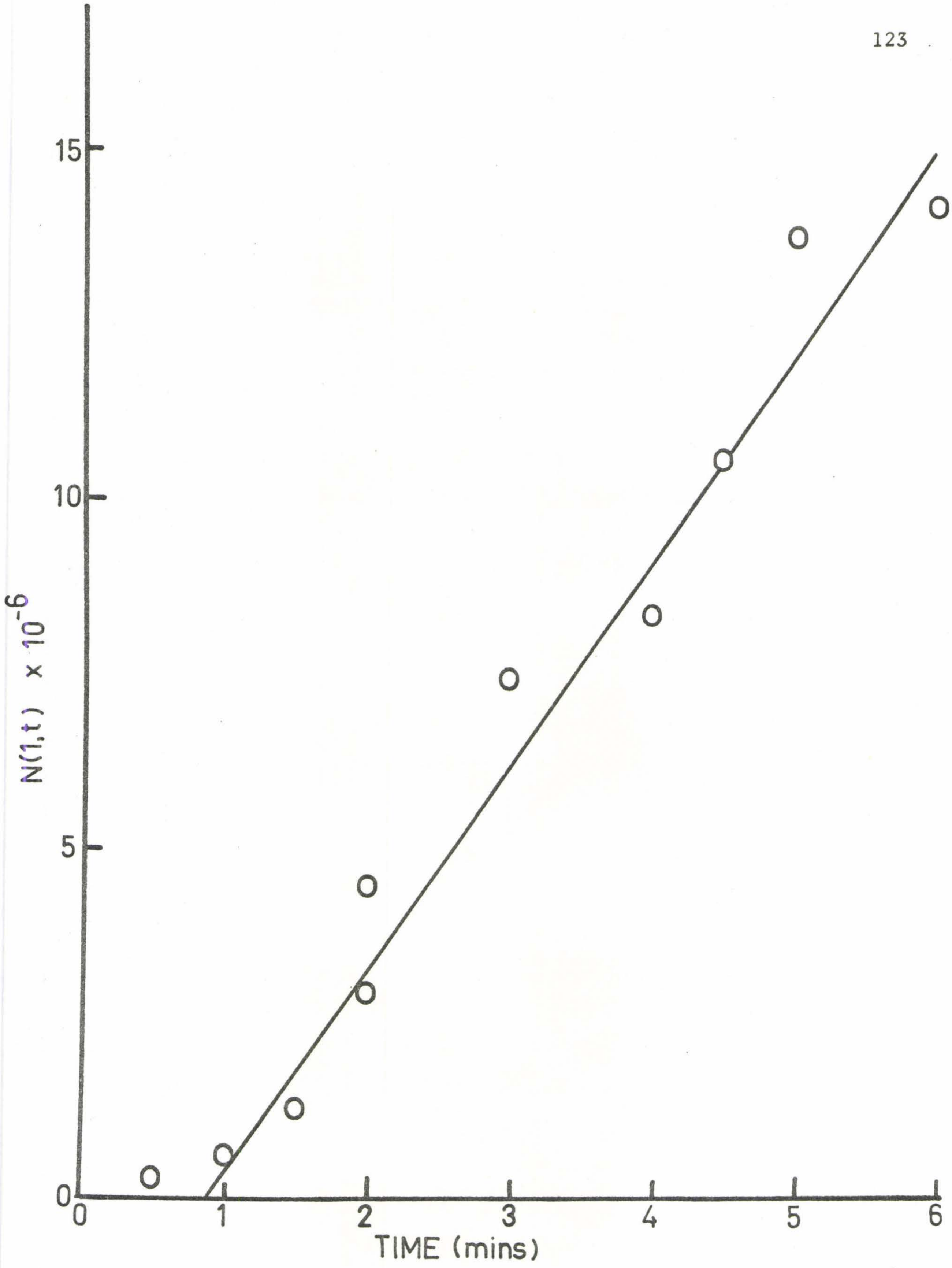

FIGURE 41. Variation of the number of nickel nioximate crystals formed with time ($c_0 = 3.75 \times 10^{-4}$M).

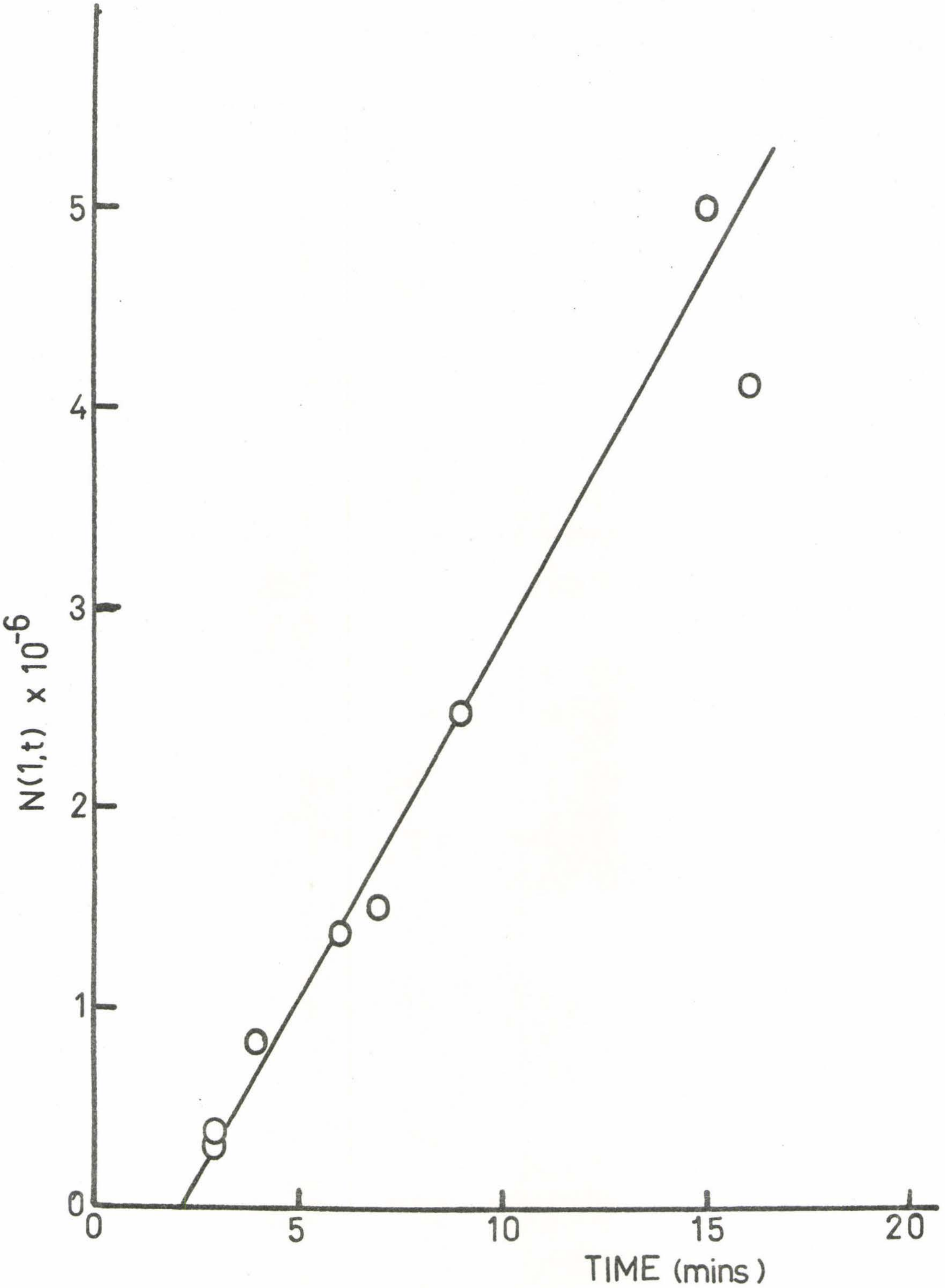

FIGURE 42. Variation of the number of nickel nioximate crystals formed with time (c_0= 2.5 x 10^{-4}M).

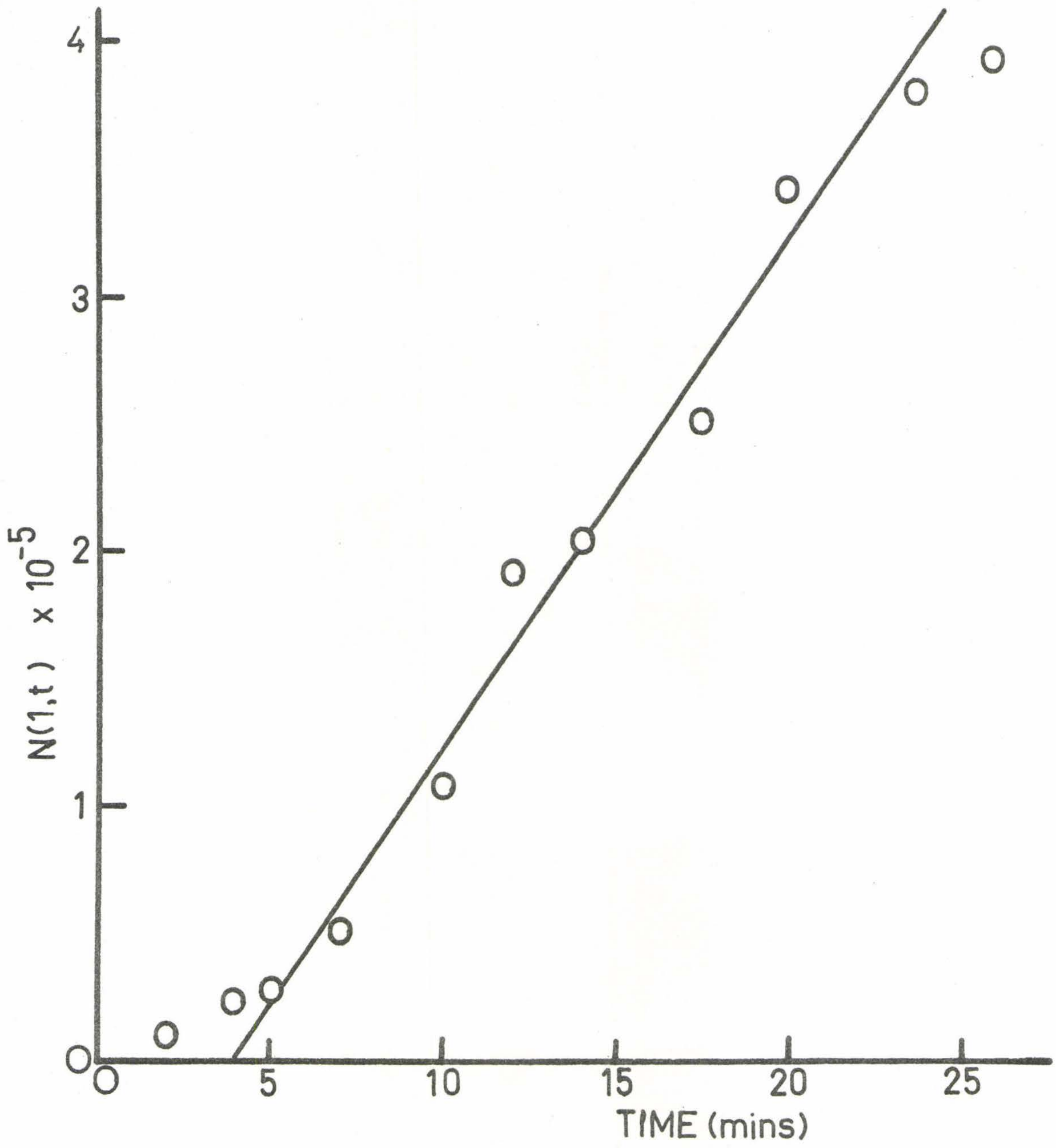

FIGURE 43. Variation of the number of nickel nioximate crystals formed with time (c_0= 2.0 x 10^{-4}M).

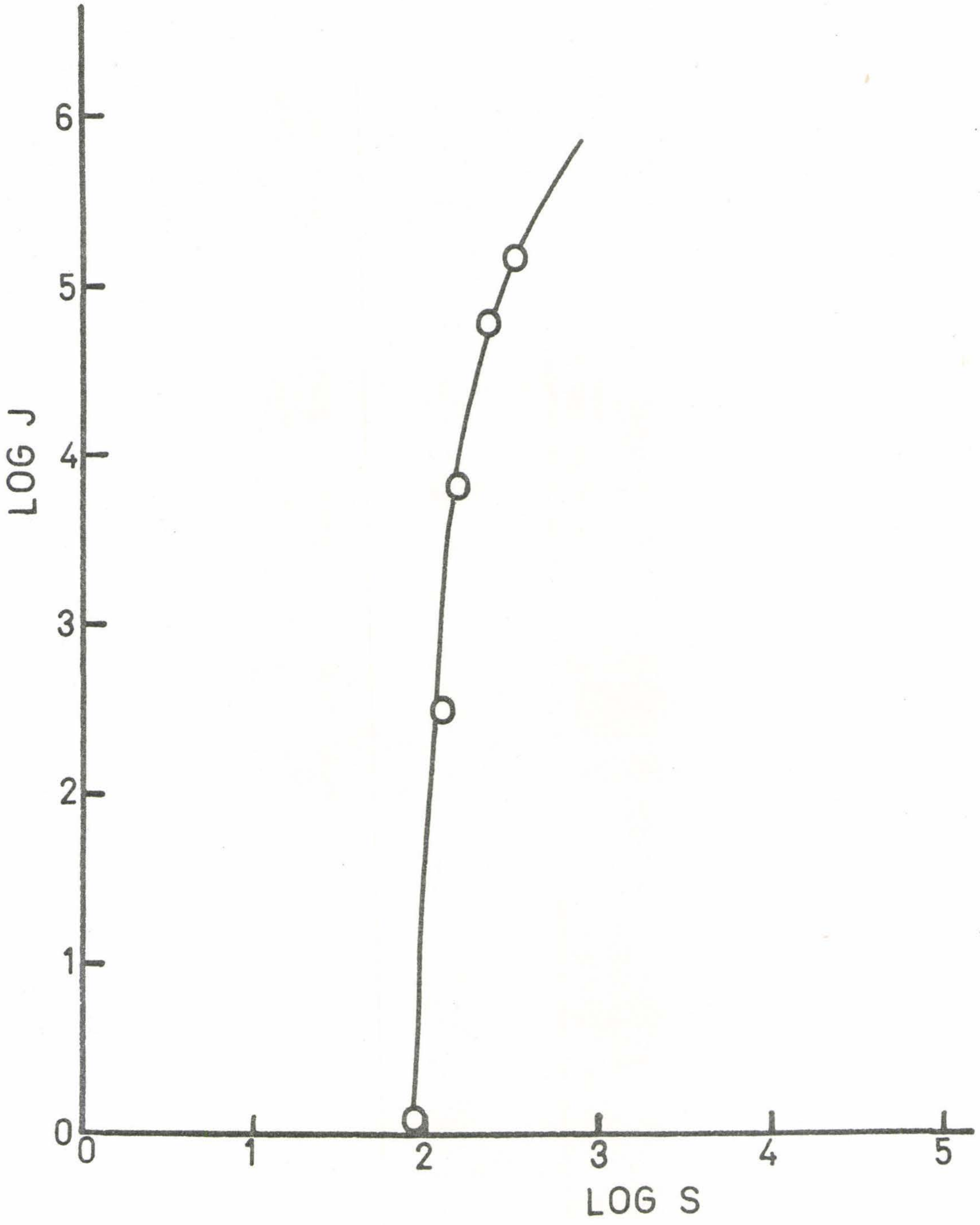

FIGURE 44. Variation of log J with log S for nickel nioximate.

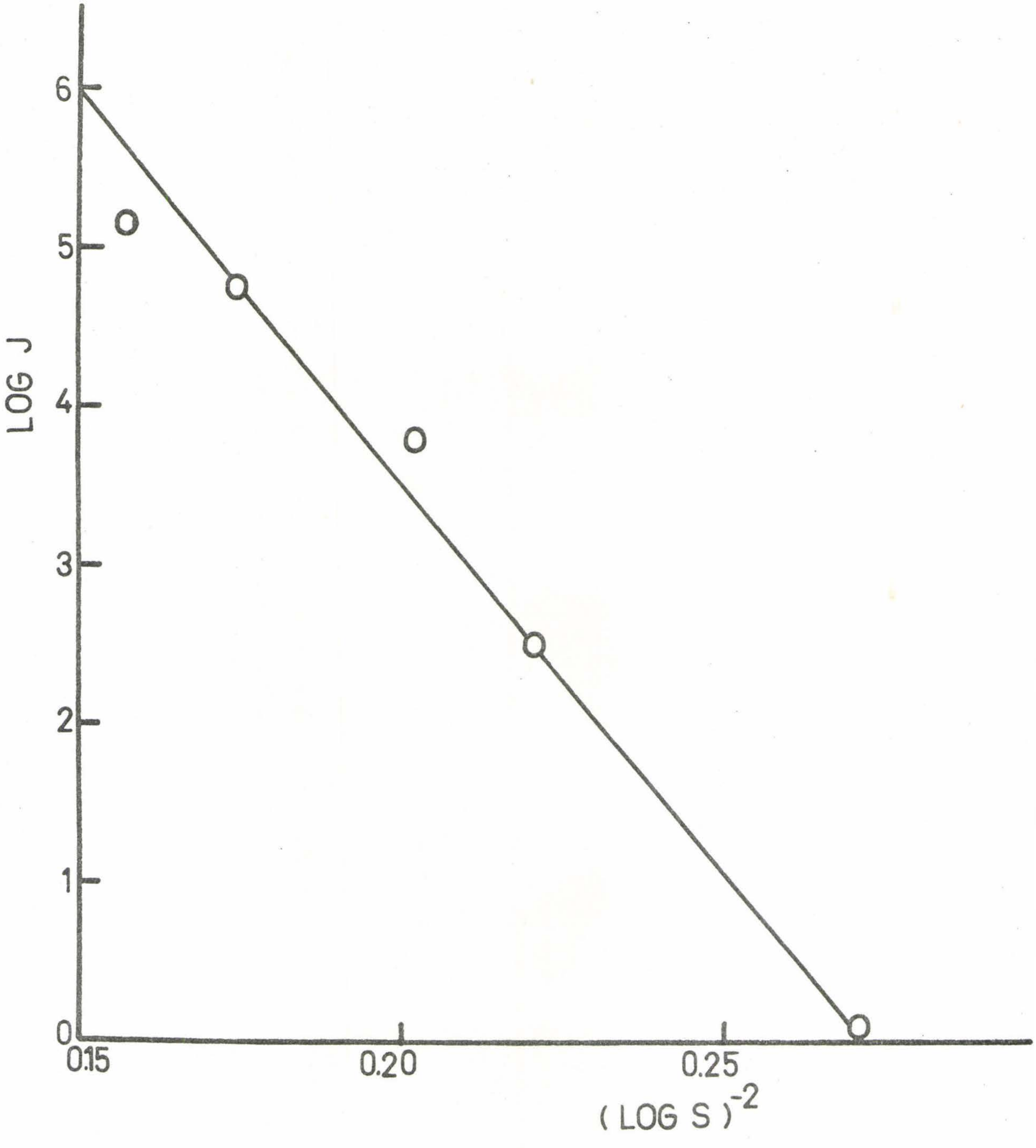

FIGURE 45. Variation of log J with (log S)$^{-2}$ for nickel nioximate.

Figure 45 shows the variation of log J with $(\log S)^{-2}$. The relationship is linear, satisfying the relationship calculated assuming a homogeneous nucleation mechanism. Log A, found by extrapolation to $(\log S)^{-2} = 0$ is 13.55. The slope of the straight line gives a value, for the surface free energy σ, of 13.5 ergs cm^{-2} assuming a rod shaped nucleus of dimensions 1 × 1 × 10 1. If a spherical nucleus is assumed σ is found to be 24 ergs cm^{-2}. The critical supersaturation S*, corresponding to J = 1, is 96 and the corresponding critical nucleus contains 14 molecules.

3.D.4. The evaluation of the nucleation rate J

The most important parameter measured in the preceeding experiments was the rate of nucleation J. As has been stated earlier, one of the purposes of this thesis was to measure the functional dependence of the rate of nucleation J on the supersaturation S. In order to measure J in an experiment in which the supersaturation is built up rapidly by direct mixing several assumptions must be made. The first is that a steady state equilibrium is attained between clusters of various sizes giving a constant rate of nucleation until the supersaturation is depleted by nucleation and crystal growth. The second is that the supersaturation is immediately constant throughout the solution after mixing. If local excesses of supersaturation are attained then there will be large variations in the rate of nucleation in different parts of the solution. Unfortunately, it is not possible to experimentally test either of the above assumptions. If local excesses of supersaturation do exist then it would be difficult to reproduce rates of nucleation from one experiment to another. This was indeed found experimentally but this irreproducibility is equally well accounted for by the critical exponential dependence, as proposed by the classical nucleation theory, of the rate of nucleation on the supersaturation.

The rate of nucleation is defined as the rate at which nuclei add one molecule to become larger than the critical nucleus. It is not possible to observe this event directly and any attempt to measure J from measurements made on detectable sizes must necessarily, therefore, contain approximations and errors. Moreover it is very important to ensure that the variation in these measurements at detectable sizes do in fact result from a variation in J and not from a variation in some other parameter, e.g., crystal growth.

In these experiments the variation, with time, of the total number of crystals detectable by the counter, N(1,t), was measured. For the three nickel oximates studied and for all initial supersaturations for each chelate, the plots of N(1,t) versus time showed the same general shape. They all had an initial linear portion which rose to a maximum, e.g., Figures 16, 18, 30, and 31. Therefore from this linear portion the rate of appearance of crystals to the detector, $(\frac{\partial N}{\partial t})_{d=1}$, could be measured for each initial supersaturation. The relationship between this parameter, $(\frac{\partial N}{\partial t})_{d=1}$, and the rate of nucleation, $(\frac{\partial N}{\partial t})_{d=0}$, will be a function of the rate of crystal growth. If the rate of growth is simply dependent upon the size of the crystal then it is easily shown that $(\frac{\partial N}{\partial t})_{d=1} = (\frac{\partial N}{\partial t})_{d=0}$. However for all the types of crystal growth described in Section (1.D.2) the rate of crystal growth dr/dt is also dependent on some power of the concentration, c. The concentration changes throughout the precipitation process, in a sigmoidal fashion, the asymptotes being c_o, the initial concentration, and s, the final concentration (the equilibrium solubility). The exact shape of this sigmoidal curve is dependent on the relative rates of crystal growth and nucleation. Two extreme cases may be identified. The first is the instance in which the rate of crystal growth is very fast, so that a crystal reaches a detectable size almost instantly after it has nucleated and that the growth time is small compared with the time over which nucleation occurs. In this case it is a very good approximation to put the rate of nucleation equal to the rate of appearance. The second extreme is one in which crystals grow very slowly and do not reach detectable size until after nucleation has ceased. In this instance crystals will be very monodisperse and will all grow to a detectable size under approximately the same supersaturation conditions. Here again the rate of nucleation may be equated with the rate of appearance. In the experiments reported here the existence of a linear relationship between the total number formed and time also indicates that the rate of appearance is a good approximation to the rate of nucleation. If the rate of crystal growth had a major effect the relationship would be curved. This can be shown from mathematical considerations. Lastly, the magnitude of errors in the measurement of J must be considered with reference to the many decades over which J is measured (see Figure 21). Large errors in the measurement of J will therefore be minor when log J is plotted against log S. For these reasons therefore the rate of nucleation J was equated with the rate of appearance of crystals with diameter above 1 μ.

Most authors have measured the rate of nucleation in this way. In droplet experiments with both pure liquids and aqueous solutions, crystals are assumed to be visible immediately after nucleation. For measurements of the rate of nucleation in bulk solution Nielsen (67) has used a slightly different approach. This approach has been to find the rate of nucleation by dividing the total number $N(0,\infty)$ of particles formed by the induction period. The induction period is an ill-defined period of time depending largely on how it is measured. It is often measured as that time occurring after mixing at which crystals just begin to be detected. The induction period is then a function of the detection method and has been determined visually (67) or photographically (60). Nielsen (104) has also shown that if the induction period is defined mathematically as that period of time, after mixing, at which the degree of reaction α ($\alpha = 1 - c_t/c_o$) is equal to 0.5, then the rate of nucleation J, is approximately equal to $N(0,\infty)/t_{0.5}$, for crystal growth that is either diffusion controlled or polynucleation controlled. The rate of nucleation is here equated with the rate of appearance of crystals. This rate is the slope of the total number of crystals versus time plot. The slope may be approximately defined as the total number of particles formed divided by the time taken for the total number of appear. This time will certainly be of the same order of magnitude as the induction period irrespective of how it is defined.

The calculation of J from the induction period and its calculation from the rate of appearance of crystals will therefore be of the same order of magnitude. As J varies drastically with S and the results are drawn in log-log form (Figures 22, 34, 44) the calculation of J using either of these methods will show curves with similar functional dependencies of J on S.

3.D.5. The nucleation parameters A, i* ,σ and S*

The nucleation parameters, A, i*, σ and S* found for the three nickel dioximates studied here are shown in Table 17. Experimentally the value of the pre-exponential factor A (Equation [15]) can only be found from a measurement of the functional dependence of J on S. Most authors have not measured this dependence and in order to calculate other nucleation parameters A is usually assumed to be approximately 10^{30}. Where the value of A has been measured experimentally its value has been found to lie in the range 10^3 - 10^{25} (80,90,91), many orders of magnitude less than the value calculated (Table 2). The values obtained in the present work were also much lower than 10^{30}. The values of A obtained, however, involve extrapolation to $(\log S)^{-2} = 0$ on the plot of log J versus $(\log S)^{-2}$ (Figures 23, 35, 45). While the plots are linear in the region shown it is not known what the relationship is at values of $(\log S)^{-2}$ closer to zero. The values are however in good agreement for those obtained (76) for other nickel and palladium dioximates. The explanation of the discrepancy between the values of A obtained here and those predicted

TABLE 17

Nucleation parameters for the nickel dioximates

Compound	A cm^{-3} sec^{-1}	σ ergs cm^{-2}	i*	S*
Nickel dimethylglyoximate	9.4	13.0	12	77
Nickel heptoximate	11.3	13.2	13	65
Nickel nioximate	13.6	13.5	14	96

by the classical theory may be due to errors in the theory. Dunning (71) has pointed out that entropy effects may play an important role in determining the value of the pre-exponential factor. These effects are neglected in the classical theory. The entropy change due to desolvation of the monomers before cluster formation and also the structural complexity of the monomers may be cited here. It is interesting to note that in the present study the value of A for nickel dimethylglyoximate is the lowest. Of the chelates studied nickel dimethylglyoximate has been shown (101) to be most solvated.

The values of σ obtained for the chelates studied here may be compared with the values obtained by Walton and Thompson (71) for nickel dimethylglyoximate and by Hileman and Velazquez (76) for nickel and palladium nioximates and heptoximates (Table 2). The values of σ found in the present study were lower, by a factor of two to three, than those found by Walton and Hileman. These authors, however, calculated σ assuming a spherical nucleus, whereas the values reported here are calculated assuming a rod shaped nucleus of dimensions $1 \times 1 \times 10\ l$. If a spherical nucleus is assumed these values of σ change from approximately 13 ergs cm^{-2} to 24 ergs cm^{-2}. The form of Equation [15] is such that σ is very insensitive to large changes in any parameter. In theory σ should include the energy contributed from edges, corners and faces of the crystal nucleus. The value of σ quoted here therefore is some average of all these.

The size of the critical nucleus at the critical supersaturation (the theory predicts that the size of the critical nucleus will vary with supersaturation) has attracted the interest of many authors who have attempted to relate it to the dimensions of the unit cell or to some other primary process at the molecular or ionic level. For the nickel chelates Banks and Anderson (101) have shown that they all exist in solution exclusively as the molecular monomer and not as solvated ions of Ni^{2+} and HD^- (HD^- represents the singly ionized dioxime ion). The primary process in the nucleation of these chelates is therefore the build up of clusters by the addition of molecules of $Ni(HD)_2$. The values obtained in this study are much lower than those calculated (Table 2), using a value of 10^{30} for A, by Hileman and Velazquez (76). They can be compared with other non ionic large molecules (Table 2). It does not seem reasonable in view of the assumptions made in the calculation of the various parameters and in the theory, to attempt to analyze this size in terms of unit cell dimensions.

3.E. Crystal Growth of Nickel Dioximates

As the nucleation event itself can not be directly observed it is only possible to gain information regarding it by observing the crystals after they have grown to a detectable size. The purpose of these crystal growth studies was to determine what types of crystal growth laws were followed by the nickel dioximate crystals and what implications, if any, could be drawn regarding the initial nucleation event.

The more important types of crystal growth laws have been listed in Section 1.D.2. These are diffusion controlled growth, poly-nucleation controlled growth and mono-nucleation controlled growth. It is convenient to describe the progress of any precipitation reaction in terms of α, the degree of reaction, defined as

$$\alpha = \frac{c_o - c_t}{c_o} \qquad [27]$$

where c_o is the initial concentration of solute and c_t is the concentration at time t. In general a precipitation reaction starts slowly, then accelerates and finally levels off as the supersaturation becomes closely equal to the equilibrium solubility. A plot of α versus t will therefore be sigmoidal with asymptates at $\alpha = 1$ and $\alpha = 0$ for all types of crystal growth. The final shape is complicated by competing types of growth and by transfer of growth control.

If it is assumed that heterogeneous nucleation is occurring then all crystals will start to grow at the same time. For this instance it has been shown (104) that it is possible to calculate the functional relationship between α and t for all the types of crystal growth laws and so to relate the shape of the α versus t sigmoidal curve to the type of crystal growth occurring. For diffusion, poly-nucleation and mono-nucleation controlled growth α has been related to t by equations of the type

$$t = KI \qquad [28]$$

where K is a constant depending on the type of crystal growth law, and I (a chronomal) is a function of α (this function also depends on the type of crystal growth law). These chronomals and their theoretical values for all values of α have been given by Neilsen (104) for the three types of crystal growth law mentioned above. Experimentally these types of crystal growth may then be distinguished by plotting the experimental time versus the values of the chronomals for the corresponding experimental α. The plot should be linear, as given by Equation [28], when a particular growth law is obeyed.

When homogeneous nucleation is considered the situation is much more complicated and it is not possible to rigorously solve the equations relating the degree of reaction to time. The first step in the approximate evaluation of this relationship is to calculate the concentration of unprecipitated solute at any time t. This concentration may be written (106, 107)

$$c_t = c_o - \frac{\rho\omega}{w}\int_0^t J(c_\tau)r_{\tau,t}^{\,3}\,d\tau \qquad [29]$$

where ρ is the crystal density,

ω is a shape factor,

w is the molecular weight of the solute,

$r_{\tau,t}$ is the radius, at time t, of a crystal nucleated at time τ,

$J(c_\tau)$ is the rate of nucleation at concentration c_τ,

and ωr^3 is the volume of any crystal.

It was shown earlier (Section 1.D.2.) that if the relationship between log J and log S is approximately linear over several decades, the rate of nucleation is given by

$$J = k_n c^n \qquad [17]$$

Equation [17] is sufficiently accurate for use in Equation [29] to calculate c_t. By substituting this value for J and the value of $r_{\tau,t}$ calculated from the diffusion controlled growth law, in Equation [29] the following relationship between α and t is obtained (106,107)

$$\alpha = (\omega^2\rho^2 k_n{}^2 2^3 D^3 w^{-2})^{1/5} c_o{}^{(2n+1)/5} \int_0^t (1-\alpha)_\tau \{\int_\tau^t (1-\alpha)_\theta d\theta\}^{3/2} d\tau \qquad [30]$$

where τ and θ are integration variables proportional to time.

Similar equations relating the degree of reaction, α, to time have been calculated (108) for homogeneous nucleation followed by poly- and mono-nucleation controlled growth. These equations cannot be rigorously solved, as they contain the integral of the time dependent degree of reaction. Important approximations may, however, be made when α is close to zero (i.e., at the beginning of the precipitation) and when α is close to 1 (i.e., at the end of the precipitation).

When α is close to zero the approximations for diffusion, poly-nucleation and mono-nucleation controlled growth are (108) respectively:

$$\alpha = k_1\ t^{5/2} \qquad [31]$$

$$\alpha = k_2\ t^4 \qquad [32]$$

$$\alpha = k_3[(1-k_4t)^{-2} - 1] \qquad [33]$$

When α is close to 1 the corresponding approximate equations are

$$\alpha = 1 - \exp(-\ k_5t) \qquad [34]$$

$$\alpha = 1 - k_6t^{-[1/(p-1)]} \qquad [35]$$

$$\alpha = 1 - k_7t^{-[1/(m-1)]} \qquad [36]$$

The constants k_1 to k_7 depend on the type of crystal growth process. As in the case of heterogeneous nucleation these equations [31,32, 33,34,35, and 36] may all be reduced to the form

$$t = KI \qquad [28]$$

where K is a constant and I (the chronomal) is a function of α. The chronomals for Equations [34], [35] and [36] (i.e., when α is close to 1) are very similar to those calculated for heterogeneous nucleation and have very similar values.

In the experiments carried out in this investigation (described in Section 3.D.) the variation with time and initial supersaturation of the size distribution of the crystals formed for the three nickel dioximates were measured. The degree of reaction, α, at any particular time is easily found when the size distribution at that time is known. The calculation is as follows. The concentration of solute at time t is given by

$$c_t = c_o - \frac{\rho \cdot \omega}{w} \int_0^{\infty} (\frac{\partial N}{\partial r}) r^3 dr \qquad [37]$$

hence

$$\alpha_t = \frac{\omega\rho}{c_o w}\int_0^\infty (\frac{\partial N}{\partial r})\cdot r^3 dr \qquad [38]$$

The size distributions were measured and recorded as plots of $(\frac{\partial N}{\partial d})_t = \frac{1}{2}(\frac{\partial N}{\partial r})_t$, versus d. This diameter size distribution curve may be simply converted to a volume size distribution curve, i.e., a plot of $(\frac{\partial N}{\partial d})_t \frac{d^3}{8}$ versus d. The area under this curve is therefore $\int_0^\infty (\frac{\partial N}{\partial d})_t \frac{d^3}{8} dd = \int_0^\infty (\frac{\partial N}{\partial r})_t r^3 dr$. The area under the volume size distribution curve was therefore measured and the value substituted in Equation [38]. This gave a series of values of α for each time in each sequence of experiments with varying initial supersaturation.

The accuracy of the values of α measured in the above way was subject to limitations. Firstly, the shape factor was estimated to have that value, which made the mass of the final size distribution to have the same mass as that calculated from the initial concentrations of the reactants. The shape factor was different for different supersaturations but in all instances had a value of 15 to 20 (the shape assumed was $\omega r \times r \times r$). This value was confirmed by visual observation. The shape factor was also assumed to be the same for all crystals of different sizes within one size distribution. Secondly for any size distribution recorded there were a certain number of crystals below the detection level of the counter. In all the calculations of the degree of reaction the total mass of the crystals present was assumed to be the same as the mass of those crystals above the detection limit. The error, due to this assumption, was worst early in the precipitation when a large proportion of the crystals were below the detection limit. However, as those crystals of largest size contributed most towards the total weight of the precipitated the error was small in all cases and negligible where most of the crystals were above the lower limit of detection. Upper estimates of the magnitude of this error may be made as follows. If the final crystal number is N then suppose all size distributions at earlier times have the same number of crystals, N, below the detection limit (1μ) and have a diameter 0.5 μ. The weight of these crystals will be $\frac{\omega}{8}\rho N(0.5)^3$. This weight is added to the weight found above 1μ and a new estimated α calculated. In all cases this amount of undetectable mass is probably grossly exaggerated. Table 18 shows comparisons between α found experimentally by ignoring the mass below the detection limit and α calculated using the exaggerated estimate above. The comparison is made for three initial concentrations of nickel dimethylglyoxime. The table shows that the two values of α are very close even for very low values of α when the comparison is worst. The experimental value of α was therefore used in all subsequent calculations. The variation of α with t, for each initial supersaturation, is shown in Appendix 2 for nickel dimethylglyoximate.

There are two potential pieces of information to be gained from the investigation of the variation of α with t. The first of these is the type of nucleation process occurring in the precipitation. The second is the type (or types) of crystal growth occurring throughout the precipitation. The results obtained here do not permit any reliable information to be obtained directly about the

TABLE 18

Experimental and estimated values for the degree of reaction for nickel dimethylglyoxime.

$c_0 = 5.0 \times 10^{-4}$		$c_0 = 2.5 \times 10^{-4}$		$c_0 = 1.0 \times 10^{-4}$	
α_{exp}	α_{est}	α_{exp}	α_{est}	α_{exp}	α_{est}
0.039	0.057	0.017	0.028	0.087	0.098
0.074	0.092	0.092	0.102	0.200	0.209
0.142	0.159	0.225	0.231	0.285	0.293
0.570	0.578	0.327	0.333	0.439	0.445
0.729	0.735	0.729	0.732	0.640	0.644
0.925	0.927	0.941	0.942	0.852	0.853

early part of the reaction where the crystals are less than 1μ in diameter and undetectable by the counter. For example, it is not possible to make the assumption that α is close to zero (Equations [31], [32] and [33]) and investigate whether the dependence of α on t indicates heterogeneous or homogeneous nucleation combined with a particular type of crystal growth. It is possible however that the dependence of α on t later in the reaction will indicate whether homogeneous or heterogeneous nucleation is occurring. As has been stated earlier the approximate chronomal for homogeneous nucleation, for α close to 1, has values very close to the chronomals for heterogeneous nucleation. This is true for the chronomals corresponding to all of the types of crystal growth. Bransom and Dunning (107) and Nielsen (59) have shown that, as the rate of nucleation varies very rapidly with supersaturation most of the nuclei are formed when α is small. Most of the change in α therefore occurs due to crystal growth on particles already formed. The situation is therefore both qualitatively and mathematically similar to the case where most of the crystal growth has occurred on heterogeneous sites. The approximate equations [34], [35] and [36], at α close to 1, should therefore also be good approximations over most of the range where α is measurable. A plot of the chronomals against time will therefore not distinguish between the two possible nucleation processes. This is especially so since both the sets of chronomals involve drastic assumptions regarding the average size and shapes of the nuclei and crystals.

The data can however be used to indicate what type of crystal growth law is obeyed.

The growth law is determined by plotting the chronomals derived from Equations [34], [35], and [36] versus time. (These are the chronomals derived assuming a homogeneous nucleation process. Those derived (104) for a heterogeneous process, having very similar values, could equally well be used). Figure 46 shows plots of the chronomal, $-\ln(1-\alpha)$, for diffusion controlled growth, versus time for several initial supersaturations of nickel dimethylglyoximate. Figure 47 shows plots of the chronomal, $(\frac{1}{1-\alpha})^p$, for poly-nucleation controlled growth, versus time for the corresponding initial supersaturations of nickel dimethylglyoximate. The plots in Figure 47 are for the particular case where $p = 3$. From these plots it can be seen that the experimental data only satisfy the functional relationship derived assuming that diffusion controlled growth is taking place. Plots of the chronomal for mono-nucleation controlled growth versus time show more curvature than those for poly-nucleation controlled growth (Figure 47). Similar plots of the chronomal for diffusion controlled growth, for nickel heptoximate and nickel nioximate are shown in Figure 48. (Figure 48 is drawn from values of α, t and the chronomals given in Appendix 2.) In these instances, also, the experimental data only satisfies the relationship required assuming diffusional controlled growth.

The results then show that for detectable crystals of the nickel dioximates studied, the growth was controlled by diffusion of the monomers to the surface. At very early stages in the precipitations (i.e., at small values of α), the results were not sufficiently

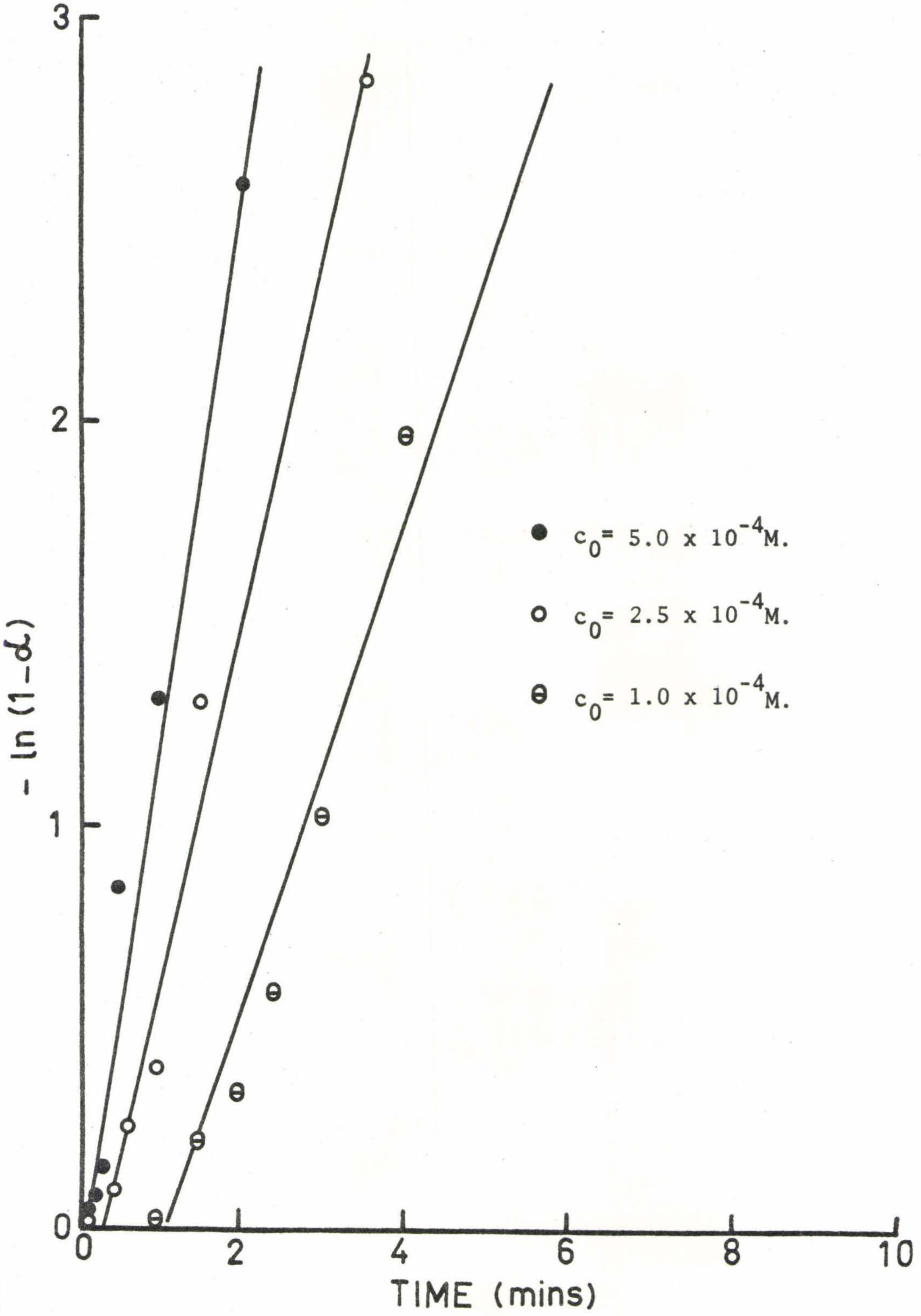

FUGURE 46. Variation of -ln (1-α) with time for three initial concentrations of nickel dimethylglyoximate.

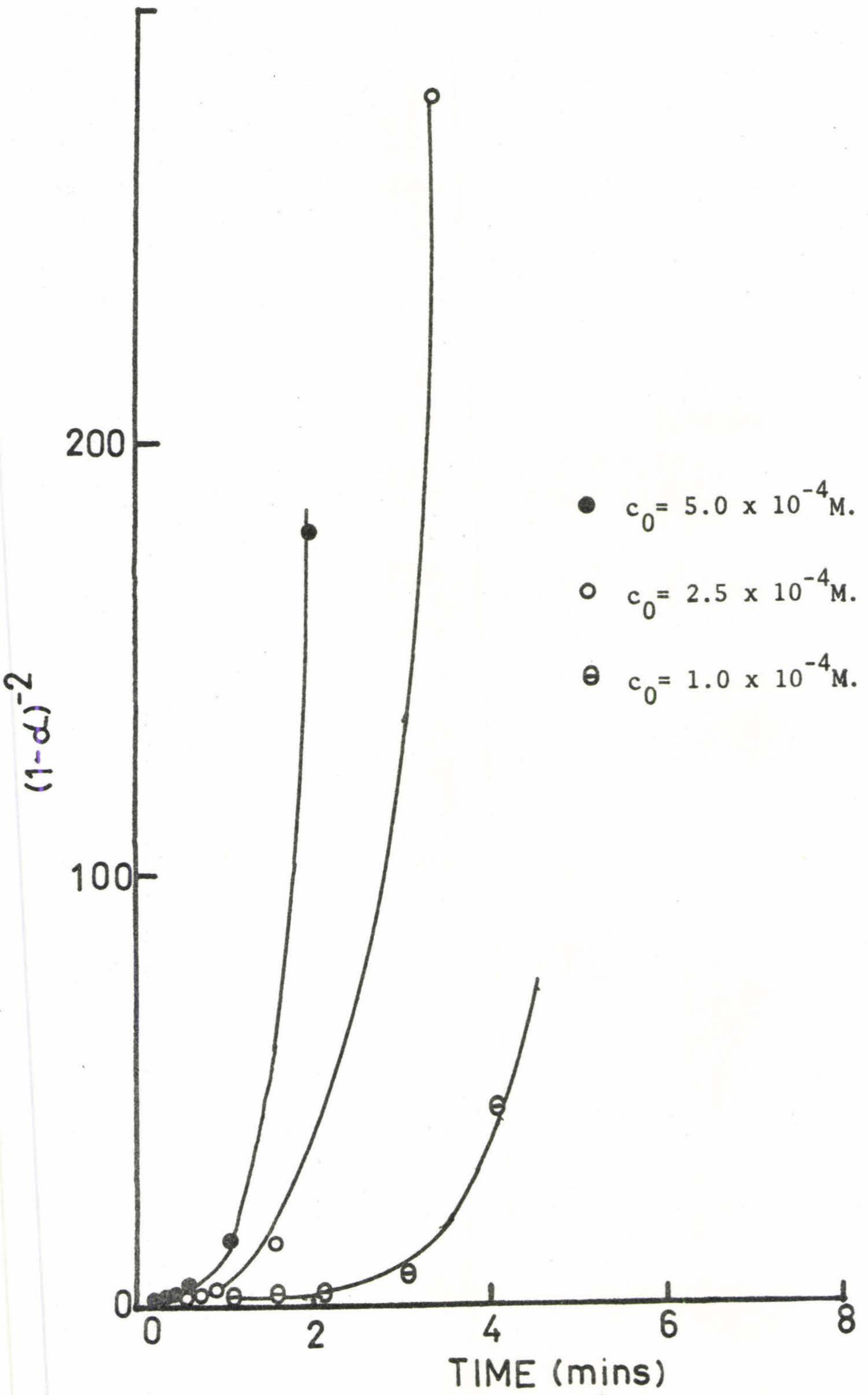

FIGURE 47. Variation of $(1-\alpha)^{-2}$ with time for three initial concentrations of nickel dimethylglyoximate.

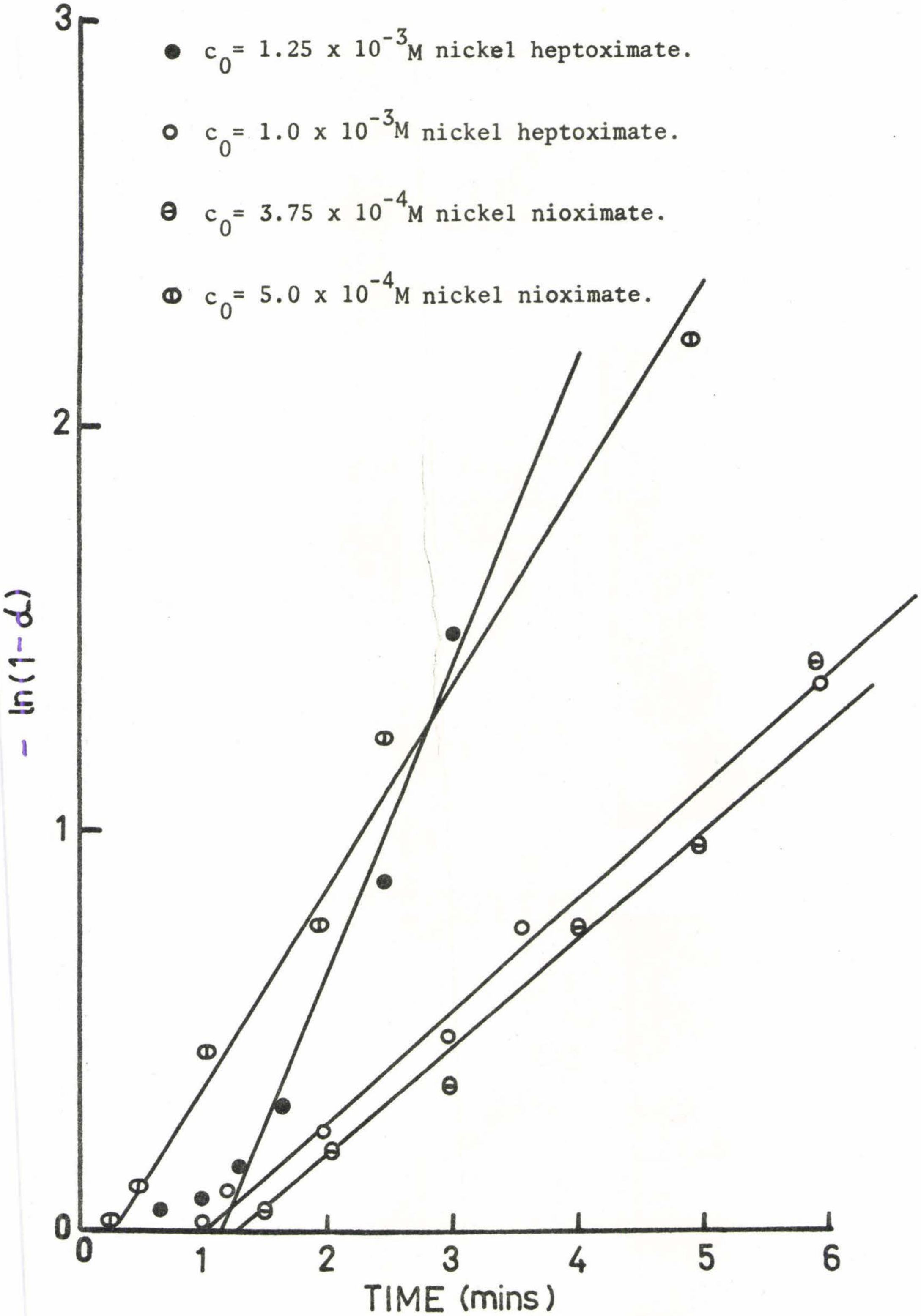

FIGURE 48. Variation of -ln (1-α) with time for nickel heptoximate and nickel nioximate.

accurate or precise to distinguish between the various growth laws. It is probable, for very small crystals below the limit of detection of the counter, that the growth is not limited by diffusion but by a nucleation controlled mechanism. Also it was not possible to determine whether the nucleation step was heterogeneous or homogeneous because of the similarity of the respective sets of chronomals, the assumptions made in their derivation and the imprecision and assumptions made in experimentally determining α.

4. SUMMARY AND CONCLUSIONS

1. A system was set up using a Coulter counter, a multichannel analyser and magnetic tape recorder in conjunction with computer analysis of the data to rapidly measure the size distribution of particles, with a wide size range, suspended in an electrolyte. The system was calibrated using spheres of known size distributions. Rapid mixing techniques combined with a stopped flow dilution method were used to produce crystal suspensions suitable for measurement using the counting system. The standard spheres and barium sulphate crystals were used to test the methods of producing the suspensions. For barium sulphate the nucleation parameters calculated from the size distribution data agreed with those found by many other investigators.

2. These mixing and counting techniques were then used to obtain the variation of the size distribution with time, of the crystals formed when three nickel dioximates were precipitated. A set of size distribution versus time data was obtained for various initial nickel dioximate supersaturations.

3. The shape of the size distribution curves and the variation of the shape with time and supersaturation indicated that homogeneous nucleation was taking place for each of the nickel dioximates.

4. The total number of crystals appearing above the lower limit of detection of the counter showed an initial linear rise with time,

for all supersaturations and all chelates. The slope of this initial linear portion was equated with the rate of nucleation, J.

5. A linear plot of log J versus $(\log S)^{-2}$ was obtained for all the compounds studied. This result supports the functional relationship predicted by the classical nucleation theory (Equation [15]).

6. Values of the pre-exponential factor, A, of the order of $10^9 - 10^{14}$ $\text{cm}^{-3}\text{sec}^{-1}$ were obtained for the chelates studied. These were compared with the theoretical value of approximately 10^{27} and the possible reasons for the discrepancy discussed.

7. The value found for the surface free energy of all the nickel dioximates was 13 ergs cm^{-2}. The number of molecules in the critical nucleus, when J = 1, was found to be from 12-14. These values compared favourably with those obtained by other authors.

8. Crystal growth studies indicated that, over the period where the progress of the reaction could be followed experimentally, the rate controlling step was the diffusion of the nickel dioximate molecules from the bulk solution to the crystal surface.

9. It was found impossible to use variation of the degree of reaction, α, with time as a criterion for distinguishing between heterogeneous and homogeneous nucleation.

10. Future Work.

This investigation was limited to the study of the nucleation of nickel dioximates and indicated that similar nucleation parameters could be obtained for these chelates even though they were precipitated under different experimental conditions. It would be of great interest to extend this study to other metal chelates of much greater structural difference and investigate any variation in the experimental nucleation parameters in relation to the differences in structure.

The development of new and improved experimental methods is of continuing importance to the understanding of nucleation phenomena. This work has underlined the fact that it is important to study the growing crystals as soon as possible after formation of the critical nuclei. Future work could improve on the techniques for measuring size distributions, with the objectives of instantaneous measurement and of lowering the size of the smallest crystals which may be detected.

5. APPENDICES

APPENDIX 1.

COMPUTER PROGRAMME TO CALCULATE AND PRINTOUT OVERALL SIZE DISTRIBUTIONS.

```
$JOB               000523 HANNA J D              100    010   030
$PAUSE PLEASE READ TAPE RHT 006 ON T.U. 2 AT 556BPI
$IBJOB        NOMAP,NODECK
$IBFTC
      DIMENSION AMP(10),IA(6000),SB(300),DIA(300),BG(300),AL(300)
      READ (5,20) AMP(1),AMP(2),AMP(3),AMP(4),AMP(5),AMP(6),AMP(7),
     $ AMP(8),AMP(9),AMP(10)
   20 FORMAT (10F6.0)
      READ (5,21) NA,AM,CCU,POS,ST,CUR,AMIN
   21 FORMAT (I4,6F7.0)
      Y = (0.52362*(ST**3.0))/(AM*CCU*POS)
      D = (Y*AMP(1)*CUR*AMIN/0.52362)**0.3333
      DO 10 JA = 1,NA
      DA = 0.0
      NH = 1
      SC = 0.0
      SD = 0.0
      DO 11 JB = 1,10
      M = 2049
      IF (JA.EQ.5.AND.JB.EQ.5) GO TO 26
      CALL RDTAPE (IA,M)
   26 CONTINUE
      DA = DA-0.5
      IF (JB.NE.) GO TO 12
      DA = D
   12 CONTINUE
      DB = (Y*AMP(JB)*CUR*600.0/0.52362)**0.33333
      XA = (DB-DA)/0.1
      NXA = XA
      DO 13 JC = 1,NXA
      PA = (0.52362*(DA**3.0))/(Y*AMP(JB)*CUR)
      DA = DA+ 0.1
      PB = (0.52362*(DA**3.0))/(*AMP(JB)*CUR)
      SA = 0.0
      NPA = PA
      NPB = PB
      XPA = NPA
      XPB = NPB
      XDA = PA-XPA
      XDB = PB-XPB
```

APPENDIX 1 (CTD)

```
      DO 14 JD = NPA,NPB
      AA = IA(JD)
      SA = SA+AA
   14 CONTINUE
      ADA = IA(NPA-1)
      ADB = IA(NPB+1)
      SA = SA-(XDA*ADA)+(XDB*ADB)
      SB(NH) = DA
      DIA(NH) + DA
      IF (JA.NE.1) GO TO 23
      BG(NH) = SB(NH)
   23 CONTINUE
      IF (JA.EQ.1) GO TO 22
      SB(NH) = SB(NH)-BG(NH)
   22 CONTINUE
      AD = SB(NH)
      IF (SB(NH).LT.1.0) AD = 1.0
      AL(NH) = ALOG10 (AD)
      SC = SC+SB(NH)
      NH = NH+1
   13 CONTINUE
   11 CONTINUE
      WRITE (6,18) JA
   18 FORMAT (25H SIZE DISTRIBUTION SERIES, I4)
      JG = 1
      JH = 129
      DO 15 JE = 1,32
      WRITE(6,16) (SB(JF),DIA(JF),AL(JF),JF = JG,JH 32)
   16 FORMAT (5(F8.0,F6.2,F6.2))
      JG = JG+1
      JH = JH+1
   15 CONTINUE
      WRITE (6,17)SC,SD
   17 FORMAT (2F14.0)
   10 CONTINUE
      STOP
      END
$IBLDR KENTAP        08/11/65
$CDICT KENTAP
$TEXT  KENTAP
$DKEND KENTAP
$ENTRY
$IBSYS
```

APPENDIX 2.

Variation of the degree of reaction, α, and the corresponding chronomals, with time, for various initial concentrations of the nickel dioximates.

Concentration and chelate.	Time (secs)	α	$-\ln(1-\alpha)$	$(1-\alpha)^{-2}$
$c_0 = 5.0 \times 10^{-4}$M	10	0.039	0.039	1.08
nickel	15	0.074	0.076	1.16
dimethylglyoximate	20	0.142	0.154	1.36
	30	0.570	0.844	5.13
	60	0.729	1.37	13.6
	120	0.925	2.59	179
$c_0 = 2.5 \times 10^{-4}$M	10	0.017	0.017	1.03
nickel	30	0.092	0.097	1.10
dimethylglyoximate	38	0.225	0.254	1.66
	60	0.327	0.395	2.20
	90	0.729	1.31	13.6
	210	0.941	2.82	283
$c_0 = 1.0 \times 10^{-4}$M	60	0.087	0.091	1.20
nickel	90	0.200	0.223	1.56
dimethylglyoximate	120	0.285	0.335	1.96
	150	0.439	0.578	3.17
	180	0.640	1.02	7.70
	240	0.852	1.90	45.3

APPENDIX 2 (ctd).

$c_0 = 5.0 \times 10^{-5}M$	90	0.001	0.001	1.00
nickel	240	0.011	0.011	1.02
dimethylglyoximate	480	0.069	0.072	1.16
	900	0.298	0.298	1.82
	1500	0.437	0.353	2.40
	1800	0.989	0.628	7.23
$c_0 = 1.25 \times 10^{-3}M$	41	0.069	0.072	1.16
nickel	60	0.075	0.079	1.17
heptoximate	80	0.117	0.125	1.28
	100	0.251	0.289	1.78
	150	0.586	0.881	5.82
	180	0.785	1.54	21.7
$c_0 = 1.0 \times 10^{-3}M$	60	0.006	0.006	1.01
nickel	75	0.101	0.107	1.23
heptoximate	120	0.219	0.247	1.64
	180	0.392	0.498	2.71
	210	0.534	0.763	4.60
	360	0.741	1.35	14.8
$c_0 = 5.0 \times 10^{-4}M$	15	0.044	0.045	1.09
nickel	30	0.097	0.102	1.23
nioximate	65	0.363	0.451	2.46
	120	0.524	0.742	4.41
	150	0.701	1.21	11.1
	300	0.892	2.22	85.7

APPENDIX 2 (ctd).

$c_0 = 3.75 \times 10^{-4}$M	90	0.059	0.061	1.13
nickel	120	0.236	0.269	1.71
nioximate	180	0.313	0.376	2.12
	240	0.533	0.761	4.58
	300	0.625	0.982	7.12
	360	0.757	1.41	16.9

6. BIBLIOGRAPHY

1. Fahrenheit, D. B., Phil. Trans. Roy. Soc., 39, 78, (1724).
2. Lowitz, J. T., Crells. Chemische Annalen, 1, 3, (1795).
3. Gay Lussac, J. L., Ann. de Chimie, 87, 225, (1813).
4. Gay Lussac, J. L., Ann. chim. phys., 11, 296, (1819).
5. Podkopev, A., Teor. Osn. Khim. Tekhnol., 3(3), 376 (1969).
6. Hem, S. L., Ultrasonics, 5, 202 (1967).
7. Berdysheva, N. A., Ageeva, M. A., Tyrurin, Y. N., Tr. Ural. Nauch. Issled. Khim. Inst., 12, 251, (1966).
8. Todoriev, N. K., Iovchev, M. P. Godisknik. Mashinno. Electrote. Khn. Inst., 10(3), 117 (1961).
9. Kukoz, K. I., Akust. Magn. Obrab. Veshchestv., 15, (1966).
10. Schroeder, H., von Dusch, Leibigs Annalen, 89, 232, (1853); 109, 35, (1859).
11. De Coppet, L. C., Ann. Chim. Phys., 6, 275 (1875).
12. Ostwald, W., Z. Phys. Chem., 22, 289, (1897); 34, 493, (1900).
13. Tamman, G., "States of Aggregation", van Nostrand, New York (1926).
14. Von Weirman, P. P., Chem. Rev., 2, 217 (1926).
15. Leckenby, R. E., Robbins, E. J., Proc. Roy. Soc. London, 280A, 409, (1964).
16. Idem, ibid., 291A, 389 (1966).
17. Cuthbert, E. R., Preece, E. R., Turnbull, A. H., Appl. Spect. 19, 18, (1965).
18. Greene, F. T., Milne, T. A., J. Chem. Phys., 39, 3150 (1963); 47, 4095 (1967).

19. Szilard, L., see Farkas L., Reference 21.

20. Volmer, M., Weber, A., Z. Phys. Chem. (Leipzig), 119, 277 (1926).

21. Farkas, L., Z. Phys. Chem. (Leipzig), A125, 326 (1927).

22. Stranski, I. N., Z. Phys. Chem. (Leipzig), B26, 732 (1935).

23. Becker, R., Doring, W., Ann. Physik., 24, 719 (1935).

24. Zeldovich, J. B., Acta Physicochimica, U.R.S.S., 18, 1 (1943).

25. Mayer, J. E., J. Chem. Phys., 5, 67 (1937).

26. Frenkel, J., J. Chem. Phys., 7, 200 (1939).

27. Becker, R., Discuss. Farad. Soc., 5, 55 (1949).

28. Rodebush, W. H., Chem. Revs., 44, 269 (1949).

29. Reiss, H., Z. Electrochem., 56, 459 (1952).

30. Dunning, W. T., Discuss. Farad. Soc., 30, 9 (1961).

31. Lothe, J., Pound, G. M., J. Chem. Phys., 36, 2080 (1962).

32. Oriani, R. A., Sundquist, B. E., J. Chem. Phys., 38, 2082 (1963).

33. Reiss, H., Katz, J. L., J. Chem. Phys., 46, 2496 (1967).

34. Lothe, J., Pound, G. M., J. Chem. Phys., 48, 732 (1968).

36. Dunning, W. J., "Chemistry of the Solid State", 159, Butterworths, London, (1955).

37. Dunning, W. J., "Nucleation", 1, Marcel Dekker, New York, (1969).

38. Andres, R. P., ibid., 69.

39. Lothe, J., Pound, G. M., ibid., 109.

40. Bradley, R. S., Quart. Revs., 5, 315 (1951).

41. Holloman, J. H., Turnbull, D., Prog. Met. Phys., 4, 368 (1953).

42. Nielsen, A. E., "Kinetics of Precipitation", 11, Pergamon Press, (1964).

43. Frenkel, J., "Kinetic Theory of Liquids", Oxford University Press,

Oxford (1946).

44. Rodebush, W. H., Chem. Revs., 44, 269 (1949).

45. Kurt, F., Z. Phys., 131, 185 (1952).

46. Reference 39, loc. cit., 127.

47. Reference 39, loc. cit., 124.

48. Sutugin, A. G., Phys. Lett. A, 29(5), 233 (1969).

49. Kantrowitz, A., J. Chem. Phys., 19, 1097 (1951).

50. Probstein, R. F., J. Chem. Phys., 19, 619 (1951).

51. Andres, R. P., Boudart, M., J. Chem. Phys., 42, 2057 (1965).

52. Courtney, W. G., J. Chem. Phys., 36, 2009 (1962).

53. Abraham, F. F., J. Chem. Phys., 51, 1632 (1969).

54. Turnbull, D., Fisher, J. C., J. Chem. Phys., 17, 71 (1948).

55. Volmer, M., Flood, H., Z. Physik Chem., A170, 273 (1934).

56. Powell, C. F., Proc. Roy. Soc. London, A119, 553 (1928).

57. Katz, J. L., Ostermier, B. J., J. Chem. Phys., 47, 478 (1967).

58. Hill, P. G., J. Fluid Mech., 25, 593 (1966).

59. Nielsen, A. E., Crystal Growth, Supplement to J. Phys. Chem. Solids, Oxford, New York, 419 (1967).

60. Nielsen, A. E., Krist. Tech., 4, 17 (1969).

61. Christiansen, J. A., Acta. Chem. Scand., 5, 676 (1951).

62. Melia, T. P., Moffitt, W. P., J. Colloid. Sci., 19, 433 (1964).

63. Hileman, O. E., Talanta, 14, 138 (1967).

64. Thompson, S., Gordon, L., Talanta, 14, 137 (1967).

65. White, M. L., Frosst, A. A., J. Colloid. Sci., 14, 247 (1959).

66. Newkirk, J. P., Turnbull, D., J. Appl. Phys., 26, 579 (1955).

67. Nielsen, A. E., Acta. Chem. Scand., 15, 441 (1961).

68. Turnbull, D., Vonnegut, B., Ind. Eng. Chem., 44, 1292 (1952).

69. Melia, T. P., Moffitt, W. P., Nature, 201, 1024 (1964).

70. Dunning, W. J., Notley, N. T., Z. Electrochem., 61, 55 (1957).

71. Dunning, W. J., Shipman, A. J., Proc. Agric. Ind. Tenth Int. Congress (Madrid), 1954.

72. Duke, F. R., Brown, L. M., J. Amer. Chem. Soc., 76, 1443 (1954).

73. Howich, L. C., U.S. At. Ener. Comm., ORO-2954-3 (1969).

74. Rihs, T., Thurston, M. C., Talanta, 17, 123 (1970).

75. Packter, A., Chauhan, P., Saunders, D. F., Krist. Tech., 4, 45 (1969).

76. Hileman, O. E., Velazquez, J., Talanta, 17, 623 (1970).

77. Thompson, S., Walton, A. G., U.S. At. Ener. Comm., COO-582-14 (1967).

78. Mealor, D., Townshend, A., Talanta, 13, 1069 (1966).

79. Walton, A. G., "Nucleation", 297, Marcel Dekker, New York (1969).

80. Nielsen, A. E., Proc. Intern. Symp. Nucleation Phenomena, Cleveland, 17 (1965).

81. Collins, F. C., Leinweber, J. P., J. Phys. Chem., 60, 389 (1956).

82. Klein, D. H., Driy, J. A., Talanta, 13(2), 289 (1966).

83. Walton, A. G., Microchim. Acta., 3, 422 (1963).

84. Enustun, B. V., Turkevich, J., J. Amer. Chem. Soc., 82, 4502 (1960).

85. Takiyama, K., Bunseki Kaguki, 18, 728 (1969).

86. Klein, D. H., Gordon, L., Walnut, T. H., Talanta, 3, 187 (1959).

87. Walton, A. G., "Formation and Properties of Precipitates," Interscience, 30 (1967).

88. Sokol, V. A., Bromberg, A. V., Tr. Uses. Nauch. Issled. Inst. Khim. Reactivov. Osobo. Christ. Khim. Vestchesto., 30, 342 (1967).

89. Haberman, N., Gordon, L., Talanta, 11, 1591 (1964).

90. Clegg, G., Melia, T. P., Talanta, 14, 989 (1967).

91. Hileman, O. E., Velazquez, J., Can. J. Chem., 48, 2896 (1970).

92. Newkirk, J. B., Turnbull, D., J. Appl. Phys., 26, 579 (1955).

93. Klein, D. H., Smith, M. D., Talanta, 15, 229 (1968).

94. Klein, D. H., Smith, M. D., Driy, J. A., Talanta, 14, 937 (1968).

95. Hlabse, T., Walton, A. G., Anal. Chim. Acta., 33, 373 (1965).

96. Van Hook, A., Frulla, F., Ind. Eng. Chem., 44, 1305 (1952).

97. Hamilton, J. A., Kantsky, J. A., Walton, A. G., Nature, 204, 1085 (1964).

98. Levine, J., National Advisory Committee for Aeronautics, Note 2234 (1950).

99. Strickland-Constable, R. F., "Kinetics and Mechanism of Crystallization", Academic Press, London (1968).

100. Godycki, E. L., Rundle, R. E., Acta. Cryst., 6, 487 (1953).

101. Banks, C. V., Anderson, S., Inorg. Chem., 2, 112 (1963).

102. Nielsen, A. E., Acta. Chem. Scand., 11, 1512 (1957).

103. Takiuama, K., Suito, E., Bull. Chem. Soc. Japan, 27, 121 (1954).

104. Reference 42, loc. cit., 54.

105. Roughton, F. J., Chance, B., Techniques of Organic Chemistry, Interscience, New York, 8(2), 704 (1963).